View metadata, citation and similar papers at core.ac.uk

brought to you by CORE

İSTANBUL TECHNICAL UNIVERSITY ★ INSTITUTE OF SCIENCE AND TECHNOLOGY

DYNAMIC SOIL STRUCTURE INTERACTION UNDER WAVE PROPAGATION VIA AN IMPROVED COUPLED FINITE ELEMENT-BOUNDARY ELEMENT METHODOLOGY

Ph.D. Thesis by
Ayşe Elif ÖZSOY ÖZBAY

Department : Civil Engineering

Programme : Structural Engineering

MARCH 2011

İSTANBUL TECHNICAL UNIVERSITY ★ INSTITUTE OF SCIENCE AND TECHNOLOGY

DYNAMIC SOIL STRUCTURE INTERACTION UNDER WAVE PROPAGATION VIA AN IMPROVED COUPLED FINITE ELEMENT-BOUNDARY ELEMENT METHODOLOGY

Ph.D. Thesis by
Ayşe Elif ÖZSOY ÖZBAY
(501032002)

Date of submission : **13 September 2010**
Date of defence examination: **02 March 2011**

Supervisor (Chairman) : **Prof. Dr. Pelin GÜNDEŞ BAKIR (ITU)**
Co-supervisor: **Dr. Bahattin KİMENÇE (ITU)**
Members of the Examining Committee : **Prof. Dr. Faruk YÜKSELER (YTU)**
Assoc. Prof. Dr. Abdullah GEDİKLİ (ITU)
Prof. Dr. Semih TEZCAN (BU)
Prof. Dr. Zekai CELEP (ITU)
Prof. Dr. Tuncer ÇELİK (Beykent University)

MARCH 2011

İSTANBUL TEKNİK ÜNİVERSİTESİ ★ FEN BİLİMLERİ ENSTİTÜSÜ

DİNAMİK YAPI ZEMİN ETKİLEŞİMİNİN DALGA YAYILIMI ETKİSİ ALTINDA SONLU ELEMAN-SINIR ELEMAN YÖNTEMİ İLE MODELLENMESİ

DOKTORA TEZİ

Ayşe Elif ÖZSOY ÖZBAY
(501032002)

Tezin Enstitüye Verildiği Tarih : 13 Eylül 2010
Tezin Savunulduğu Tarih : 02 Mart 2011

Tez Danışmanı : Prof. Dr. Pelin Gündeş BAKIR (İTÜ)
Eş Danışman : Öğr. Gör. Dr. Bahattin KİMENÇE (İTÜ)
Diğer Jüri Üyeleri : Prof. Dr. Faruk YÜKSELER (YTÜ)
Doç. Dr. Abdullah GEDİKLİ (İTÜ)
Prof. Dr. Semih TEZCAN (BÜ)
Prof. Dr. Zekai CELEP (İTÜ)
Prof. Dr. Tuncer ÇELİK (Beykent Üniversitesi)

MART 2011

FOREWORD

I would like to express my deep appreciation and thanks for my advisor, Prof. Dr. Pelin Gündeş BAKIR and my co-advisor, Dr. Bahattin KİMENÇE. I owe special thanks to the members of my thesis committee; Prof. Dr. Faruk YÜKSELER, Assoc. Prof. Dr. Abdullah GEDİKLİ for their helpful guidance and contribution throughout this thesis.

I am also grateful to Prof. Dr. Zekai CELEP and Prof. Dr. Tuncer ÇELİK for their suggestions and generous support.

Finally, I would like to thank to my husband Hakan ÖZBAY, my son Kerem ÖZBAY and to my dearest family for their help and endless encouragement.

March 2011

Ayşe Elif ÖZSOY ÖZBAY

Civil Engineering

TABLE OF CONTENTS

Page

FOREWORD ..... **v**
TABLE OF CONTENTS ..... **vii**
ABBREVIATIONS ..... **ix**
LIST OF TABLES ..... **xi**
LIST OF FIGURES ..... **xiii**
LIST OF SYMBOLS ..... **xv**
SUMMARY ..... **xix**
ÖZET ..... **xxi**
1. AN OVERVIEW OF THE THESIS **1**
1.1 Purpose of the Dissertation 3
1.2 The Summary of the Methodology 6
2. INTRODUCTION **9**
2.1 The Theoretical Background 10
2.1.1 Solutions in the time domain versus the frequency domain 11
2.1.2 Direct method 12
2.1.3 Substructure method 12
2.1.4 Lumped parameter models 13
3. SEISMIC WAVE PROPOGATION IN THE SOIL MEDIUM **15**
3.1 Seismic Waves 15
3.2 Equations of Motion for an Elastic Solid 17
3.3 Solution of the Wave Equations in the Elastic Medium 20
4. MODELLING OF THE SOIL MEDIUM **27**
4.1 Background 27
4.2 Green's Functions for the Harmonic Point Load acting on the Surface of an Elastic Half-Space 29
4.3 Evaluation of the Frequency Dependent Impedance Matrix of the Elastic Half-Space 36
5. IMPLEMENTATION OF THE SUBSTRUCTURE METHOD **41**
5.1 General Procedure 41
5.2 Derivation of the Numerical Methodology 43
5.3 The Summary of The Numerical Procedure 48
6. SAMPLE PROBLEM 1: 3D BRIDGE-BACKFILL SYSTEM **51**
6.1 Introduction 51
6.2 Traveling Seismic Wave Effect 51
6.3 The Sample Problem 55
6.4 The Modal Participation Factors 57
6.5 The Response of the Bridge-Backfill System under Harmonic Excitation 62
6.6 The Response of Bridge-Backfill System under Plane SH Wave Excitation 65
6.7 The Discussion of the Results 66

7. SAMPLE PROBLEM 2: 3D MULTISTORY BUILDING 71
7.1 Introduction..... 71
7.2 Simplified Equivalent Single-Degree-Of-Freedom (SDOF) System for the Coupled Soil-Structure System 71
7.3 Two-Degree-Of-Freedom System for the Coupled Soil-Structure System 74
7.4 Response of Two-Degree-Of-Freedom Model to Earthquake Ground Motion 76
7.5 Verification of the Numerical Procedure: A Simplified Three Dimensional Frame 79
7.6 Three Dimensional Modeling of A Reinforced Concrete Multistory Building..... 83
7.7 Discussion of the Results..... 86
7.7.1 Effect of the soil-structure interaction on the fundamental frequency of the structure 87
7.7.2 Effect of soil-structure interaction on the peak displacement response of the soil-structure system..... 89
7.7.3 Damage identification using the drift ratio 90
8. CONCLUSIONS AND RECOMMENDATIONS 93
8.1 Conclusions..... 94
8.2 Contributions 96
8.3 Recommendations for The Future Work 98
REFERENCES 99
APPENDICES 105
CURRICULUM VITAE 121

ABBREVIATIONS

BEM	**:** Boundary Element Method
DOF	**:** Degrees of Freedom
FAS	**:** Fourier Amplitude Spectra
FEM	**:** Finite Element Method
FEMA	**:** Federal Emergency Management Agency
FFT	**:** Fast Fourier Transform
HAZUS	**:** Hazards United States
P	**:** Primary Waves
SDOF	**:** Single Degree of Freedom
SH	**:** Secondary Waves (polarized in horizontal plane)
SV	**:** Secondary Waves (polarized in vertical plane)
SSI	**:** Soil Structure Interaction
2D	**:** Two dimensional
3D	**:** Three dimensional

LIST OF TABLES

Page

Table 5.1: The summary of the numerical procedure. 49
Table 6.1: Physical and material properties of the bridge..... 56
Table 6.2: Natural modes of the bridge-backfill system. 59
Table 6.3: Material properties of the soil for Cases A1, B1 and C1. 65
Table 7.1: Mechanical and material properties of soil-structure system..... 80
Table 7.2: Comparison of the natural frequency of the soil-structure system.. 82
Table 7.3: Comparison of the displacement amplitude values in y direction. 82
Table 7.4: The natural frequencies, the proportional damping and the effective masses for the first 20 modes. 86
Table 7.5: The summary of the results. 87
Table 7.6: Drift ratio at the threshold of the damage state for C1M building type according to HAZUS99 [16]..... 91
Table 7.7: Structural performance levels and damage given by FEMA 356 [17]. ... 91

LIST OF FIGURES

Page

Figure 1.1 : General framework of the study. 5
Figure 1.2 : The methodology developed in this study. 7
Figure 3.1 : Deformations produced by Love waves and Rayleigh waves [51]. 15
Figure 3.2 : Deformations produced by body waves: P, SV and SH-waves [52]. 16
Figure 3.3 : Reflections of P, SV and SH waves at the ground surface [14]. 17
Figure 3.4 : Reflections of P, SV and SH waves at the ground surface [50]. 18
Figure 3.5 : Free-field displacement due to seismic wave propagation. 26
Figure 4.1 : Flowchart for the calculation of half-space impedance matrix. 28
Figure 4.2 : The source and the receiver points in Cartesian coordinate system. 29
Figure 4.3 : The graph of f_{rr} versus dimensionless frequency a_0 for the Poisson's ratio of $\nu = 1/3$ and $\nu = 1/4$ [29]. 34
Figure 4.4 : The graph of $f_{\theta r}$ versus dimensionless frequency a_0 for the Poisson's ratio of $\nu = 1/3$ and $\nu = 1/4$ [29]. 35
Figure 4.5 : The graph of f_{rz} versus dimensionless frequency a_0 for the Poisson's ratio of $\nu = 1/3$ and $\nu = 1/4$ [29]. 35
Figure 4.6 : The graph of f_{zz} versus dimensionless frequency a_0 for the Poisson's ratio of $\nu = 1/3$ and $\nu = 1/4$ [29]. 36
Figure 5.1 : Flowchart for the numerical modeling of the soil-structure system. 42
Figure 6.1 : 2D Multispan bridge under the effect of SH waves [66]. 53
Figure 6.2 : The 3D bridge model under the effect of SH waves [70]. 54
Figure 6.3 : 3D Finite element model of the bridge. 55
Figure 6.4 : Solid, thin shell and membrane elements [60]. 56
Figure 6.5 : Harmonic motion in the *x* direction. 64
Figure 6.6 : Harmonic motion in the y direction. 64
Figure 6.7 : The response in the y direction for the rigid base conditions given as Case A1 (top) and Case A2 (bottom). 68
Figure 6.8 : The response in y direction for Case B1 (top) and Case B2 (bottom). . 69
Figure 6.9 : The response in *y* direction for Case C1 (top) and Case C2 (bottom)... 70
Figure 7.1 : Single degree of freedom model for soil-structure interaction [18]. 72
Figure 7.2 : Two degree of freedom system for the soil-structure system [18]. 74
Figure 7.3 : Two-degree of freedom model. 77
Figure 7.4 : Coefficients in impedance functions of a rigid massless circular footing resting on the elastic half-space [73]. 78
Figure 7.5 : Three dimensional modeling of the single story structure. 79
Figure 7.6 : Response of one story building at the foundation. 80
Figure 7.7 : Response of one story building at the first story level. 81
Figure 7.8 : Relative displacement of the first story level with respect to foundation. 81
Figure 7.9 : FEM of the building and discretization of the soil-structure interface.. 84
Figure 7.10 : Plan section of the multistory building [74]. 85
Figure 7.11 : The procedure proposed for the damage identification. 90

Figure A.1 : Mode shapes of the bridge (1-9). 106
Figure A.2 : Mode shapes of the bridge (10-17). 107
Figure A.3 : Mode shapes of the bridge (18-26). 108
Figure A.4 : Mode shapes of the bridge (31, 45, 57, 58, 71, 75). 109
Figure A.5 : Mode shapes of the bridge deck. 110
Figure B.1 : Displacement response at the foundation normalized with respect to the base excitation for the Soil A and the vertical SH wave..... 111
Figure B.2 : Displacement response at the sixth story normalized with respect to the base excitation for the Soil A and the vertical SH wave..... 111
Figure B.3 : Displacement response at the foundation normalized with respect to the base excitation for the Soil A and the horizontal SH wave. 112
Figure B.4 : Displacement response at the 6th story normalized with respect to the base excitation for the Soil A and the horizontal SH wave. 112
Figure B.5 : Displacement response at the foundation normalized with respect to the base excitation for the Soil B and the vertical SH wave..... 113
Figure B.6 : Displacement response at the 6th story normalized with respect to the base excitation for the Soil B and the vertical SH wave..... 113
Figure B.7 : Displacement response at the foundation normalized with respect to the base excitation for the Soil B and the horizontal SH wave..... 114
Figure B.8 : Displacement response at the 6th story normalized with respect to the base excitation for the Soil B and the horizontal SH wave..... 114
Figure B.9 : Ratio of the acceleration response (top/base) for the Soil A and the vertical SH wave. 115
Figure B.10 : Ratio of the acceleration response (top/base) for the Soil A and the horizontal SH wave. 115
Figure B.11 : Ratio of the acceleration response (top/base) for the Soil B and the vertical SH wave. 116
Figure B.12 : Ratio of the acceleration response (top/base) for the Soil B and the horizontal SH wave. 116
Figure C.1 : Displacement response of the story levels relative to foundation at f = 1.45 Hz for the Soil A and the vertical SH wave motion. 117
Figure C.2 : Interstory drift ratio at f = 1.45 Hz for the Soil A and the vertical SH wave motion. 117
Figure C.3 : Displacement response of the story levels relative to foundation at f = 1.45 Hz for the Soil A and the horizontal SH wave motion..... 118
Figure C.4 : Interstory drift ratio at f = 1.45 Hz for the Soil A and the horizontal SH wave motion. 118
Figure C.5 : Displacement response of the story levels relative to foundation at f = 2.15 Hz for the Soil B and the vertical SH wave motion. 119
Figure C.6 : Interstory drift ratio at f = 2.15 Hz for the Soil B and the vertical SH wave motion. 119
Figure C.7 : Displacement response of the story levels relative to foundation at f = 2.15 Hz for the Soil B and the horizontal SH wave motion..... 120
Figure C.8 : Interstory drift ratio at f = 2.15 Hz for Soil B/ horizontal SH wave... 120

LIST OF SYMBOLS

a_0	: Dimensionless Frequency
A_j	: Area of the jth Subregion
c	: Apparent Wave Velocity
c_b	: Damping of the Building (for Fixed Based Condition)
c_f	: Damping of the Foundation
[C]	: Damping Matrix of the Soil-Structure System
$[C_{11}]$	: Diagonal Damping Matrix of the Superstructure
$[C_{HS}]$	: Compliance Matrix of the Half-space
e	: Incident Angle of the Seismic Wave
f	: Reflection Angle of the Seismic Wave
$f_{rr}(a_0)$	: *rr* component of the Green's Function
$f_{\theta r}(a_0)$	: θr component of the Green's Function
$f_{\theta z}(a_0)$	: θz component of the Green's Function
$f_{zr}(a_0)$	: *zr* component of the Green's Function
$f_{zz}(a_0)$	: *zz* component of the Green's Function
$F(z)$	: Rayleigh Determinant
G	: Shear Modulus
$[G(\omega,(\underline{x}-\underline{x}_0))]$	: Green's Function Matrix
$[I]$	: Identity Matrix
$J_0(a_0 z)$	: Bessel Function of the First Kind of Zeroth-Order
$J_1(a_0 z)$	: Bessel Function of the First Kind of First Order
$J_2(a_0 z)$	: Bessel Function of the First Kind of Second Order
k	: Wave-number of the Incident Wave
k_b	: Stiffness of the Building (for the Fixed Based Condition)
k_f	: Stiffness of the Foundation
k_h	: Spring Coefficient of Foundation
[K]	: Stiffness Matrix of the Soil-Structure System
$[K_{12}]$	: Coupled Stiffness Matrix of Superstructure and Interface Region
$[K_{11}]$	: Stiffness Matrix of the Superstructure
$[K_{22}]$	: Stiffness Matrix the Soil-Structure Interface
$[K_{HS}]$	: Frequency-dependent Impedance Matrix
$[K_{ST}]$	: Effective Impedance Matrix of the Structure
m_b	: Mass of the Building
m_f	: Mass of the Foundation
[M]	: Mass Matrix of the Soil-Structure System

$[M_{11}]$	: Mass Matrix of the Superstructure
$[M_{22}]$	: Mass Matrix for the Soil-Structure Interface
M_n	: Modal Mass
M_n^*	: Effective Mass
n	: Ratio of S-Wave Velocity to P-Wave Velocity
p	: Amplitude of the Incident P-wave
$\{p_{eff}(t)\}$	: Vector of Effective Earthquake Loading
$\{P\}$	: Load Vector of the Interface Nodes with Dimension of *(3Nx1)*
$\{P_2\}$	: Vector of Forces Applied along the Interface Nodes
$\{P_{D0}\}$	: Vector of Driving Force Amplitudes Induced by Seismic Wave Motion
$\{P_s\}$	: Load Vector of the Center of Interface Element with Dimension of *(3Sx1)*
$\{P(\underline{x}_0)\}$	: Harmonic Force Vector Applied at $\underline{x}_0$
R	: Distance between the Source Point and the Receiver Point
$[R_D]$	: Dynamic Transformation Matrix
$[R_S]$	: Quasi-static Transformation Matrix
$[R_Z]$	: Rotation Matrix around *z* Axis
s	: Amplitude of the Incident S-Wave
$[T]$	: System Transformation Matrix
u	: Displacement Amplitude of Mass due to Elastic Deformation of SDOF System
u_0	: Complex Valued Displacement Amplitude of Incident Wave in *x* Direction
$u_b(t)$	: Horizontal Displacement of Foundation
u_{ff}	: Free Field Displacement in the Plane of Soil-structure System in *x* Direction
u_g	: Displacement Amplitude of the Ground Motion
$u_g(t)$	: Time Dependent Horizontal Ground Motion
$\{u_{max}\}$	: Maximum Displacement Vector
$u(t)$	: Deformation of the Structure
$u_t(t)$	: Total Horizontal Displacement of the Structural Mass
$\{u(\underline{x})\}$	: Displacement Vector of Point $\underline{x}$ on Surface of Half-Space due to Point Source
v_0	: Complex Valued Displacement Amplitude of Incident Wave in *y* Direction
v_{ff}	: Free Field Displacement in the Plane of Soil-structure System in *y* Direction
$\ddot{v}_g(t)$	: Earthquake Time History
v_p	: P-wave Velocity
v_s	: S-wave Velocity
w_0	: Complex Valued Displacement Amplitude of Incident Wave in *z* Direction

w_{ff}	: Free Field Displacement in the Plane of Soil-structure System in z Direction
x	: Coordinate in x Direction
$\underline{x}$	: Coordinate Vector of the Surface Point on the Elastic Half-space
$\underline{x}_0$	: Coordinate Vector of the Surface Point where the Harmonic Force is Applied
y	: Coordinate in y Direction
$\{y\}$	: Time Dependent Displacement Vector of the Soil-Structure System
$\{y_1\}$	: Time Dependent Displacement Vector of the Superstructure
$\{y_{1d}\}$	: Dynamic Part of the Displacement Vector
$\{y_{1s}\}$	: Static Part of the Displacement Vector
$\{y_2\}$	: Time Dependent Displacement Vector of the Interface Nodes
$\{y_{20}\}$	: Displacement Amplitude Vector of the Interface Nodes
z	: Coordinate in z Direction
$\bar{\varepsilon}$	: Volumetric Strain
ε_{xx}	: xx Component of the Normal Strain
ε_{xy}	: xy Component of the Shear Strain
ε_{xz}	: xz Component of the Shear Strain
ε_{yy}	: yy Component of the Normal Strain
ε_{yz}	: yz Component of the Shear Strain
ε_{zz}	: zz Component of the Normal Strain
ζ	: Hysteretic Damping Ratio of the Structure
ζ_{g}	: Hysteretic Damping Ratio of the Soil
ζ_N	: Modal Damping Ratio
ζ_{x}	: Hysteretic Damping Ratio of the Foundation
$\{\eta\}$	: Modal Response Amplitude Vector
$\{\dot{\eta}\}$	: First Derivative of Modal Response Amplitude Vector with respect to Time
$\{\ddot{\eta}\}$	: Second Derivative of Modal Response Amplitude Vector with respect to Time
θ_{cr}	: Critical Angle of the Incident Seismic Wave
θ_H	: Horizontal Angle of the Incident Seismic Wave
θ_V	: Vertical Angle of the Incident Seismic Wave
λ	: Lamé's First Constant
μ	: Lamé's Second Constant
ρ	: Mass Density of the Elastic Solid
$\{\sigma(\underline{x}_j)\}$	: Constant Traction at the Centroid of Subregion j
σ_{xx}	: xx Component of the Normal Stress
σ_{xy}	: xy Component of the Shear Stress
σ_{xz}	: xz Component of the Shear Stress
σ_{yy}	: yy Component of the Normal Stress

σ_{yz}	: *yz* Component of the Shear Stress
σ_{zz}	: *zz* Component of the Normal Stress
$[\Gamma]$	: Matrix of Modal Participation Factors
υ	: Poisson's Ratio
ϕ	: Displacement Phase Shift
Φ	: Potential Function Involving Pure Dilatation
Ψ	: Potential Function Involving Pure Rotation
ω	: Excitation Frequency of the Incident Wave
ω_b	: Fixed Based Natural Frequency of the Building
ω_f	: Natural Frequency of the Foundation without the Building
ω_h	: Natural Frequency of the Structure without Rocking Vibration
ω_N	: Nth Natural Frequency of the Superstructure
ω_r	: Natural Frequency of the Structure without Horizontal Vibration
ω_s	: Fixed Based Natural Frequency of the Structure
Ω	: Excitation Frequency of the Harmonic Motion
Ω_x	: Rotation about *x* Axis
Ω_y	: Rotation about *y* Axis

DYNAMIC SOIL STRUCTURE INTERACTION UNDER WAVE PROPAGATION VIA AN IMPROVED FINITE ELEMENT-BOUNDARY ELEMENT METHODOLOGY

SUMMARY

The effect of soil-structure interaction is recognized to play an important role in the seismic analysis of civil structures. The dynamic analysis of the structures in general engineering practice is based on the idealization that the structure rests on very stiff soil and the seismic motions applied at the support points are the same as the free field motions at those locations. However, the structure always interacts with the surrounding soil which leads to a change in the seismic motions at the base.

The nature and the amount of interaction mainly depend on the stiffness of the soil and the structure as well as the structure's mass properties. If the structure is founded on rock, the motion of the base is identical to the free field motion of the same point. In this case, the seismic analysis can be carried out with the assumption that the structure is excited by the specified motion. If the structure is founded on soft soil, the dynamic response of the structure will be different from the fixed-based condition. The presence of the structure will also alter the free field motion strongly at the site. Therefore, the interaction problem has to be taken into account in the seismic analysis of the structures, more so, in the case of soft soil conditions and stiff, massive structures.

Within the scope of this study, a three dimensional coupled Finite Element-Boundary Element (FE-BE) methodology is developed to analyze the dynamic soil-structure interaction under the effects of the traveling seismic waves. The dynamic response of the soil-structure systems subjected to traveling seismic waves is obtained in the frequency domain. In the seismic analysis of the system, the substructure method is employed to deal with the interaction problem. This method is based on substructuring the system as the structure and the unbound soil.

Finally, through the use of the displacement response curves of a multistory building which is obtained by the dynamic analysis employing the developed numerical procedure, a drift-based damage identification technique is proposed.

DİNAMİK YAPI ZEMİN ETKİLEŞİMİNİN DALGA YAYILIMI ETKİSİ ALTINDA SONLU ELEMAN-SINIR ELEMAN YÖNTEMİ İLE MODELLENMESİ

ÖZET

Yapıların deprem yükü altındaki dinamik çözümlemelerinde yapı-zemin etkileşiminin önemli bir etkisi olduğu bilinmektedir. Genellikle, yapıların dinamik analizinde yapının sert zemin üzerine oturduğu; dolayısı ile yapının zemin ile rijit olarak bağlandığı kabul edilmektedir. Bu durumda, yapının temele ait düğüm noktalarına gelen deprem hareketinin yer hareketi ile aynı olduğu varsayılır. Ancak, yapının zemin ile etkileşimi temele etkiyen yer hareketinin değişmesine neden olur.

Yapı-zemin etkileşimin etkisi zeminin ve üstyapının rijitliği ile üstyapının kütlesi ve geometrik özellikleriyle doğrudan ilişkilidir. Yapının sert kayalık zemin üzerinde inşa edildiği durumlar için temel hareketinin yer hareketi ile eşdeğer olduğu kabul edilebilir. Bu durumda, yapının dinamik analizi temelden etkiyen yer hareketi altında çözümlenebilir. Ancak, yapının yumuşak zemin üzerinde inşa edildiği durumlarda yapının dinamik analiz için bu yaklaşım doğru değildir. Yapı, zeminden etkiyen yer hareketinde de değişim yaratabilmektedir. Bu sebeple, özellikle zayıf zemin üzerinde inşa edilmiş ağır ve rijit yapıların dinamik analizinde yapı-zemin etkileşiminin göz önünde bulundurulması gerekmektedir.

Bu çalışmanın kapsamında, yapı-zemin etkileşimini deprem dalgaları etkisi altında incelemek için Sonlu Eleman ve Sınır Eleman Yöntemleri kullanılarak üç boyutlu sayısal bir metodoloji geliştirilmiştir. Geliştirilen metodoloji ile yapı-zemin sistemlerinin dinamik cevabı, frekans tanım alanında elde edilmiştir. Sistemin dinamik analizi için altsistem yöntemi kullanılmıştır. Bu yöntemde, iki ayrık sistem olarak modellenen yapı ve zemin ortamı, süreklilik denklemleri ve dinamik denge denklemleri kullanılarak yapı-zemin arakesitinde eşleştirilmiştir.

Geliştirilen bu teknik ile çok katlı bir yapının dinamik analizi gerçekleştirilmiş, yapının her katındaki yatay yerdeğiştirmeler elde edilerek yapıda göreli kat ötelemesi oranına bağlı hasar seviyesi belirlenmiştir. Bu şekilde, çok katlı binalarda göreli kat ötelemesine bağlı bir hasar belirleme yöntemi önerilmiştir.

1. AN OVERVIEW OF THE THESIS

Soil-structure interaction (SSI) has an important effect on the seismic response of structures especially for massive structures, which are founded on soft soil. For structures resting on stiff soil, motion of the foundation is approximately identical to the free field motion, which is the motion at the surface level of soil without the structure built on it. In this case, interaction effect of soil on the structure can be neglected. Moreover, the change in the free-field motion caused by the structure existing on it is negligible.

Considering the soft soil conditions and structures resting on large foundation areas such as bridges, not only the response of the structure is altered due to the interaction effects but also the dynamic characteristics. The most important change occurs in the fixed based fundamental frequency of the structure. In general, the interaction effect reduces the natural frequency of the structure; increases the contribution of rocking motion to the structural response and reduces the maximum base shear of the structure [1-4].

The reduction of the fundamental frequency has been stated by various studies based on vibration recordings during earthquake excitation and ambient vibration tests. The study conducted by Trifunac et al. [5,6] covers a detailed analysis on the time dependent changes of the apparent frequency of a seven-story reinforced concrete building in Van-Nuys, California based on the recorded data of 12 earthquakes. The results indicate that the system frequency changes from one earthquake to another due to “the softening” of the system and the nonlinearity of the soil.

Using the vibration recordings of 11 earthquakes belonging to the seven-story building in Van-Nuys, the authors [7] have also used wave propagation method in order to detect the structural damage. The plots of the impulse response functions computed by deconvolution of the recorded earthquake response are used for measuring the wave travel times of the vertical propagating seismic waves. The changes in the wave travel times are used to detect the changes in the structural stiffness between the two subsequent earthquakes.

In a previous study conducted by Şafak E. [8], a layered continuous model for the analysis of the seismic response of a building is proposed and the damage is detected by monitoring the changes in the parameters of each layer. The author has developed a discrete-time wave-propagation method to calculate the seismic response of the multistory buildings resting on a layered soil media and subjected to vertically propagating shear waves. Buildings are modeled considering each story as separate layers resting on the layered soil media. The response has been defined in terms of the wave travel times between the layers as well as the wave reflection and the transmission coefficients at layer interfaces. This method has been suggested as a practical tool for the damage detection from seismic records due to its ability to incorporate the soil layers under the foundation.

Clinton et al. [9] have shown that the modal parameters of a structure are affected by the earthquake history, weather conditions such as the rain, wind and the extremities in the temperature. The study has drawn attention on the mechanisms reducing the natural frequencies of the observed structure. The emphasis was made on the interaction of the structure with the surrounding soil, which causes the reduction, as well as the nonlinear softening of the superstructure itself.

Şafak E. [10] has investigated the detection and the identification of the soil-structure interaction in buildings using the vibration recordings. The author has suggested a very useful tool to identify and discriminate the effects of the SSI on the natural frequency of the fixed-based buildings. The identification process depends on the earthquake response data recorded from the top and the foundation levels. The ratio of the Fourier Amplitude Spectrum (FAS) of top-story accelerations to the foundation data has been verified theoretically and experimentally to have peaks at the fixed-based frequency of the building. Observing the deviation of the peak response values of the individual top-story and the foundation acceleration records, the proposed method enables the identification of the SSI effect without any borehole or free-field recordings from the site.

Unlike the listed studies, Çelebi and Şafak [11,12] have analyzed the acceleration response records of the buildings and concentrated on the identification of site frequencies as well as the structural frequencies using the data obtained from the roof and the ground floor. The site frequency is simply identified using the cross-spectra of the orthogonal acceleration records at any desirable level. The peaks that appear at

the cross-spectra curves corresponding to the roof or the base motions clearly indicate the site frequencies. The structural frequencies are determined using the ratio of the transfer functions. The simple spectral technique has been applied to 5 instrumented buildings in order to verify the proposed procedure.

As apparent from the above mentioned references, the emphasis in the literature is on the variation of the fundamental frequency of the structure under seismic motions. One of the reasons is that, in the earthquake resistant design of the structures based on the Response Spectrum Method [13], the base shear and the design seismic loads acting on each story level are estimated in terms of the fundamental frequency of the building. Equally important is damage identification in structures. Damage results in change in the modal parameters (frequency, mode shapes and damping ratios) of the structures. By monitoring the changes in the modal parameters, it is possible to monitor the progress of the damage in the structure. Since SSI also affects the frequencies, it is important to discriminate the effects of the SSI from the effects of the damage on the modal parameters. Thus, the effects of the SSI on the natural frequencies of the structures will be analyzed and discussed within the scope of this study.

In addition to the changes in the fundamental frequency of the structures, the response amplitude at the shifted frequency is also changed due to the soil type underlying the structure. The seismic waves that are generated due to the occurrence of an earthquake, propagate through the soil media having different mechanical properties and different layer thicknesses. Reaching the base of a structure, the seismic waves cause different types of base excitation depending on the underlying soil type. Thus, the effects of the underlying soil conditions on the response amplitude of the soil-structure system has to be investigated in details. The results of the analysis will be discussed in terms of the interstory drift ratios. Finally, the drift values will be employed to evaluate the damage state of the structure that is defined by the earthquake codes.

1.1 Purpose of the Dissertation

Within the scope of this study, a numerical procedure has been developed in order to analyze and determine the dynamic response of the structures with surface foundations under the effect of the seismic wave motion propagating in the elastic

half-space soil medium. Finite Elements Method (FEM) has been used for three-dimensional modeling of the structure that has a surface foundation. The effect of the seismic waves at the base of the structure is considered in terms of the excitation force applied at the soil-structure interface, which has been discretized by rectangular areas. The excitation force induced by the seismic wave motion has been determined by multiplying the free-field displacement vector of each interface node and the corresponding frequency-dependent impedance matrix of the elastic half-space representing the underlying soil medium. The impedance matrix is evaluated using the Green's functions that are defined for unit harmonic force acting on a specific point of the semi-infinite half-space surface [14, 15].

Implementing the described numerical model, the main objectives of this study are;

- to develop the three dimensional (3D) numerical model of the soil-structure system,
- to obtain the dynamic response of the structures for increasing the excitation frequency of the seismic waves,
- to obtain the effects of the SSI on the modal parameters of structures,
- to analyze the effect of the traveling seismic waves on the response of the structures,
- to analyze the effect of the soil conditions on the response of the soil-structure system,
- to introduce a code based damage identification methodology for the structures under the effects of the seismic waves. This methodology is based on identifying the peak displacement response of the soil-structure system; to determine the maximum interstory drift ratio of the structure; and to evaluate the code based damage state defined in HAZUS99 Technical Manual [16] or the structural performance level of the structure.

The outline of the general framework summarizing the objectives of the study and the methods that are used for achieving these objectives is given in Figure 1.1. The objectives are listed by order of phases that are performed to accomplish the final and main purpose of the thesis.

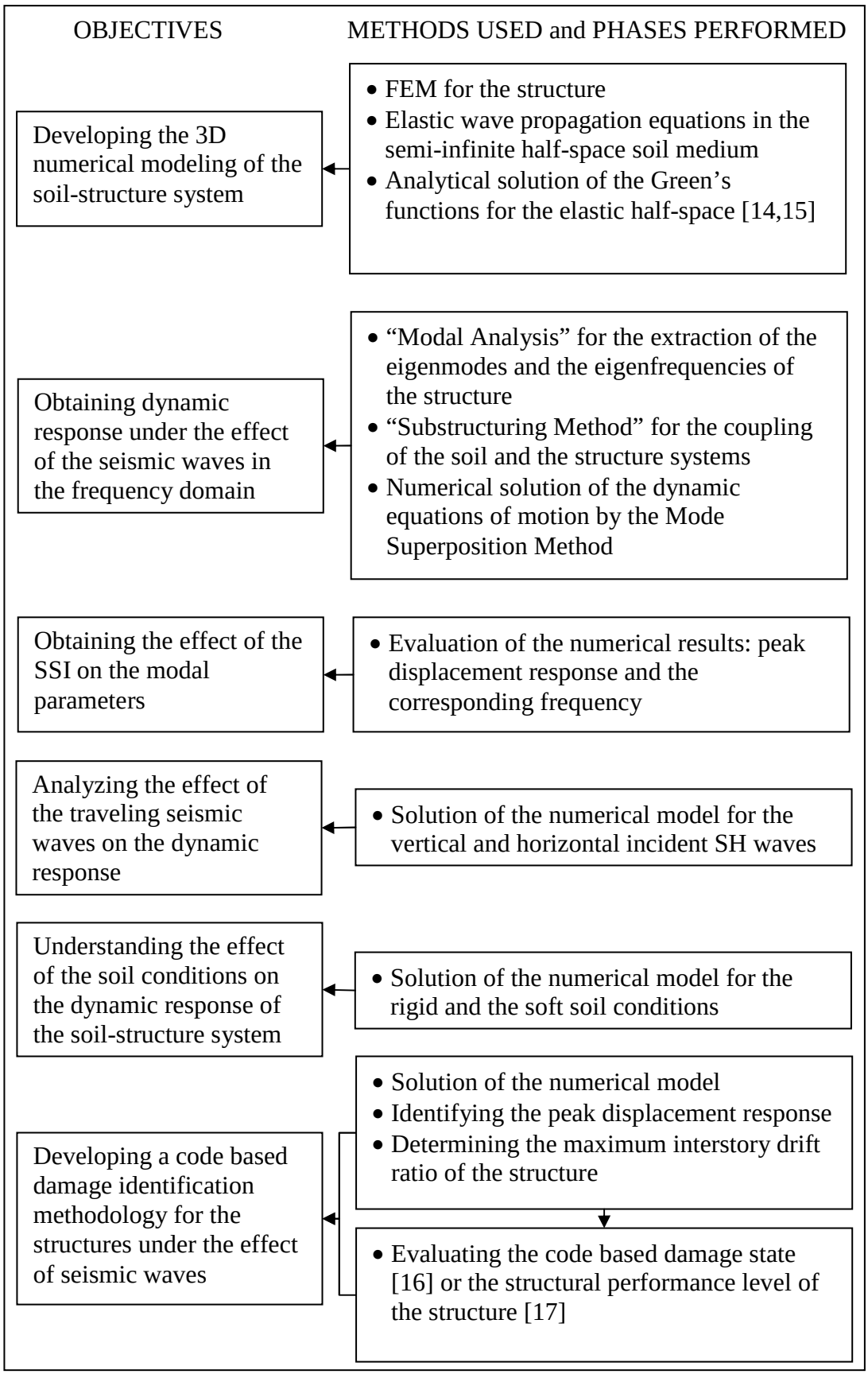

Figure 1.1 : General framework of the study.

1.2 The Summary of the Methodology

Within the scope of this thesis, a numerical study is conducted to analyze the effect of the soil-structure interaction on the dynamic response of the structures. The dynamic response is obtained by modeling the soil medium and the structure under the effect of the seismic waves.

The dynamic analysis of the soil-structure system is accomplished by the "Substructure Method". Implementing this method, the total system is divided as the structure and the unbounded soil. Then, the structure and the soil are modelled using the Finite Elements and the Boundary Element Methods, respectively. The numerical procedure is based on the analysis of the structure under the excitation force, which is induced by the free-field motion. The excitation force representing the effect of the seismic waves acts at the soil-structure interface, which is usually the contact surface of the foundation with the soil. Coupling the two substructures at the soil-structure interface is provided using the displacement compatibility and the dynamic equilibrium equations at the soil-structure interface elements.

The physical representation of the soil model mainly depends on the seismic wave motion and the dynamic-stiffness coefficients of the soil. The vector of the seismic wave motion at the soil-structure interface nodes is multiplied with the frequency-dependent impedance matrix of the soil in order to obtain the excitation force acting at the interface nodes of the soil-structure system.

The seismic input motion acting on the surface of the foundation is calculated using elastic seismic wave equations. These equations define the motion of the seismic waves, propagating through the soil, which is represented by an elastic half-space.

The dynamic stiffness of the soil is expressed in terms of the frequency-dependent impedance matrix. This matrix is calculated using the Greens' Functions [14,15] that are defined for the unit harmonic force acting on a specific point of the half-space surface.

Finally, the dynamic response of the structure is obtained by the numerical solution of the set of dynamic equilibrium equations under the base excitation induced by the seismic waves. The methodology that is developed for the numerical implementation of the numerical procedure is summarized in Fig. 1.2.

NUMERICAL OR ANALYTICAL METHODS EMPLOYED

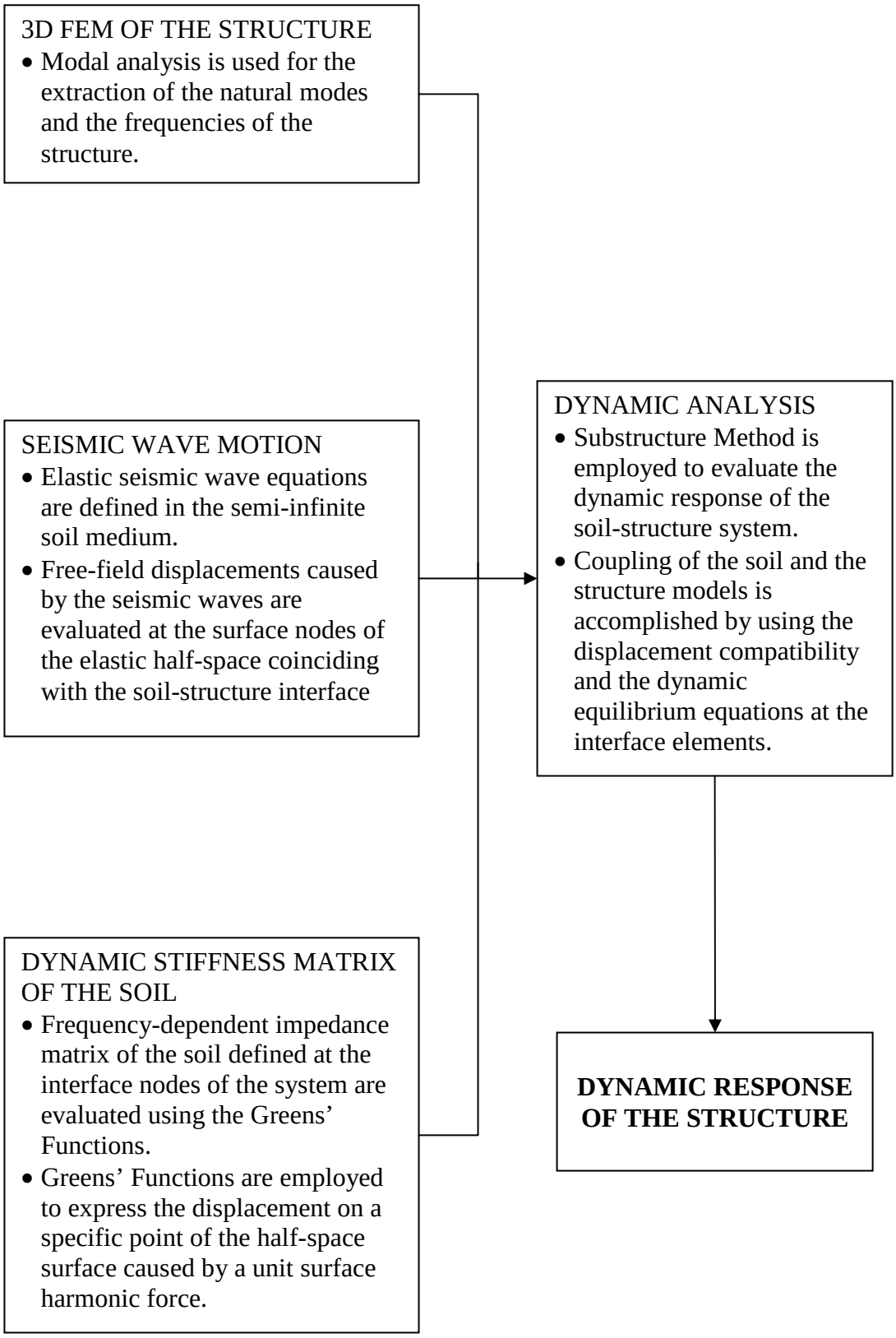

Figure 1.2 : The methodology developed in this study.

2. INTRODUCTION

This study concentrates on determining the effect of the SSI on the dynamic response of the structures. To achieve this, a numerical procedure is developed for modeling the soil-structure system under the effects of the seismic waves.

In the process of modeling the soil-structure system, the soil medium is represented as an elastic half space; the seismic excitation is regarded in the form of a free-field motion induced by the elastic seismic waves and the structure is considered to be resting on a surface foundation system. The dynamic analysis of the soil-structure system has been carried out by using the substructure method in the frequency domain. Implementing this method, the structure and the soil have been modeled using Finite Elements and Boundary Elements, respectively. The two separate systems are coupled at the soil-structure interaction surface, which is the contact area between the foundation and the soil.

The Boundary Element Method is a very convenient approach for dynamic soil structure interaction problems. Implementing this technique, the radiation condition of the semi-infinite elastic half-space is automatically encountered. Due to the use of the fundamental solutions in the half space, only a surface discretization is required leading to a reduction in the dimension of the problem by one [18]. Since the solution is obtained on the boundary surface of the volume, only a mesh on the boundary is sufficient. However, implementation of FEM necessitates the generation of the mesh through the entire domain. In addition, Finite Elements Method necessitates the implementation of the non-reflective boundaries at the edge elements in order to prevent trapping of the wave energy within the system. In the solution process of the Finite Element model, the element integrals are easy to evaluate. On the contrary, the BEM integrals are harder to evaluate which contain integrands that become singular at specific points [19]. Therefore, each technique has both advantageous and disadvantageous features in terms of the computational efficiency. The chose of the method depends on the type of the problem that is encountered.

The interaction surface is discretized by four-noded rectangular elements. Considering the interface nodes each having three translational degrees of freedom, the surface foundation is regarded as a flexible base. Thus, the free-field displacement and the excitation force induced by the seismic waves are transmitted through the nodes that compose the interaction surface.

The dynamic stiffness of the soil-foundation system is represented by the frequency-dependent impedance matrix. Generation of this matrix is performed by;

- The evaluation of the Green's Functions matrix at each node of the interface;
- Transforming Green's Functions matrix from polar to Cartesian coordinate system;
- Evaluation of the compliance matrix using the transposed Green's Functions matrix for the total interaction surface;
- Inversion of the compliance matrix.

Combining the sub-steps of the numerical procedure, the three-dimensional dynamic analysis of the soil-structure system can be carried out by running the developed program. The final numerical procedure is capable of obtaining the displacement and acceleration response of any nodal point of the structure and the foundation which is excited by the seismic waves through the soil. Implementing the procedure on a multistory building, the maximum interstory drift ratio of each story level is computed using the peak displacement amplitude. Therefore, the maximum interstory drift ratio values can be employed to identify "the damage state" or the "structural performance level" defined by HAZUS99 [16] and FEMA 356 [17], respectively.

2.1 The Theoretical Background

Various numerical methods have been developed for the analysis of the interaction problem, which can be classified in two main groups as the direct method and the substructure method.

For the numerical analysis of the semi-infinite soil medium, an interaction surface enclosing the structure is determined. The characteristics of the nodes lying on the surface represent the overall features of the unbounded soil domain existing on the

exterior region of the surface [20]. The location of the interaction surface can be selected arbitrarily. In the substructure method, the surface is regarded to coincide with the soil-structure interface, whereas it coincides with an artificial boundary within which the soil is modeled in the direct method.

In addition to these two techniques, simple physical models are the alternative approaches for the analysis of the dynamic soil-structure interaction problem. Implementing these models, a small number of degrees of freedom and a few springs, dashpots and masses with frequency-independent coefficients are used in order to represent the dynamic stiffness, damping and mass properties of the underlying soil. The three types of simple physical models in the literature are the truncated cones, the spring-dashpot-mass models and the methods with a prescribed wave pattern in the horizontal plane [21].

2.1.1 Solutions in the time domain versus the frequency domain

The dynamic interaction problem can be analyzed in the frequency domain or in the time domain. The solution in the frequency domain has many advantages. Since the Green's functions of a semi-infinite half-space are usually computed in the frequency domain and are less singular than in the time domain, this approach is much more favorable.

Furthermore, the frequency domain approach permits splitting the problem into separate parts as the soil and the structure through the use of the frequency-dependent impedance coefficients.

Considering the linear soil-structure interaction problems, material damping can be easily defined in terms of the harmonic motions. Thus, using the complex response method, the soil-structure interaction analysis is easier to handle in the frequency domain than the time domain [22].

However, the computational efficiency of the numerical solution in the time domain is higher than the frequency domain in the nonlinear dynamic soil-structure problems, which is beyond the scope of this study.

2.1.2 Direct method

In the direct method, response of the structure and the soil within the artificial boundary, which is termed as the near-field, are modeled using a finite number of elements. Appropriate boundary conditions should be determined in order to represent the missing soil existing on the exterior region of the interaction surface [23]. As the soil is modeled up to infinity, the reflections of the outwardly propagating waves should be absorbed through the interpretation of a transmitting boundary on behalf of the artificial boundary. The effects of the surrounding soil, which is termed as far-field is analyzed approximately by imposing these transmitting boundaries along the interface of the near field and the far field. The model proposed by Lymser and Kuhlmeyer [24] implements the simplest type of transmitting boundaries as viscous boundaries, which are represented by simple dashpots. Engquist and Majda [25], Liao and Wong [26] have proposed local, non-consistent boundaries whereas Weber [27] implemented the type of boundaries which were based on transfer functions.

In the direct method, the solution of the equations of motion for the soil-structure system may be conducted in the frequency or in the time domain. Since this method does not use the superposition of the displacement, it has the advantage of including the nonlinear effects through the use of the equivalent linear method. However, it has the disadvantage of high computational expense and coarser models can be obtained for structures using the direct method.

2.1.3 Substructure method

Implementation of the substructure method is based on splitting the complete model into two parts as the soil and the structure using the principles of compatibility and displacements at the foundation level. For the soil-structure interaction, the dynamic response of the soil-structure system is obtained by introducing the free field motion at the foundation level.

In the substructure method, the structure is normally modeled using the finite elements. The properties of the unbounded soil on the exterior of the interaction surface are represented by a boundary condition at the interface nodes reflecting the effects of the soil mesh extending to infinity.

If the dynamic analysis is performed in the frequency domain, the excitation is decomposed into a Fourier series and the response is determined independently for each Fourier term corresponding to a specified frequency. The boundary condition in the frequency domain is determined using the frequency dependent dynamic stiffness coefficients. These coefficients relate the displacement amplitudes with the force amplitudes, which should be fully coupled at the interface nodes for the frequency domain.

For the dynamic analysis in the time domain, the convolution integrals of the dynamic stiffness coefficients and the related displacements are evaluated in the time domain in order to determine the forces. The coupling of the time dimension should be provided in addition to the displacement and the force amplitudes. The dynamic stiffness coefficients can be determined using the boundary integral-equation procedure for the analysis in the time domain.

The linear analysis of the interaction problem has been carried out previously by the computer codes developed in the frequency domain, which are based on the substructure method [28, 29]. These studies enable efficient procedures for the linear interaction problem using the Fast Fourier Transform. However, the analysis in the time domain has a higher computational effort due to the recursive evolution of the convolution integrals.

The substructure method has the advantage that if the free field motion is changed, the dynamic stiffness coefficients do not have to be recalculated. In addition, the use of this method in design is more favorable than the direct method. Because, the implementation of this technique is simpler and less expensive than the direct method especially for the structures with surface foundations resting on a uniform half-space [30]. However, considering the structures with embedded foundations resting on a layered soil medium, implementation of the substructure method may be as difficult as the direct method. Therefore, choice of the method mainly depends on the type of the structure, the underlying foundation and the soil conditions.

2.1.4 Lumped parameter models

The lumped parameter model representing the linear unbounded soil in the SSI analysis mainly consists of several springs, dampers and masses with frequency-independent real coefficients. These models are chosen by arranging a variety of

connected springs, dashpots and masses with unknown parameters, whose values are determined by minimizing the total square errors between the dynamic stiffness flexibility function of the lumped-parameter model and the corresponding rigorous solution for the soil [30].

Some of the previous work employed constant values for the foundation stiffness and damping in order to represent the unbounded soil medium [31–34]. The truncated semi-infinite cone model was developed for general practices in foundation vibration in the light of the numerous studies [35–40]. Furthermore, certain discrete physical models were established leading to the lumped-parameter models which yielded consistent results with the truncated cone model [41, 42].

The transfer function of a lumped parameter in the frequency domain which is composed of a selected arrangement of springs, dampers and masses at the foundation nodes, is the dynamic stiffness or the flexibility coefficient and it can be represented by a non-linear function of these functions. These coefficients are determined by using a curve-fitting technique in order to find an optimum fit between the transfer function of the lumped parameter model and the exact solution attained by the boundary-element procedure.

Employing the lumped parameter model for the dynamic SSI analysis, the dynamic behavior of the total soil-structure system may be represented by the stiffness, damping and the mass matrices, which are assembled by the finite element model of the superstructure and the lumped parameter model for the unbounded soil. In order to remain within the framework of the substructure method which leads to a convenient representation of the dynamic SSI problem, the properties of the lumped parameter model of the soil should be independent of the properties of the structure or the total system [43].

The lumped parameter model has the advantage of easy incorporation with the conventional dynamic analysis and direct applicability to the non-linear structural analysis in the time domain leading to further developments on the improved lumped-parameter models [44–49]. Even though the lumped parameter models represent the linear behavior of the unbounded soil, the nonlinear behavior of the structure can also be taken into consideration [30].

3. SEISMIC WAVE PROPOGATION IN THE SOIL MEDIUM

3.1 Seismic Waves

The seismic waves produced by an earthquake motion are the body waves and the surface waves. The body waves which can propagate through the interior part of the earth can be categorized as P-waves (primary or longitudinal waves) and the S-waves (secondary, shear or transverse waves having two components as SV and SH). The surface waves are mainly produced by the interaction of the body waves with the surface layers of the earth (Fig. 3.1). Hence, they propagate along the surface of the earth and the amplitude of the waves decrease exponentially with the depth. Rayleigh and Love waves are the important types of surface waves, which are produced by the body waves generated by the source of the earthquake motion from the interior part of the earth. Rayleigh waves have vertical and horizontal components of particle motion resulting in an elliptical movement against the propagation direction. This deformation type is due to the interaction of the P-waves and the S-waves with the surface layers. Thus, these waves can be considered as the combinations of the P-waves and the S-waves. On the contrary, Love waves that are caused by the interaction of SH-waves with a soft surface layer have only the horizontal component of the particle motion [50].

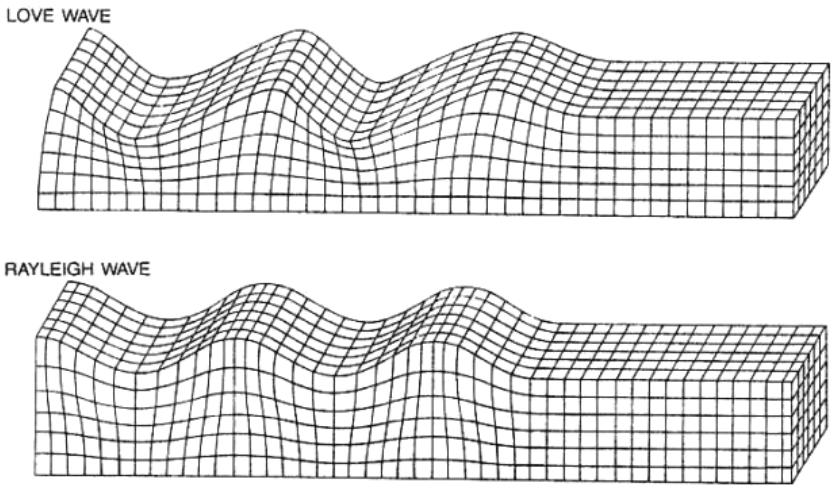

Figure 3.1 : Deformations produced by Love waves and Rayleigh waves [51].

The body wave equations are derived from the dynamic equilibrium equations of a cubical element, which represents a very small part of a homogeneous, elastic, isotropic and unbounded medium. These equilibrium equations lead to two basic wave equations referring to two extreme types of deformation; the P-wave equation that involve pure dilatational deformation without any shearing or rotation and the S-wave equation corresponding to the pure distortional deformation. Fig. 3.2 shows the direction of the propagation and the type of the deformation as they travel through the elastic material for each type of the body wave.

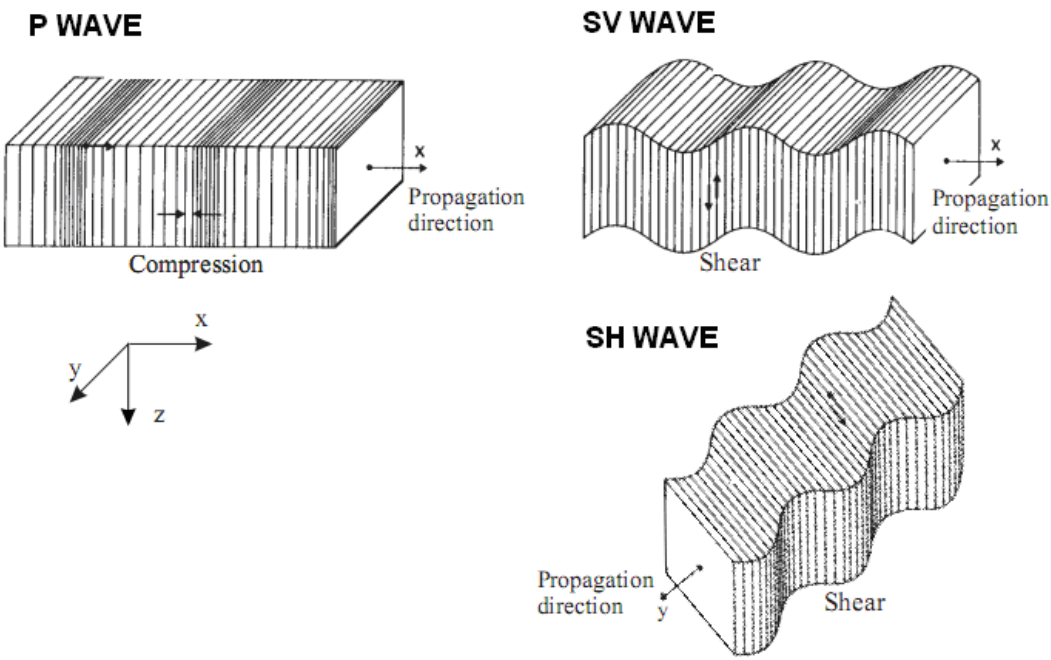

Figure 3.2 : Deformations produced by the body waves: P, SV and SH-waves [52].

The reflections of the incident P, SV and SH waves at the free surface of an elastic solid have different vertical angles according to the wave type as shown in Fig. 3.3. An incident P-wave reaching the ground surface with the vertical angle, *e* is reflected as a P-wave with the same angle and a SV-wave with the angle *f* which is greater than the vertical incidence angle. In the case of an incident SV-wave reaching the ground surface with the vertical angle *f*, the reflection is in the form of a SV-wave with an angle *f*, which is coupled with a P-wave with the angle, *e*. Since the reflection angle of P-wave *e* is smaller than *f*, the reflected P-wave occurs only in the case that $f > \theta_{cr}$ where θ_{cr} is the critical angle determined as:

$$\theta_{cr} = \cos^{-1}\left(\frac{v_s}{v_p}\right) \tag{3.1}$$

where v_s, v_p : the shear and the primary wave velocities, respectively.

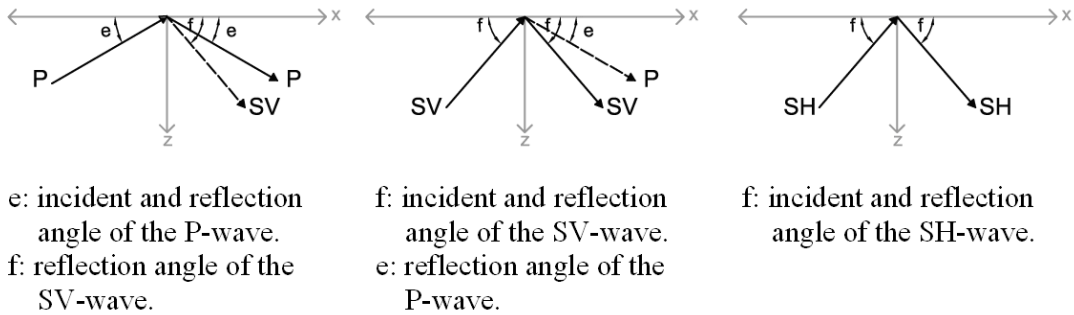

Figure 3.3 : Reflections of P, SV and SH waves at the ground surface [14].

3.2 Equations of Motion for an Elastic Solid

The derivation of the wave equations involves the solution of the dynamic equilibrium equations of the elastic solid material under the stress variation in *x*. Considering an infinitesimal elastic solid cube as shown in Fig. 3.4, the dynamic equilibrium equation for the stress variation in *x* direction is expressed as:

$$\begin{aligned}\rho.dx.dy.dz.\frac{\partial^2 u}{\partial t^2} &= \left(\sigma_{xx} + \frac{\partial \sigma_{xx}}{\partial x}dx\right)dydz - \sigma_{xx}dydz \\ &+ \left(\sigma_{xy} + \frac{\partial \sigma_{xy}}{\partial y}dy\right)dxdz - \sigma_{xy}dxdz \\ &+ \left(\sigma_{xz} + \frac{\partial \sigma_{xz}}{\partial z}dz\right)dxdy - \sigma_{xz}dxdy\end{aligned} \tag{3.2}$$

where ρ: the mass density of the elastic solid and u: the displacement in the x direction. The equation can be rewritten as:

$$\rho.\frac{\partial^2 u}{\partial t^2} = \frac{\partial \sigma_{xx}}{\partial x} + \frac{\partial \sigma_{xy}}{\partial y} + \frac{\partial \sigma_{xz}}{\partial z} \tag{3.3}$$

Similarly, the equation of motion can also be written in *y* and *z* directions as:

$$\rho.\frac{\partial^2 u}{\partial t^2} = \frac{\partial \sigma_{yx}}{\partial x} + \frac{\partial \sigma_{yy}}{\partial y} + \frac{\partial \sigma_{yz}}{\partial z} \tag{3.4}$$

$$\rho.\frac{\partial^2 u}{\partial t^2}=\frac{\partial \sigma_{zx}}{\partial x}+\frac{\partial \sigma_{zy}}{\partial y}+\frac{\partial \sigma_{zz}}{\partial z} \qquad \textbf{(3.5)}$$

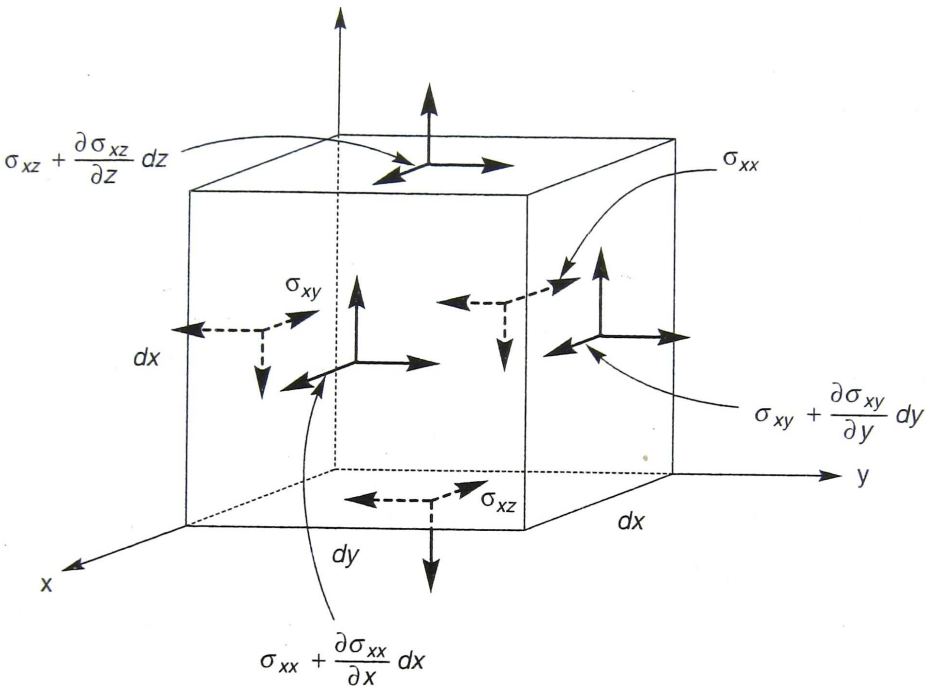

Figure 3.4 : Reflections of P, SV and SH waves at the ground surface [50].

Using the Hooke's Law for the isotropic, linear and elastic materials, the stress and strain components are defined as:

$$\begin{aligned} \sigma_{xx} &= \lambda\bar{\varepsilon}+2\mu\varepsilon_{xx}\ , & \sigma_{xy} &= \mu\varepsilon_{xy} \\ \sigma_{yy} &= \lambda\bar{\varepsilon}+2\mu\varepsilon_{yy}\ , & \sigma_{yz} &= \mu\varepsilon_{yz} \\ \sigma_{zz} &= \lambda\bar{\varepsilon}+2\mu\varepsilon_{zz}\ , & \sigma_{zx} &= \mu\varepsilon_{zx} \end{aligned} \qquad \textbf{(3.6)}$$

where $\bar{\varepsilon}=\varepsilon_{xx}+\varepsilon_{yy}+\varepsilon_{zz}$ is the volumetric strain and λ, μ: the Lame's constants. Implementing the stress-strain relationships into the equations of motion in *x*, *y* and *z* directions Eq. (3.6) into Eqs. (3.3), (3.4) and (3.5) yields;

$$\rho.\frac{\partial^2 u}{\partial t^2}=\frac{\partial}{\partial x}\left(\lambda\bar{\varepsilon}+2\mu\varepsilon_{xx}\right)+\frac{\partial}{\partial y}\left(\mu\varepsilon_{xy}\right)+\frac{\partial}{\partial z}\left(\mu\varepsilon_{xz}\right) \qquad \textbf{(3.7)}$$

$$\rho.\frac{\partial^2 u}{\partial t^2}=\frac{\partial}{\partial x}\left(\lambda\bar{\varepsilon}+2\mu\varepsilon_{xx}\right)+\frac{\partial}{\partial y}\left(\mu\varepsilon_{xy}\right)+\frac{\partial}{\partial z}\left(\mu\varepsilon_{xz}\right) \qquad \textbf{(3.8)}$$

$$\rho.\frac{\partial^2 u}{\partial t^2} = \frac{\partial}{\partial x}\left(\lambda\bar{\varepsilon} + 2\mu\varepsilon_{xx}\right) + \frac{\partial}{\partial y}\left(\mu\varepsilon_{xy}\right) + \frac{\partial}{\partial z}\left(\mu\varepsilon_{xz}\right) \tag{3.9}$$

Using the Laplacian operator which is defined as $\nabla^2 = \frac{\partial^2}{\partial x^2} + \frac{\partial^2}{\partial y^2} + \frac{\partial^2}{\partial z^2}$, the three equations given above are expressed as:

$$\rho.\frac{\partial^2 u}{\partial t^2} = (\lambda + \mu)\frac{\partial \bar{\varepsilon}}{\partial x} + \mu\nabla^2 u \tag{3.10}$$

$$\rho.\frac{\partial^2 u}{\partial t^2} = (\lambda + \mu)\frac{\partial \bar{\varepsilon}}{\partial y} + \mu\nabla^2 v \tag{3.11}$$

$$\rho.\frac{\partial^2 u}{\partial t^2} = (\lambda + \mu)\frac{\partial \bar{\varepsilon}}{\partial z} + \mu\nabla^2 w \tag{3.12}$$

Differentiating the Eqs. (3.10), (3.11) and (3.12) with respect to *x*, *y* and *z*, respectively; and adding the equations, the first type of wave equation is derived as below;

$$\frac{\partial^2 \bar{\varepsilon}}{\partial t^2} = \left(\frac{\lambda + 2\mu}{\rho}\right).\nabla^2 \bar{\varepsilon} \tag{3.13}$$

The resulting equation describes the dilatational wave, which is named as the P-wave equation since the volumetric strain $\bar{\varepsilon}$ involves the pure dilatational deformations without any shearing or rotation. Referring to the P-wave equation, the velocity of the p-wave is defined as:

$$v_p = \sqrt{\frac{\lambda + 2\mu}{\rho}} \tag{3.14}$$

The P-wave velocity can also be expressed in terms of the Poisson's ratio υ and the shear modulus *G*, using the relationships between the elastic material properties and the Lame's constants;

$$v_P = \sqrt{\frac{2G(1-\upsilon)}{\rho(1-2\upsilon)}} \tag{3.15}$$

where the shear modulus $G = \mu$ and the Poisson's ratio υ is defined as:

$$\upsilon = \frac{\lambda}{2(\lambda + \mu)} \tag{3.16}$$

Similarly, the shear wave equation (S-wave) is derived by differentiating Eq. (3.11) with respect to *z* and Eq. (3.12) with respect to *y*. Subtracting the resulting equations yields;

$$\rho \frac{\partial^2}{\partial t^2}\left(\frac{\partial w}{\partial y} - \frac{\partial v}{\partial z}\right) = \mu.\nabla^2\left(\frac{\partial w}{\partial y} - \frac{\partial v}{\partial z}\right) \tag{3.17}$$

Since the rotation about the *x* axis is defined as $\Omega_x = \frac{\partial w}{\partial y} - \frac{\partial v}{\partial z}$, Eq. (3.17) is rewritten as:

$$\frac{\partial^2 \Omega_x}{\partial t^2} = \frac{\mu}{\rho}\nabla^2 \Omega_x \tag{3.18}$$

The resulting equation defines the distortional wave or the S-wave of the rotation about the *x* axis. Finally, using Eq. (3.18), the shear wave velocity (S-wave) is derived as:

$$v_S = \sqrt{\frac{G}{\rho}} \tag{3.19}$$

3.3 Solution of the Wave Equations in the Elastic Medium

In this section, the solution of the wave equations is encountered for three types of plane waves generated in an elastic, homogeneous and isotropic half-space. Initially, the propagation of the P and the SV waves is investigated and the wave motion equations are obtained at the ground surface. Secondly, the propagation of the SH wave is determined in terms of the surface displacement equations.

The displacements in the *x* and the *z* directions induced by the seismic waves can be expressed in terms of the two potential functions Φ and Ψ as:

$$u = \frac{\partial \Phi}{\partial \mathrm{x}} + \frac{\partial \Psi}{\partial z} \tag{3.20}$$

$$w = \frac{\partial \Phi}{\partial z} - \frac{\partial \Psi}{\partial \mathrm{x}} \tag{3.21}$$

Using the stress-strain relationships in three dimensional space, the volumetric strain, $\bar{\varepsilon}$ and the rotation about *y* axis, Ω_y can also be expressed as:

$$\bar{\varepsilon} = \frac{\partial u}{\partial \mathrm{x}} + \frac{\partial w}{\partial \mathrm{z}} = \frac{\partial}{\partial \mathrm{x}}\left(\frac{\partial \Phi}{\partial \mathrm{x}} + \frac{\partial \Psi}{\partial z}\right) + \frac{\partial}{\partial \mathrm{z}}\left(\frac{\partial \Phi}{\partial \mathrm{x}} - \frac{\partial \Psi}{\partial z}\right) = \nabla^2 \Phi \tag{3.22}$$

$$2\Omega_y = \frac{\partial u}{\partial \mathrm{z}} - \frac{\partial w}{\partial \mathrm{x}} = \frac{\partial}{\partial \mathrm{z}}\left(\frac{\partial \Phi}{\partial \mathrm{x}} + \frac{\partial \Psi}{\partial z}\right) - \frac{\partial}{\partial \mathrm{z}}\left(\frac{\partial \Phi}{\partial \mathrm{x}} - \frac{\partial \Psi}{\partial z}\right) = \nabla^2 \Psi \tag{3.23}$$

The dynamic equilibriums in *x* and *z* directions are defined as:

$$\rho \frac{\partial^2 u}{\partial t^2} = (\lambda + \mu)\frac{\partial \bar{\varepsilon}}{\partial \mathrm{x}} + \mu \nabla^2 u \tag{3.24}$$

$$\rho \frac{\partial^2 w}{\partial t^2} = (\lambda + \mu)\frac{\partial \bar{\varepsilon}}{\partial \mathrm{z}} + \mu \nabla^2 w \tag{3.25}$$

Substituting Equations (3.20) and (3.21) into (3.24) and (3.25) yield;

$$\rho \frac{\partial}{\partial \mathrm{x}}\left(\frac{\partial^2 \Phi}{\partial t^2}\right) + \rho \frac{\partial}{\partial \mathrm{z}}\left(\frac{\partial^2 \Psi}{\partial t^2}\right) = (\lambda + 2\mu)\frac{\partial}{\partial \mathrm{x}}\left(\nabla^2 \Phi\right) + \mu \frac{\partial}{\partial \mathrm{z}}\left(\nabla^2 \Psi\right) \tag{3.26}$$

$$\rho \frac{\partial}{\partial \mathrm{z}}\left(\frac{\partial^2 \Phi}{\partial t^2}\right) - \rho \frac{\partial}{\partial \mathrm{x}}\left(\frac{\partial^2 \Psi}{\partial t^2}\right) = (\lambda + 2\mu)\frac{\partial}{\partial \mathrm{z}}\left(\nabla^2 \Phi\right) - \mu \frac{\partial}{\partial \mathrm{x}}\left(\nabla^2 \Psi\right) \tag{3.27}$$

Using the above equations, the two potential functions are derived as:

$$\frac{\partial^2 \Phi}{\partial \mathrm{t}^2} = v_p^2 \nabla^2 \Phi \tag{3.28}$$

$$\frac{\partial^2 \Psi}{\partial \mathrm{t}^2} = v_s^2 \nabla^2 \Psi \tag{3.29}$$

It is evident that the first potential function involves pure dilatation and the latter involves rotation given by the Equations (3.28) and (3.29). Solutions of the potential functions have the exponential forms as given below:

$$\Phi = F(z)e^{i(\omega t - kx)} \tag{3.30}$$

$$\Psi = G(z)e^{i(\omega t - kx)} \tag{3.31}$$

where ω: the excitation frequency of the incident wave; k: the wave-number defined in terms of the excitation frequency and the apparent wave velocity defined as $k = \omega / c$. Substituting Eq. (3.30) and (3.31) into (3.28) and (3.29) yields;

$$\frac{d^2F}{dz^2} + \left(\frac{\omega^2}{v_P^2} - k^2 \right) F = 0 \tag{3.32}$$

$$\frac{d^2G}{dz^2} + \left(\frac{\omega^2}{v_S^2} - k^2 \right) G = 0 \tag{3.33}$$

The general solutions for the second-order differential equations are;

$$F(z) = A_1 e^{qz} + A_2 e^{-qz} \tag{3.34}$$

$$G(z) = B_1 e^{sz} + B_2 e^{-sz} \tag{3.35}$$

where;

$$q^2 = k^2 - \frac{\omega^2}{v_P^2} \tag{3.36}$$

$$s^2 = k^2 - \frac{\omega^2}{v_S^2} \tag{3.37}$$

Finally, two displacement potential functions are obtained as:

$$\Phi = A_1 e^{qz + i(\omega t - kx)} + A_2 e^{-qz + i(\omega t - kx)} \tag{3.38}$$

$$\Psi = B_1 e^{sz+i(\omega t-kx)} + B_2 e^{-sz+i(\omega t-kx)} \quad \textbf{(3.39)}$$

Since the potential functions are defined for pure dilatation and distortion respectively, the coefficients A_1, B_1, A_2 and B_2 denote the incident and the reflected waves for the P and SV-waves. These coefficients are determined from the boundary conditions at the ground surface.

Considering an incident P-wave, the amplitude B_1 involving the incident SV-wave is zero in Eq. (3.39). Since the shear and the normal stress at the ground surface is zero as a boundary condition, the ratios of A_2/A_1 and B_2/A_1 are expressed as [14];

$$\frac{A_2}{A_1} = \frac{4\tan e \tan f - (1+3\tan^2 f)^2}{4\tan e \tan f + (1+3\tan^2 f)^2} \quad \textbf{(3.40)}$$

$$\frac{B_2}{A_1} = \frac{-4\tan e(1+3\tan^2 f)^2}{4\tan e \tan f + (1+3\tan^2 f)^2} \quad \textbf{(3.41)}$$

The relationship between the cosines of the incident P-wave and the reflected SV wave angles, e and f is dependent on the primary and shear wave velocities, v_p and v_s as given below;

$$\cos^2 e = \frac{v_P^2}{v_S^2}\cos^2 f \quad \textbf{(3.42)}$$

Using the solutions of the potential functions and the amplitude ratios given above, the free field motion due to an incident P-wave at the ground surface is finally determined as:

$$\begin{Bmatrix} u \\ v \\ w \end{Bmatrix} = p \begin{Bmatrix} u_0 \\ v_0 \\ w_0 \end{Bmatrix} e^{i(\omega t-kx)} \quad \textbf{(3.43)}$$

where p: the amplitude of the incident P-wave. The surface displacement amplitudes u_0, v_0 and w_0 of the P-wave are defined as:

$$u_0 = (\cos e)\left[1 + \frac{A_2}{A_1} - \frac{B_2}{A_1}\tan f\right] \quad \textbf{(3.44)}$$

$$v_0 = 0 \quad \textbf{(3.45)}$$

$$w_0 = -(\sin e)\left[1 - \frac{A_2}{A_1} - \frac{B_2}{A_1}\cot e\right] \quad \textbf{(3.46)}$$

In the case of an incident SV wave reaching the ground surface, the coefficient A_1 which involves the amplitude of an incident P-wave is zero. Applying the same boundary conditions which are still valid for SV-waves, the ratios of A_2/B_1 and B_2/B_1 are expressed as [14]:

$$\frac{A_2}{B_1} = \frac{4\tan f(1+3\tan^2 f)}{4\tan e\tan f + (1+3\tan^2 f)^2} \quad \textbf{(3.47)}$$

$$\frac{B_2}{B_1} = \frac{4\tan e\tan f - (1+3\tan^2 f)^2}{4\tan e\tan f + (1+3\tan^2 f)^2} \quad \textbf{(3.48)}$$

The relationship between the cosines of the incident SV-wave and the reflected P wave angles, f and e is given as:

$$\cos^2 f = \frac{v_S^2}{v_P^2}\cos^2 e \quad \textbf{(3.49)}$$

where v_p and v_s are the primary and shear wave velocities. The above equation yields real values of the reflection wave angle, e for the incident wave angles of $e \geq \theta_{cr}$ where $\theta_{cr} = \cos^{-1}\left(\frac{v_S}{v_P}\right)$. The free field displacement vector caused by the incident SV-wave at the ground surface can be finally determined as:

$$\begin{Bmatrix} u \\ v \\ w \end{Bmatrix} = s \begin{Bmatrix} u_0 \\ v_0 \\ w_0 \end{Bmatrix} e^{i(\omega t - kx)} \tag{3.50}$$

where s : the amplitude of the incident SV-wave. The displacement amplitudes in the plane of the SV-wave propagation i.e. *x'- y'-z'* coordinate system are expressed as:

$$u_0 = -(\sin f)\left[1 - \frac{B_2}{B_1} + \frac{A_2}{B_1}\cot f\right] \tag{3.51}$$

$$v_0 = 0 \tag{3.52}$$

$$w_0 = -(\cos f)\left[1 + \frac{B_2}{B_1} + \frac{A_2}{B_1}\tan e\right] \tag{3.53}$$

Unlike the P and the SV-waves, SH-wave is reflected as a SH-wave, which has an amplitude independent of the vertical incident angle (Fig. 3.3). The particle motion has a horizontal direction, which is normal to the plane of the wave propagation (Fig. 3.2). Since the total wave energy is reflected as a SH wave, the horizontal displacement at the free surface is twice that of the incident wave. The ground motion induced by the incident SH wave is obtained using Eq. (3.52) where s is the amplitude of the incident SH wave;

$$\begin{Bmatrix} u \\ \mathrm{v} \\ \mathrm{w} \end{Bmatrix} = \begin{Bmatrix} 0 \\ 2s \\ 0 \end{Bmatrix} e^{i(\omega t - kx)} \tag{3.54}$$

The formulations that are derived to determine the surface displacements induced by an incident P, SV or SH wave are defined in the vertical plane of the wave propagation. However, the coordinate system of a structure may not coincide with that of the incident wave as given in Fig. 3.5. Therefore, the wave motion reaching the ground surface has to be rotated into the coordinate system of the structure using the horizontal angle between the vertical plane of the wave motion and the vertical plane of the structure.

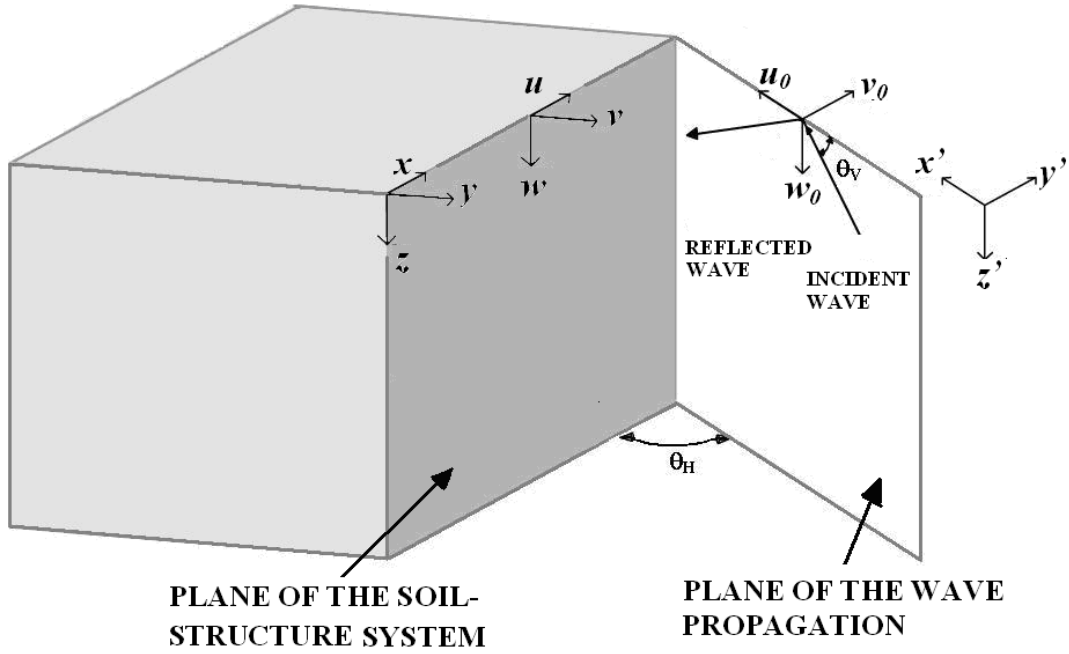

Figure 3.5 : Free-field displacement due to seismic wave propagation.

Hence, the free-field displacement vector at the interface nodes of the soil-structure system is obtained by multiplying the surface wave displacement vector with the rotation matrix, $[R_z]$ in order to rotate the displacement vector with an angle of θ_H around the global z axis. The rotation matrix around the z axis, $[R_z]$ is defined as:

$$[R_Z] = \begin{bmatrix} \cos\theta_H & -\sin\theta_H & 0 \\ \sin\theta_H & \cos\theta_H & 0 \\ 0 & 0 & 1 \end{bmatrix} \qquad \textbf{(3.55)}$$

The resulting free field displacement defined in the plane of the soil-structure system is obtained as:

$$\begin{Bmatrix} u_{ff} \\ v_{ff} \\ w_{ff} \end{Bmatrix} = \begin{bmatrix} \cos\theta_H & -\sin\theta_H & 0 \\ \sin\theta_H & \cos\theta_H & 0 \\ 0 & 0 & 1 \end{bmatrix} \begin{Bmatrix} u_0 \\ v_0 \\ w_0 \end{Bmatrix} e^{i(\omega t - kx\cos\theta_H - ky\sin\theta_H)} \qquad \textbf{(3.56)}$$

where u_0, v_0 and w_0 are the complex valued displacement amplitudes of the incident waves [29].

4. MODELLING OF THE SOIL MEDIUM

4.1 Background

The soil medium is represented by a semi-infinite elastic half-space and the interaction surface is flexible but the soil-structure system is fully bonded at the interface. The interaction surface is defined by rectangular elements, which also match with the geometry of the finite element model of the structure. Thereby, the coupling of the soil-structure system is achieved using the displacement compatibility at the interaction nodes. The frequency-dependent impedance matrix representing the complex-valued dynamic stiffness matrix of the soil-structure system under the seismic excitation is calculated utilizing the Green's functions on the surface of the elastic half space.

The Green's functions that are defined for an elastic half space have aroused from the solution of Lamb's problem, which deals with the elastic displacements resulting from the disturbance in an elastic half space. This pioneering work "On Propagation of tremors over the surface of an elastic solid" by Lamb [15] mainly concerns the wave motion generated at the surface of an elastic half-space due to the concentrated loads at the surface or the interior part of the half-space. Both harmonic time dependent and impulsive loads that are applied along a line or at a specific point are considered for the solution of the problem. After the work of Lamb, which is referred to as Lamb's Problem due to his contribution to the theory of wave propagation, many researchers have studied on the same problem such as Ewing et al. [14], Graff [53] and Achenbach [54].

In the previous study conducted Dendrou et. al. [29] for the dynamic analysis of the bridge-backfill systems, the solution of the Lamb's problem provided by Ewing et al. [15] has been evaluated in order to calculate the Green's functions for the elastic half-space. The Green's functions given by Dendrou et. al. [29] are employed to evaluate the frequency-dependent impedance matrix of the soil-structure system in this study.

Obtaining the impedance matrix of the soil-structure system for each excitation frequency, the force vector induced by the seismic wave motion is calculated by the multiplication of the impedance matrix and the free field displacement vector at the same excitation frequency. The calculation of frequency-dependent impedance matrix of the half-space is expressed in the form of a flowchart in order to summarize numerical procedure as given in Fig. 4.1.

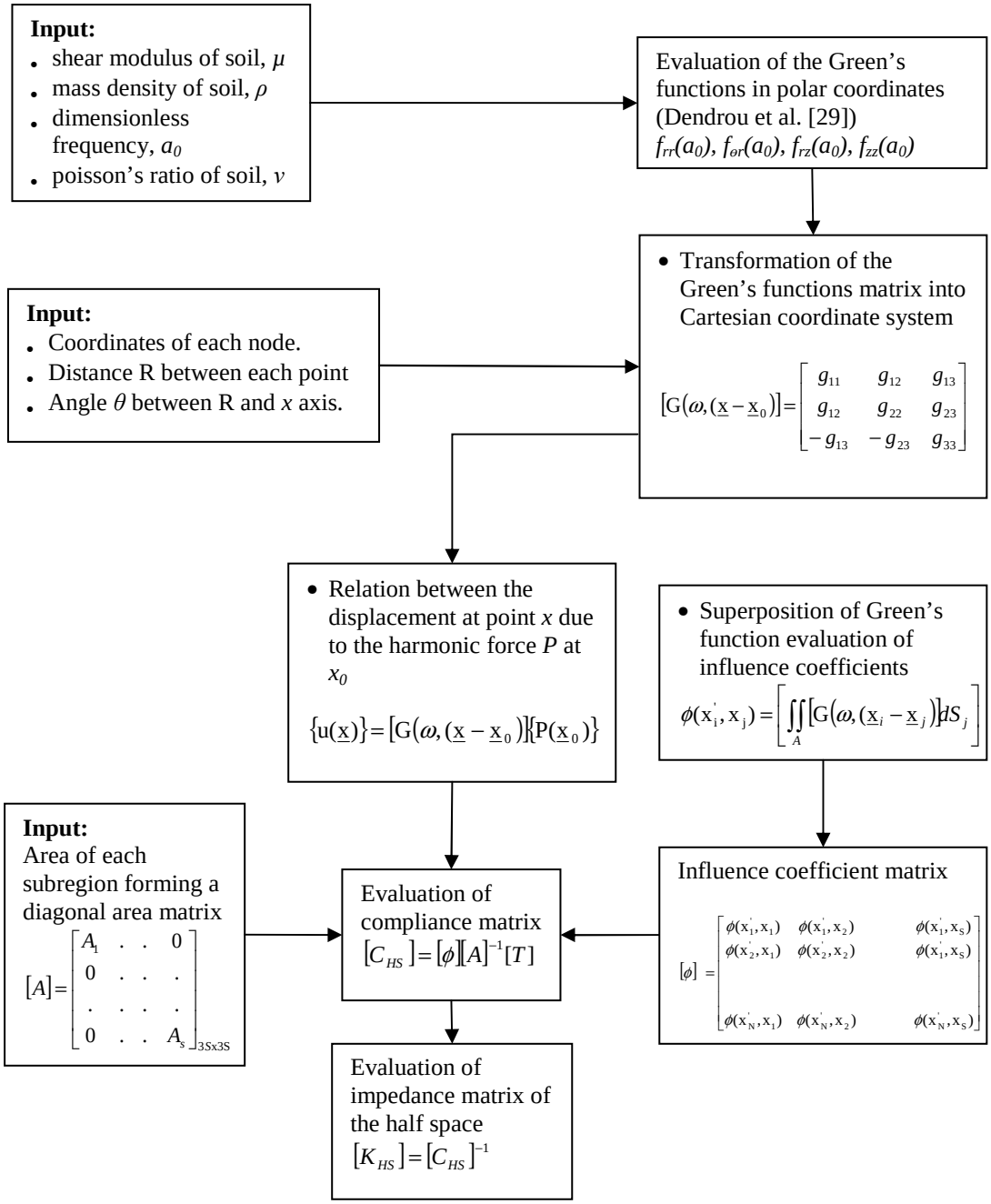

Figure 4.1 : Flowchart for the calculation of half-space impedance matrix.

4.2 Green's Functions for the Harmonic Point Load acting on the Surface of an Elastic Half-Space

Considering a harmonic point load acting on the surface of an elastic half space, the displacement vector $\{u\}$ of any point $\underline{x}$ on the surface due to the point source is expressed in terms of the Green's function matrix $[G(\omega,(\underline{x}-\underline{x}_0))]$ and the harmonic force vector $\{P(\underline{x}_0)\}$ acting at point $\underline{x}_0$ as given in Eq. (4.1).

$$\{u(\underline{x})\}=\begin{Bmatrix} u_x \\ u_y \\ u_z \end{Bmatrix} e^{i\omega t} = [G(\omega,(\underline{x}-\underline{x}_0))]\{P(\underline{x}_0)\} \qquad \textbf{(4.1)}$$

where $\underline{x}$: vector containing the coordinates of the surface point where the displacement is calculated; $\underline{x}_0$: vector containing the coordinates of the surface point where the harmonic force is applied; $\{P(\underline{x}_0)\}$: harmonic force applied at $\underline{x}_0$; ω: excitation frequency. The vector notation for the force and the displacement on the surface of elastic half-space is given in Fig. 4.2.

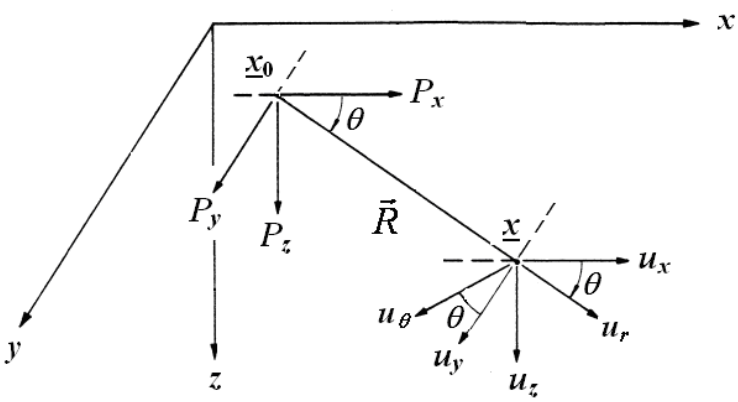

Figure 4.2 : The source and the receiver points in the Cartesian coordinate system.

Green's function matrix $[G(\omega,(\underline{x}-\underline{x}_0))]$ is composed of the displacement Green's functions, which are originally defined in polar coordinate system. Since the finite elements model of the structure is developed in the Cartesian coordinate system, the soil-structure interaction surface is also discretized by rectangular subregions. Therefore, the components of the Green's function matrix, which have been defined and evaluated in polar coordinates, are transformed into Cartesian coordinates.

The displacement vector at point $\underline{x}_0$ in the polar coordinate system can be transformed into the Cartesian coordinate system as:

$$\{u(\underline{x})\}=\begin{Bmatrix} u_x(\underline{x}) \\ u_y(\underline{x}) \\ u_z(\underline{x}) \end{Bmatrix}=\begin{bmatrix} \cos\theta & -\sin\theta & 0 \\ \sin\theta & \cos\theta & 0 \\ 0 & 0 & 1 \end{bmatrix}\begin{Bmatrix} u_r(\underline{x}) \\ u_\theta(\underline{x}) \\ u_z(\underline{x}) \end{Bmatrix} \qquad \textbf{(4.2)}$$

The components of the force vector at point $\underline{x}_0$ in Cartesian coordinate system are given as:

$$\{P(\underline{x}_0)\}=\begin{Bmatrix} P_x(\underline{x}_0) \\ P_y(\underline{x}_0) \\ P_z(\underline{x}_0) \end{Bmatrix}=\begin{Bmatrix} P_r(0) \\ P_\theta(\pi/2) \\ P_z \end{Bmatrix} \qquad \textbf{(4.3)}$$

The relationship between the harmonic point source and the displacement vector by given by Eq. 4.1 is revised using the Eqs. (4.2) and (4.3);

$$\begin{Bmatrix} u_r(\underline{x}) \\ u_\theta(\underline{x}) \\ u_z(\underline{x}) \end{Bmatrix}=\frac{1}{\mu R}\begin{bmatrix} f_{rr}\cos\theta & f_{rr}\cos(\theta-\pi/2) & f_{rz} \\ f_{\theta r}\sin\theta & f_{\theta r}\sin(\theta-\pi/2) & f_{\theta z} \\ f_{rz}\cos\theta & f_{rz}\cos(\theta-\pi/2) & f_{zz} \end{bmatrix}\begin{Bmatrix} P_x(\underline{x}_0) \\ P_y(\underline{x}_0) \\ P_z(\underline{x}_0) \end{Bmatrix} \qquad \textbf{(4.4)}$$

where μ: shear modulus of the soil; R: distance between the point that the force is applied (source) and the point at which the displacement is calculated (receiver); θ: angle between R and x axis. Substituting Eq. (4.2) into Eq. (4.4) and using $f_{\theta z}=0$ and $f_{rz}=-f_{zr}$, the Green's functions matrix in the Cartesian coordinate system is finally derived as:

$$[\mathrm{G}(\omega,(\underline{x}-\underline{x}_0)] = \frac{1}{\mu R}\begin{bmatrix} f_{rr}\cos^2\theta - f_{\theta r}\sin^2\theta & (f_{rr}+f_{\theta r})\cos\theta\sin\theta & f_{rz}\cos\theta \\ (f_{rr}+f_{\theta r})\cos\theta\sin\theta & f_{rr}\sin^2\theta - f_{\theta r}\cos^2\theta & f_{rz}\sin\theta \\ -f_{rz}\cos\theta & -f_{rz}\sin\theta & f_{zz} \end{bmatrix} \quad \textbf{(4.5)}$$

In the case of a concentrated impulsive load, the solution of the displacement as an elastodynamic problem is named as the fundamental singular solution or the Green's function of the medium [55,56]. Considering a point load applied harmonically on the surface of the halfspace, the displacement is expressed in terms of the displacement and the traction Green's functions for which the surface of the halfspace is traction free as a boundary condition.

The Green's functions are obtained by the integral solutions of the displacement potential functions defined for the elastic wave propagation. The derivation of the Green's functions for the surface point source for the elastic half-space is given in Ewing et al. [14]. Each component of the Green's function matrix is as follows:

$$f_{rr}(a_0) = \frac{a_0}{4\pi}\left[\int_0^\infty \frac{z\sqrt{z^2-1}\{J_2(a_0 z)-J_0(a_0 z)\}dz}{F(z)} + \int_0^\infty \frac{z}{\sqrt{z^2-1}}\{J_2(a_0 z)+J_0(a_0 z)\}dz\right] \quad \textbf{(4.6)}$$

$$f_{\theta r}(a_0) = \frac{a_0}{4\pi}\left\{\int_0^\infty \frac{z\sqrt{z^2-1}\{J_2(a_0 z)+J_0(a_0 z)\}dz}{F(z)} + \int_0^\infty \frac{z}{\sqrt{z^2-1}}\{J_2(a_0 z)-J_0(a_0 z)\}dz\right\} \quad \textbf{(4.7)}$$

$$f_{zz}(a_0) = -\frac{a_0}{2\pi}\int_0^\infty \frac{z\sqrt{z^2-n^2}\,J_0(a_0 z)dz}{F(z)} \quad \textbf{(4.8)}$$

$$f_{zr}(a_0) = -f_{rz}(a_0) \quad \textbf{(4.9)}$$

$$f_{\theta z}(a_0) = 0 \quad \textbf{(4.10)}$$

where the Rayleigh Determinant is determined as:

$$F(z) = (2z^2-1)^2 - 4z^2\sqrt{(z^2-n^2)(z^2-1)}$$

The ratio of the shear and primary wave velocity is defined as:

$$n = \frac{v_S}{v_P} = \sqrt{\frac{1-2\nu}{2(1-\nu)}}$$

and the dimensionless frequency is given as:

$$a_0 = \frac{\omega R}{v_s}$$

Using the Ewing's approach [14], Denrdou et al. [29] have evaluated the Green's functions replacing the integrals by the contour integrals in the complex plane. Evidently, these contour integrals have singular point at *z=s* where *F(s) = 0* and branch points at *z* = 1 and *z* = *n*. Before applying the Cauchy's Theorem, the branch cuts have been introduced in the complex plane. The integrals are partitioned into six parts in order to evaluate numerically. In such a case, each component of the Green's functions is expressed as below:

$$f_{rr} = \frac{a_0}{4\pi}\left(I_5 - I_6 + I_3 + I_4\right) \qquad \textbf{(4.11)}$$

$$f_{rz} = \frac{a_0}{2\pi} I_2 \qquad \textbf{(4.12)}$$

$$f_{\theta r} = \frac{a_0}{4\pi}\left(I_5 + I_6 + I_3 - I_4\right) \qquad \textbf{(4.13)}$$

$$f_{zz} = -\frac{a_0}{2\pi} I_1 \qquad \textbf{(4.14)}$$

where

$$I_1 = \int_0^\infty \frac{z\sqrt{z^2 - n^2}\, J_0(a_0 z)dz}{F(z)} \qquad \textbf{(4.15)}$$

$$I_2 = \int_0^\infty \frac{z^2(2z^2 - 1) - 2\sqrt{z^2 - n^2}\sqrt{z^2 - 1} J_1(a_0 z)dz}{F(z)} \qquad \textbf{(4.16)}$$

$$I_3 = \int_0^\infty \frac{z J_2(a_0 z)dz}{\sqrt{z^2 - 1}} \qquad \textbf{(4.17)}$$

$$I_4 = \int_0^\infty \frac{z J_0(a_0 z)dz}{\sqrt{z^2 - 1}} \qquad \textbf{(4.18)}$$

$$I_5 = \int_0^\infty \frac{z\sqrt{z^2-1}J_2(a_0 z)dz}{F(z)} \tag{4.19}$$

$$I_6 = \int_0^\infty \frac{z\sqrt{z^2-1}J_0(a_0 z)dz}{F(z)} \tag{4.20}$$

The static values of the Green's functions are defined for the excitation frequency, $\omega = 0$ by Love [57] as given below:

$$f_{rr}(0) = \frac{1}{2\pi} \tag{4.21}$$

$$f_{rz}(0) = \frac{-n^2}{4\pi(1-n^2)} \tag{4.22}$$

$$f_{\theta r}(0) = \frac{-1}{4\pi(1-n^2)} \tag{4.23}$$

$$f_{zz}(0) = \frac{1}{4\pi(1-n^2)} \tag{4.24}$$

$$f_{zr}(0) = -f_{rz}(0) \tag{4.25}$$

$$f_{\theta z}(0) = 0 \tag{4.26}$$

Since the dynamic analysis of the soil-structure system is carried out in the frequency domain, the integrals are evaluated for the specific excitation frequencies sequentially in the numerical procedure.

The plots of the real and the complex parts of the Green's functions for the Poisson's ratio $\nu = 1/3$ and $\nu = 1/4$ of the soil medium are presented in Figs. 4.3 through 4.6. It is observed that $f_{rr}(a_0)$ is not affected by the change in the Poisson's ratio of the soil medium as shown in Fig. 4.3. The rest of the functions f_{rr}, $f_{\theta r}$, f_{rz}, f_{zz} are slightly increased with the decrease of Poisson's ratio.

Since the integration of the functions in the complex plane possess singularities at Rayleigh Pole, $F(s)=0$ and branch points associated with the terms $\sqrt{z^2-n^2}$ and $\sqrt{z^2-1}$, the evaluation of the integrals are partitioned into intervals of $0 \le z \le n$ and $n \le z \le 1$ using the procedure given by Ewing [14]. Therefore, the variation of Poisson's ratio essentially affect the limits and the contents of the integrals defined by the ratio of the shear wave velocity and the primary wave velocity as $n = \frac{v_S}{v_P} = \sqrt{\frac{1-2\nu}{2(1-\nu)}}$.

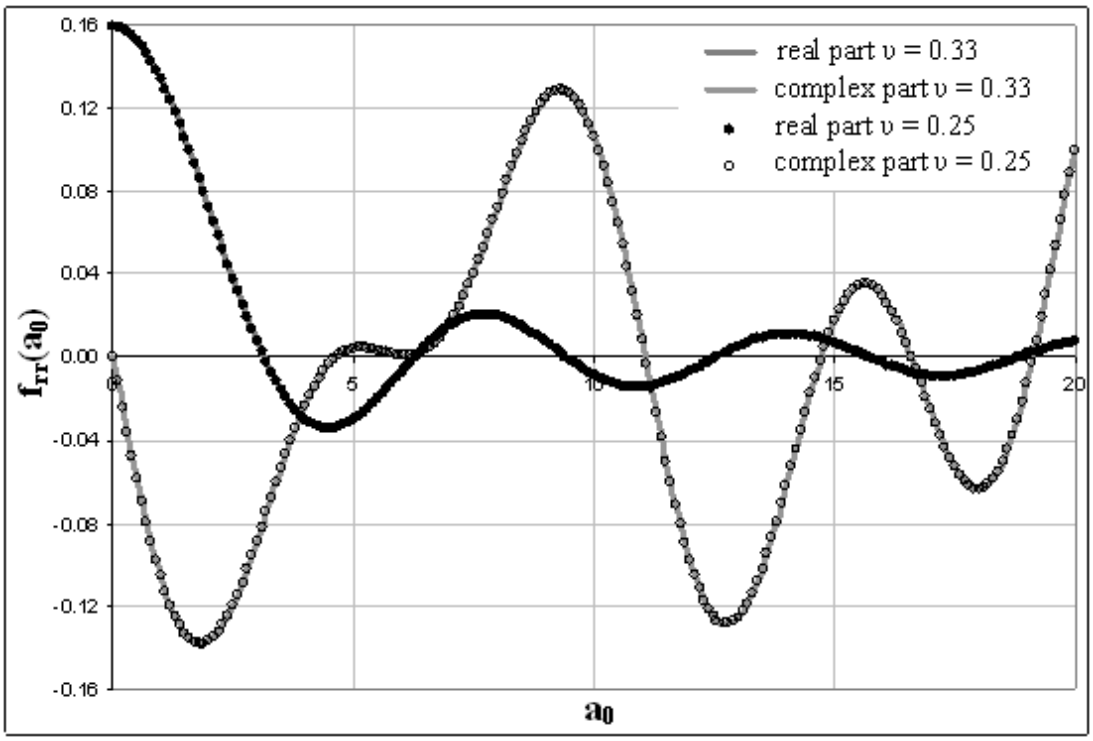

Figure 4.3 : The graph of f_{rr} versus dimensionless frequency a_0 for the Poisson's ratio of $\nu = 1/3$ and $\nu = 1/4$ [29].

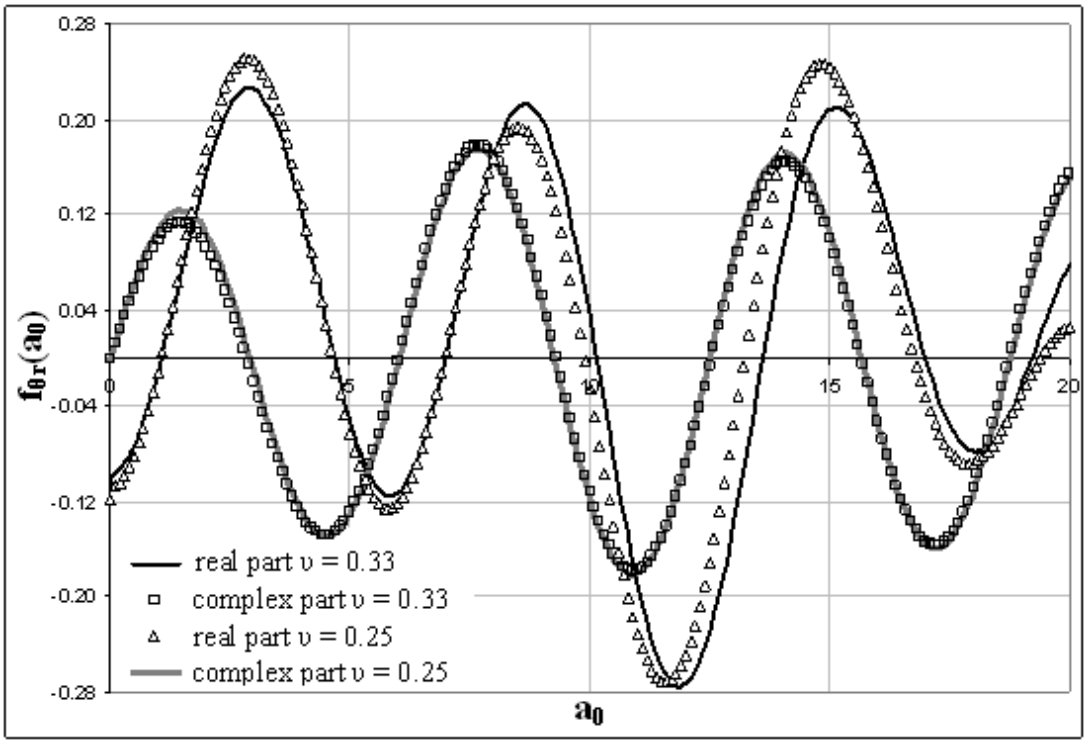

Figure 4.4 : The graph of $f_{\theta r}$ versus dimensionless frequency a_0 for the Poisson's ratio of $\nu = 1/3$ and $\nu = 1/4$ [29].

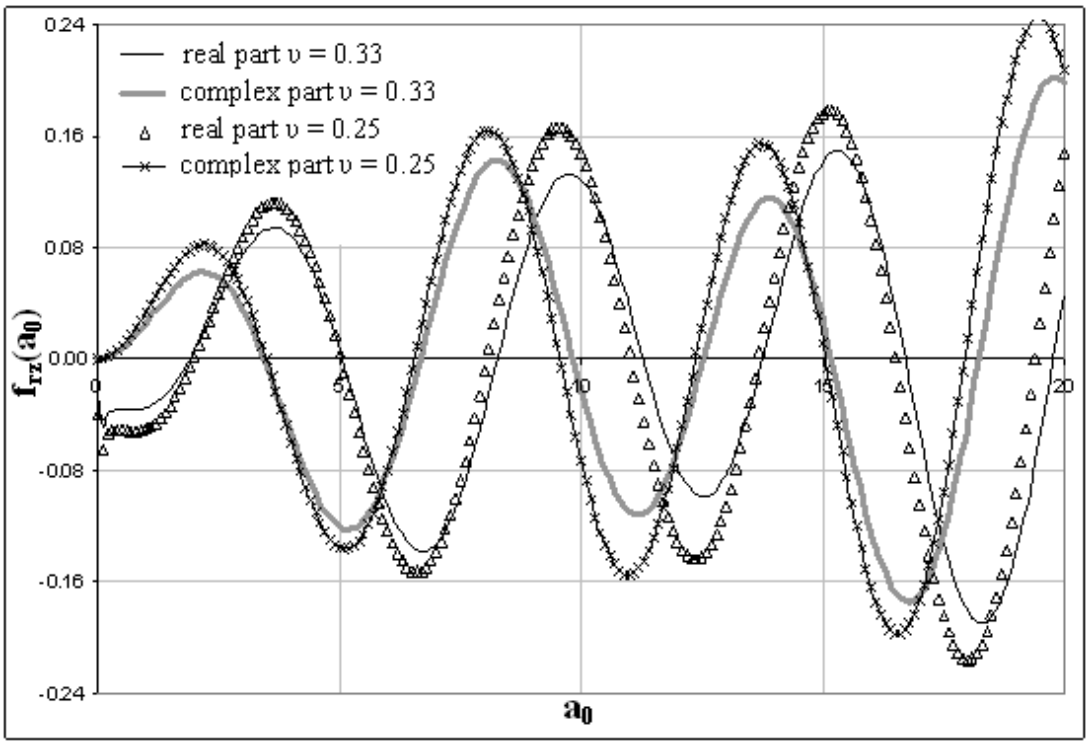

Figure 4.5 : The graph of f_{rz} versus dimensionless frequency a_0 for the Poisson's ratio of $\nu = 1/3$ and $\nu = 1/4$ [29].

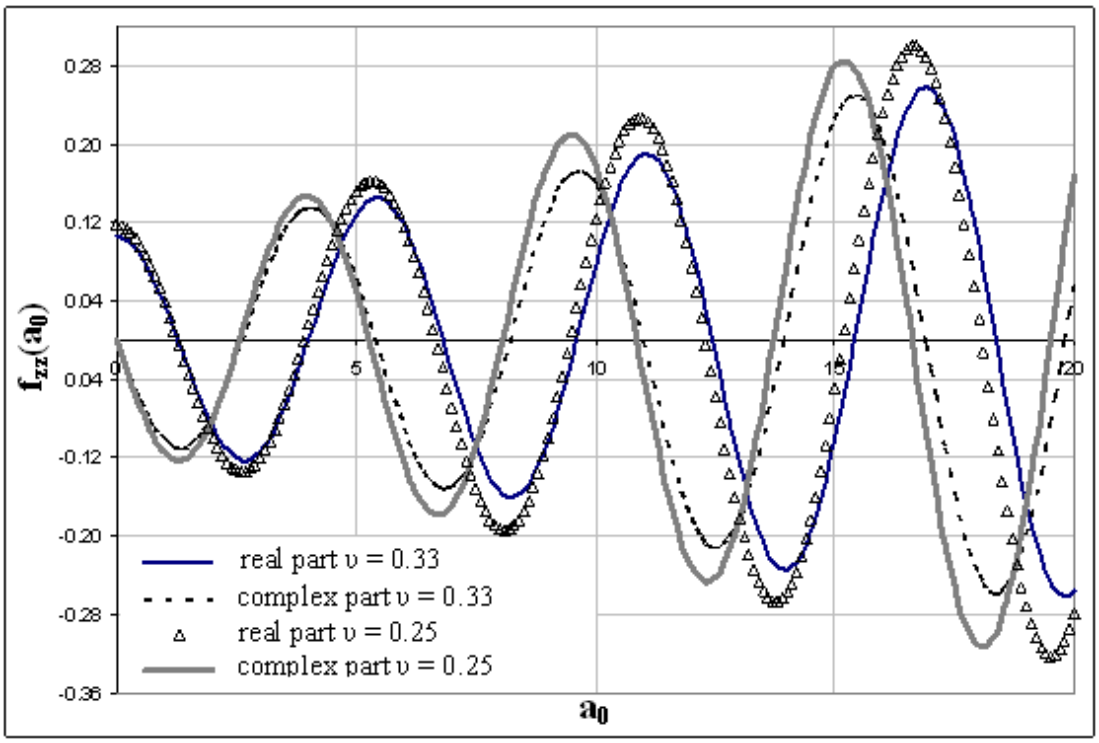

Figure 4.6 : The graph of f_{zz} versus dimensionless frequency a_0 for the Poisson's ratio of $\nu = 1/3$ and $\nu = 1/4$ [29].

4.3 Evaluation of the Frequency Dependent Impedance Matrix of the Elastic Half-Space

Green's functions matrix has been previously defined in terms of the harmonic point source, $\{P(\underline{x}_j)\}e^{i\omega t}$ applied at point $\underline{x}_j$ and the surface displacement vector $\{u(\underline{x}_i)\}$ at $\underline{x}_i$;

$$\{u(\underline{x}_i)\} = \begin{Bmatrix} u_x \\ u_y \\ u_z \end{Bmatrix} e^{i\omega t} = [\mathrm{G}(\omega, (\underline{x}_i - \underline{x}_j))]\{P(\underline{x}_j)\}e^{i\omega t} \qquad \textbf{(4.27)}$$

For the dynamic analysis of soil-structure system with a surface foundation, the interface surface is discretized by the rectangular areas of $A_j(x)$. The generation of the impedance matrix involves determining the displacement vector at any nodal point $\underline{x}_i$ of the rectangular interface due to the unit harmonic force at each nodal point $\underline{x}_j$. Considering constant stress traction over the total interface area, Eq. (4.27) defining the displacement due to a single point load is superposed for unit point harmonic load applied at each interface node. Therefore, Eq. (4.27) is rewritten as:

$$\{u(\underline{x}_i)\} = \iint_A [G(\omega, (\underline{x}_i - \underline{x}_j))].\{\sigma(\underline{x}_j)\}.dS_j =$$
$$\sum_{j=1}^{S} \iint_{Aj} [G(\omega, (\underline{x}_i - \underline{x}_j))].\{\sigma_j(\underline{x}_j)\}.dS_j \qquad \textbf{(4.28)}$$

where $\{\sigma(\underline{x}_j)\}$: constant traction at the centroid of subregion j and A_j : area of the jth subregion.

Wong [58] has studied the dynamic response of the deformable soil under the effect of the seismic excitations. The research focuses on the determination of the soil impedance and driving forces induced by the seismic waves at the foundation-soil interface. The results of this study reveal that the stress distribution is sensitive to the shape of the foundation. However, the impedance evaluated by integrating the stress values and the driving force are not affected by the shape of the foundation. Therefore, the integration can be discretized by an approximate area in order to simplify the integration process as given in Eq. (4.28).

In the previous study conducted by Elorduy et al. [59], each subregion has been represented by square elements. Since the evaluation of Green's functions for the concurrent points $\underline{x}_i = x_j$ is difficult due to the singularity, $\frac{1}{|(\underline{x}_i - \underline{x}_j)|}$. The researchers kept the source points at the center of each square element and the receiver points were shifted to the nodes of the square elements. A similar procedure has been developed by Dendrou et al. [29] for the computation of the impedance matrix. In this procedure, the integration of the Green's functions are accomplished considering the source point as the centroid of the rectangular element and the receiver point as the node composing the interface area.

To implement the proposed procedure, the Eq. (4.28) has been revised as:

$$\{u(\underline{x}_i)\} = [\phi]\ \{\sigma_j(\underline{x}_j)\} \qquad \textbf{(4.29)}$$

where the matrix $[\phi]$ is written as:

$$[\phi] = \begin{bmatrix} \phi(x_1^{'}, x_1) & \phi(x_1^{'}, x_2) & . & . & \phi(x_1^{'}, x_S) \\ \phi(x_2^{'}, x_1) & \phi(x_2^{'}, x_2) & . & . & \phi(x_1^{'}, x_S) \\ . & . & . & . & . \\ . & . & . & . & . \\ \phi(x_N^{'}, x_1) & \phi(x_N^{'}, x_2) & . & . & \phi(x_N^{'}, x_S) \end{bmatrix} \quad \textbf{(4.30)}$$

Each component of the matrix $[\phi]$ is determined by the integration of the Green's function matrix over the discretized interface surface;

$$\phi(x_i^{'}, x_j) = \left[\iint_A \mathrm{G}\left(\omega, (\underline{x}_i - \underline{x}_j)\right) dS_j \right] \quad \textbf{(4.31)}$$

The constant traction vector can be rewritten as $\{\sigma_j(\underline{x}_j)\} = [A]^{-1}\{P_s(\underline{x}_j)\}$ where $[A]$ is the diagonal matrix, which consists of the area of each rectangular element. The load vector $\{P_s(\underline{x}_j)\}$ with the dimensions of *(3Sx1)* is obtained as:

$$\{P_s\} = [T]\{P\} \quad \textbf{(4.32)}$$

where $\{P\}$: the load vector having a dimension of *3Nx1* and $[T]$: the transformation matrix with the dimensions of *(3Sx3N)*. *N* and *S* are the number of nodes of the interface and the number of subregions, respectively. Using transformation matrix $[T]$, the point loads applied at the corners of subregions are shifted to the center of each element.

The generation of the transformation matrix is based on transforming the nodal point force into equivalent forces acting at the centroids of the subregions nearby the original nodal source. Three different types of transformation are possible: the transformation of the point source acting on an interior node, on an edge node or on a corner node.

Using the transformation matrix and the nodal force vector, the displacement vector $\{u\}$ in Eq. (4.29) is rewritten as:

$$\{u\} = [\phi]\{\sigma_s\} = [\phi].[A]_D^{-1}[T]\{P\} \quad \textbf{(4.33)}$$

Eventually, the compliance matrix of the half-space, $[C_{HS}]$ defined as:

$$\{u\} = [\phi]_{.}[A]^{-1}[T]\{P\} = [C_{HS}]\{P\} \quad \textbf{(4.34)}$$

$$[C_{HS}] = [\phi]_{.}[A]_{D}^{-1}[T] \quad \textbf{(4.35)}$$

Since the frequency-dependent impedance matrix, $[K_{HS}]$ is the inverse of the compliance matrix, $[C_{HS}]$ it is calculated as:

$$[K_{HS}] = [C_{HS}]^{-1} \quad \textbf{(4.36)}$$

5. IMPLEMENTATION OF THE SUBSTRUCTURE METHOD

5.1 General Procedure

The dynamic analysis of the soil-structure system has been carried out using the substructure method. Implementation of the numerical model for the substructure method has been accomplished by partitioning the soil and the structure system and analyzing each system separately. The finite element modeling of the superstructure has been developed using ANSYS [60] software and modeling of soil medium has been conducted by a special MATLAB code [61] developed within the scope of this dissertation.

The free field motion induced by the seismic waves has been determined by the computer program developed in this study using the elastic wave theory, which has been explained in Chapter 3. The impedance matrix for each excitation frequency at the interface nodes has been obtained sequentially within a numerical loop of the computer program as given in Chapter 4. The evaluation of the impedance matrix has been formulated employing the fundamental solutions for the homogeneous half-space. Finally, the output data produced by the two subprograms for the seismic wave motion and the impedance matrix of the soil medium have been multiplied in order to calculate the excitation force vector caused by the incident wave at the interface nodes as given below;

$$\{P\} = [K_{HS}].\{u_{ff}\} \qquad \textbf{(5.1)}$$

Using the compatibility equations for the displacement at the interface nodes, the equations of motion for the total system are formulated in the matrix form and solved numerically. The overall numerical procedure is summarized in Figure 5.1.

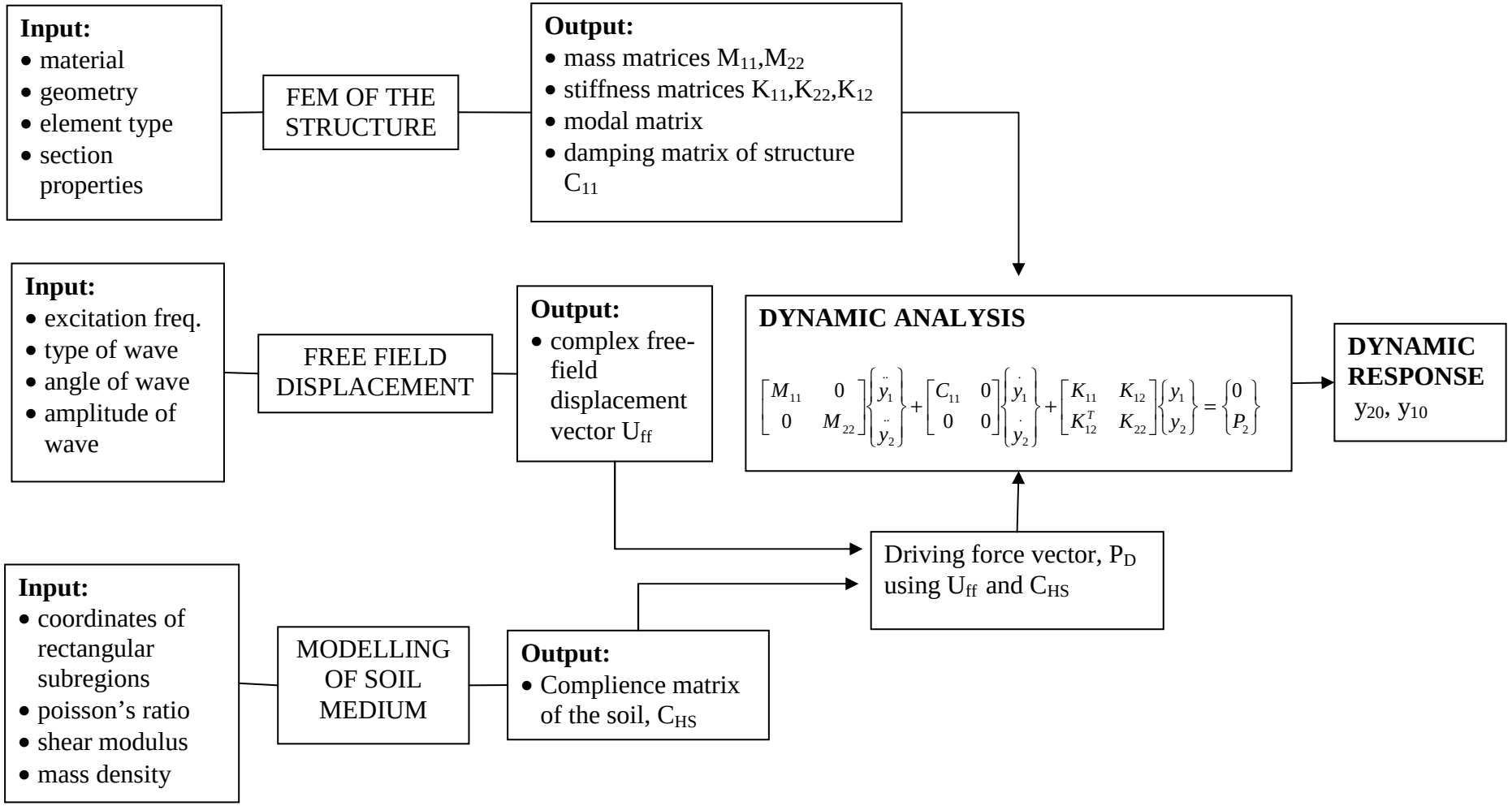

Figure 5.1 : Flowchart for the numerical modeling of the soil-structure system.

5.2 Derivation of the Numerical Methodology

Finite element modeling of the superstructure necessitates the generation of the structural geometry using a number of nodes. Employing the substructure method, the nodes of the structure are categorized as the structural nodes and the nodes belonging to the soil-structure interface surface. Therefore, the matrices composing the set of the equations of motion for the dynamic analysis are also partitioned as the structure and the soil-structure interface.

The dynamic response of the soil-structure system, $\{y\}$ is accomplished by the solution of the dynamic equilibrium equations given as:

$$[M]\{\ddot{y}\}+[C]\{\dot{y}\}+[K]\{y\}=\{P\} \qquad \textbf{(5.2)}$$

where [M], [C] and [K] are mass, damping and stiffness matrices. The displacement vector $\{y\}$ defined in the time domain is composed of the superstructure displacements $\{y_1\}$ and the displacements of the interface nodes, $\{y_2\}$. Using the substructure method, Equation (5.2) is rewritten as:

$$\begin{bmatrix} M_{11} & 0 \\ 0 & M_{22} \end{bmatrix}\begin{Bmatrix} \ddot{y}_1 \\ \ddot{y}_2 \end{Bmatrix}+\begin{bmatrix} C_{11} & 0 \\ 0 & 0 \end{bmatrix}\begin{Bmatrix} \dot{y}_1 \\ \dot{y}_2 \end{Bmatrix}+\begin{bmatrix} K_{11} & K_{12} \\ K_{12}^T & K_{22} \end{bmatrix}\begin{Bmatrix} y_1 \\ y_2 \end{Bmatrix}=\begin{Bmatrix} 0 \\ P_2 \end{Bmatrix} \qquad \textbf{(5.3)}$$

where $[M_{11}]$: the mass matrix of the superstructure; $[M_{22}]$: the mass matrix for the soil-structure interface; $[C_{11}]$: the diagonal damping matrix of the superstructure; $[K_{11}]$: the stiffness matrix of the superstructure; $[K_{22}]$: the stiffness matrix the soil-structure interface; $[K_{12}]$: the coupled stiffness matrix of the superstructure and the interface region and $\{P_2\}$: the vector of the forces applied along the interface nodes.

The response of the structure, $\{y_1\}$ is defined by the static and the dynamic parts as given in Eq. (5.4). Using quasi-static transmission of the free field motion, the static part of the displacement vector $\{y_{1s}\}$ can be expressed in terms of the displacement vector of the interface nodes $\{y_2\}$ as given in Eq. (5.6).

$$\{y_1\}=\{y_{1s}\}+\{y_{1d}\} \qquad \textbf{(5.4)}$$

$$[K_{11}]\{y_{1s}\}+[K_{12}]\{y_2\}=\{0\} \quad \textbf{(5.5)}$$

$$\{y_{1s}\}=-[K_{11}]^{-1}[K_{12}]\{y_2\}=[R_s]\{y_2\} \quad \textbf{(5.6)}$$

$[R_s]$ is the quasi-static transformation matrix which is derived using the static part of the equilibrium equation [62,18]. Using Eq. (5.4), the first row of the matrix of the dynamic equilibrium equation is expressed as:

$$[M_{11}].\{\ddot{y}_{1s}+\ddot{y}_{1d}\}+[C_{11}].\{\dot{y}_{1s}+\dot{y}_{1d}\}+[K_{11}].\{y_{1s}+y_{1d}\}+[K_{12}].\{y_2\}=\{0\} \quad \textbf{(5.7)}$$

Substituting Eq. (5.6) in Eq. (5.7) yields;

$$\begin{aligned}&[M_{11}].[R_S].\{\ddot{y}_2\}+[M_{11}].\{\ddot{y}_{1d}\}+[C_{11}].[R_S].\{\ddot{y}_2\}+[C_{11}].\{\dot{y}_{1d}\}+\ldots\\&[K_{11}].[R_S].\{y_2\}+[K_{11}].\{y_{1d}\}+[K_{12}].\{y_2\}=\{0\}\end{aligned} \quad \textbf{(5.8)}$$

Since $[K_{11}].[R_S].\{y_2\}+[K_{12}].\{y_2\}=\{0\}$, Eq. (5.7) is finally expressed in the form of;

$$[M_{11}].\{\ddot{y}_{1d}\}+[C_{11}].\{\dot{y}_{1d}\}+[K_{11}].\{y_{1d}\}=-([M_{11}].[R_S].\{\ddot{y}_2\}+[C_{11}].[R_S].\{\dot{y}_2\}) \quad \textbf{(5.9)}$$

Dendrou et al. [29] has neglected the effect of the damping on the forcing function and obtained Eq. (5.9) as:

$$[M_{11}].\{\ddot{y}_{1d}\}+[C_{11}].\{\dot{y}_{1d}\}+[K_{11}].\{y_{1d}\}=-[M_{11}].[R_s].\{\ddot{y}_2\} \quad \textbf{(5.10)}$$

The dynamic part of the displacement vector $\{y_{1d}\}$ is expressed in terms of the eigenvectors of the structure as given below;

$$\{y_{1d}\}=[\Phi].\{\eta\} \quad \textbf{(5.11)}$$

where $\{\eta\}$ is the vector of the modal response amplitudes and $[\Phi]$ is the modal matrix. Substituting Eq. (5.11) into (5.10) and using the orthogonality conditions, Eq. (5.12) is obtained for each free vibration mode of the superstructure, which is given below;

$$[I].\{\ddot{\eta}\}+[2\omega_N\zeta_N].\{\dot{\eta}\}+[\omega_N^2].\{\eta\}=-[\Phi]^T([M_{11}].[R_S].\{\ddot{y}_2\}+[C_{11}].[R_S].\{\dot{y}_2\}) \quad \textbf{(5.12)}$$

where $[I]$: the identity matrix; $\{\dot{\eta}\}$ and $\{\ddot{\eta}\}$: the first and second derivatives of the vector of modal response amplitudes with respect to time; $[\omega_N^2]$: the diagonal matrix containing the square of the nth natural frequency; $[\Phi]$: the modal matrix containing the eigenvectors of the superstructure and ζ_N: the modal damping ratio which is proportional to the mass and the stiffness matrices of the structure. The orthogonality conditions are as follows;

$$[\Phi]^T[M_{11}].[\Phi]=[I] \quad \textbf{(5.13)}$$

$$[\Phi]^T[C_{11}].[\Phi]=[2\omega_N\zeta_N] \quad \textbf{(5.14)}$$

$$[\Phi]^T[K_{11}].[\Phi]=[\omega_N^2] \quad \textbf{(5.15)}$$

The modal matrix, $[\Phi]$ is normalized to the mass matrix, $[M_{11}]$. Expressing the displacement vector of the interface nodes, $\{y_2\}$ and the vector of the modal response amplitudes, $\{\eta\}$ in the form of harmonic motion with an excitation frequency of Ω, the Eq. (5.12) can be rearranged as:

$$\begin{aligned}&\{-[\Omega^2]+i[2\Omega\omega_N\xi_N]+[\omega_N^2]\}.\{\eta_0\}=\\&-[\Phi]^T\{-\Omega^2[M_{11}].[R_S]+i\Omega[C_{11}].[R_S]\}\{y_{20}\}\end{aligned} \quad \textbf{(5.16)}$$

where $\{y_2\}=\{y_{20}\}e^{i\Omega t}$; $\{\eta\}=\{\eta_0\}e^{i\Omega t}$. Finally, the displacement amplitude, $\{\eta_0\}$ in the frequency domain in Eq. (5.16) is obtained as:

$$\{\eta_0\}=[S]^{-1}\{\Omega^2[\Gamma]-i\Omega[\Phi]^T[C_{11}].[R_s]\}.\{y_{20}\} \quad \textbf{(5.17)}$$

where $[\Omega^2]$ is the diagonal matrix containing the square of the excitation frequency and $[S]$ is given as:

$$[S] = -[\Omega^2] + i[2\Omega\omega_N\xi_N] + [\omega_N^2] \quad \textbf{(5.18)}$$

Multiplying both sides of Eq. (5.18) by $e^{i\Omega t}$, the dynamic part of the displacement vector of the structure $\{y_{1d}\}$ is expressed in terms of the displacement vector of the interface modes $\{y_2\}$ as given below;

$$\{y_{1d}\} = \left[\Omega^2[\Phi]\,[S]^{-1}[\Gamma] - i\Omega[\Phi]\,[S]^{-1}[\Phi]^T[C_{11}]\,[R_s]\right]\{y_{20}\}e^{i\Omega t} \quad \textbf{(5.19)}$$

where $[\Gamma]$ is the matrix of modal participation factors which is obtained as:

$$[\Gamma] = [\Phi]^T[M_{11}][R_S] \quad \textbf{(5.20)}$$

The diagonal damping matrix $[C_{11}]$ can also be expressed as:

$$[C_{11}] = [M_{11}].[\Phi].[2\omega_N\xi_N].[\Phi]^T[M_{11}] \quad \textbf{(5.21)}$$

which has been given as an alternative formulation for the evaluation of the damping matrix by Clough and Penzien [62]. Substituting the above expression into Eq. (5.19) yields;

$$\{y_{1d}\} = \left[\Omega^2[\Phi].[S]^{-1}[\Gamma] - i\Omega[\Phi].[S]^{-1}[2\omega_N\xi_N].[\Phi]^T[M_{11}].[R_s]\right]\{y_{20}\}e^{i\Omega t} \quad \textbf{(5.22)}$$

Rearranging the matrices that are multiplied by the displacement vector $\{y_2\}$, Eq. (5.18) is finally obtained as:

$$\{y_{1d}\} = [R_D]\{y_2\} \quad \textbf{(5.23)}$$

where the dynamic transformation matrix $[R_D]$ is defined as:

$$[R_D] = \Omega^2[\Phi][S]^{-1}[\Gamma] - i\Omega[\Phi][S]^{-1}[2\omega_N\xi_N][\Phi]^T[M_{11}][R_s] \quad \textbf{(5.24)}$$

Eventually, the relationship between the displacement vector of the structure $\{y_1\}$ and the interface nodes $\{y_2\}$ is derived as:

$$\{y_1\} = [T]\{y_2\} = [T]\{y_{20}\}e^{i\Omega t} \tag{5.25}$$

$$[T] = [R_S] + [R_D] \tag{5.26}$$

where $[R_S]$: the static transformation matrix; $[R_D]$: the dynamic transformation matrix and $[T]$: the system transformation matrix. Using the relationship between the displacement vector of the structure $\{y_1\}$ and the interface nodes $\{y_2\}$, the second row of the matrix in Eq. (5.3) can be rewritten as:

$$[M_{22}]\left\{\ddot{y}_2\right\} + [K_{12}]^T[T]\left\{y_2\right\} + [K_{22}]\{y_2\} = \{P_2\} \tag{5.27}$$

Similar to the displacement vector of the interface nodes which has been defined as $\{y_2\} = \{y_{20}\}e^{i\Omega t}$, the force vector applied along the interface, $\{P_2\}$ is also expressed in terms of a harmonic excitation which is given as $\{P_2\} = \{P_{20}\}e^{i\Omega t}$. Therefore, Eq. (5.27) is rearranged as:

$$[K_{ST}]\{y_{20}\} = \{P_{20}\} \tag{5.28}$$

where the matrix $[K_{ST}]$ represents 'the effective impedance matrix' of the structure as given below;

$$[K_{ST}] = -\Omega^2[M_{22}] + [K_{12}]^T[T] + [K_{22}] \tag{5.29}$$

The vector of the forces applied along the interface, $\{P_2\}$ is decomposed as the driving forces and the resisting forces as given below:

$$\{P_2\} = \{P_{20}\}e^{i\Omega t} = [\{P_{D0}\} + \{P_{R0}\}]\ e^{i\Omega t} \tag{5.30}$$

The vector of driving force amplitudes $\{P_{D0}\}$ is composed of the force amplitudes, which are induced by the seismic wave motion. Using the Green's functions, the driving forces along the interface nodes have been previously defined in terms of the

impedance matrix of the half-space, $[K_{HS}]$ and the free field motion, $\{u_{ff}\}$ as given below:

$$\{P_{DO}\} = [K_{HS}].\{u_{ff}\} \tag{5.31}$$

Using the compatibility of the displacements at the interface nodes, the vector of the resisting force amplitudes is given as:

$$\{P_{RO}\} = -[K_{HS}].\{y_{20}\} \tag{5.32}$$

Substituting Eq. (5.30) into (5.28), the vector of the response amplitudes along the interface, $\{y_{20}\}$ can be obtained as:

$$\{y_{20}\} = [K_{ST} + K_{HS}]^{-1}\{P_{DO}\} \tag{5.33}$$

where $[K_{ST} + K_{HS}]$ is the impedance matrix of the soil-structure system. Since $\{y_1\} = [T].\{y_2\}$, the response of the superstructure is finally expressed as:

$$\{y_1\} = [T]\,[K_{ST} + K_{HS}]^{-1}\{P_{DO}\}e^{i\Omega t} \tag{5.34}$$

5.3 The Summary of The Numerical Procedure

This chapter includes the numerical procedure that has been implemented for the dynamic analysis of the soil-structure systems. The solution of the dynamic soil-structure interaction problem has been encountered using the substructure method. The detailed derivation of the formulation has been explained in the previous sections of this chapter. The numerical procedure is summarized in Table 5.1.

The numerical procedure is mainly based on the methodology developed by Dendrou et al. [29] for dynamic analysis of soil-structure interaction problems. The authors have used the substructure method for the coupling of the soil and the structure systems. The formulation of the dynamic transformation matrix, $[R_D]$ in the previous study has been derived neglecting the effect of damping on the dynamic transformation matrix. However, this assumption has led to the overestimation of the

response amplitudes of the soil-structure system under the effect of the seismic waves. As a contribution of this thesis, an alternative formulation has been developed including the effect of the damping on the dynamic transformation matrix, $[R_D]$. The damping matrix which is implemented in this study is an alternative formulation of the damping matrix given by Clough and Penzien [62]. The dynamic response amplitudes of the soil-structure systems using the new formulation developed in this study are more realistic than the previous methodology.

Table 5.1: The summary of the numerical procedure.

STAGE	**DESCRIPTION AND FORMULATION OF THE PROCEDURE**
Assembling the element matrices using Finite Element Method	The mass, and the stiffness matrices have been partitioned into the components of the superstructure and the interface. $\begin{bmatrix} M_{11} & 0 \\ 0 & M_{22} \end{bmatrix} \begin{Bmatrix} \ddot{y}_1 \\ \ddot{y}_2 \end{Bmatrix} + \begin{bmatrix} C_{11} & 0 \\ 0 & 0 \end{bmatrix} \begin{Bmatrix} \dot{y}_1 \\ \dot{y}_2 \end{Bmatrix} + \begin{bmatrix} K_{11} & K_{12} \\ K_{12}^T & K_{22} \end{bmatrix} \begin{Bmatrix} y_1 \\ y_2 \end{Bmatrix} = \begin{Bmatrix} 0 \\ P_2 \end{Bmatrix}$ **Structure:** M_{11}, K_{11}, C_{11} **Interface:** M_{22}, K_{22} **Coupling:** K_{12}
Eigenvalue analysis	The interface nodes have been assumed to be fixed at the base. The modal matrix is obtained by mass normalization. $[\Phi]^T [M_{11}][\Phi] = [I]$ $[\Phi]^T [C_{11}][\Phi] = [2\omega_N \zeta_N]$ $[\Phi]^T [K_{11}][\Phi] = [\omega_N^2]$
Calculation of the dynamic and the static transformation matrices	$\{y_1\} = \{y_{1s}\} + \{y_{1d}\}$ $\{y_{1s}\} = [R_s]\{y_2\}$ and $\{y_{1d}\} = [R_D]\{y_2\}$ $[R_s] = -[K_{11}]^{-1}[K_{12}]$ $[R_D] = \Omega^2 [\Phi]_. [S]^{-1} [\Gamma] - i\Omega [\Phi][S]^{-1} [2\omega_N \xi_N]_. [\Phi]^T [M_{11}]_. [R_s]$ $[S] = -[\Omega^2] + i[2\Omega\omega_N \zeta_N] + [\omega_N^2]$

Table 5.1 (Continued): The summary of the numerical procedure.

STAGE	DESCRIPTION AND FORMULATION OF THE PROCEDURE
Calculation of the transformation matrix	$\{y_1\}=[T]\{y_2\}$ $[T]=[R_S]+[R_D]$
Calculation of the effective impedance matrix for the structure	$[K_{ST}]\{y_{20}\}=\{P_{20}\}$ $[K_{ST}]=-\Omega^2[M_{22}]+[K_{12}]^T[T]+[K_{22}]$
Determination of the vector of driving force amplitude	$\{P_{DO}\}=[K_{HS}]\{u_{ff}\}$ $[K_{HS}]$:Half-space impedance matrix $\{u_{ff}\}$: Free-field motion of the interface nodes
Determination of the vector of interface displacement amplitudes	$\{y_{20}\}=[K_{ST}+K_{HS}]^{-1}\{P_{DO}\}$
Determination of the response of the structure	$\{y_1\}=[R_S+R_D].[K_{ST}+K_{HS}]^{-1}\{P_{DO}\}e^{i\Omega t}$

6. SAMPLE PROBLEM 1: 3D BRIDGE-BACKFILL SYSTEM

6.1 Introduction

This chapter includes the dynamic analysis of a bridge-backfill system under the effect of the traveling SH waves, which has been previously analyzed by Dendrou et al. [63]. The authors have discussed the traveling seismic wave effect on the dynamic response of the soil-structure system. The same bridge model has been regenerated and examined using the numerical procedure that is developed in this study. The solution of the soil-structure model has been conducted implementing the same geometrical and material properties of the structure and the soil with the previous study. Comparing the results of the dynamic analyses, it has been observed that the response curves of the bridge-backfill system obtained using the numerical procedure developed in this study are in good agreement with the previous one.

After the verification of the computer program that is implemented in this study, the same bridge-backfill system has been analyzed for three different soil types in order to observe the effect of soil conditions on the dynamic response of the soil-structure system.

Eventually, the dynamic response for each case has been obtained by the revised substructure methodology including the effect of the damping on the dynamic transformation matrix of the system. The results of the analyses are discussed in detail.

6.2 Traveling Seismic Wave Effect

The influence of the dynamic soil structure interaction on the response of the structures becomes more important, if the size of a structure is large such as a bridge or a large dam. The effect of the soil-structure interaction may appear in two types according to the size and geometry of the foundation. The first effect is named as the kinematic interaction. In this type of interaction, the foundation serves as a filtering effect to the seismic waves by its geometry. The other type of interaction, which is

called as the traveling wave effect, occurs when the characteristic length of the structure is in the same order as the wavelength of the seismic waves. In this case, the ground motion changes to a great extent along the length of the structure. The traveling wave effect becomes important depending on the size of the structure and on the type, frequency and direction of the seismic wave [64].

In general, the dynamic response of the structures is carried out with the assumption that the structure is under the same input excitation applied simultaneously at the entire base. This assumption may be sufficient for a structure with moderate building dimensions. However, seismic waves traveling along the soil-structure interface may cause a non-uniform effect if the length of the structure is close to the seismic wavelength. In this case, amplitude and phase angle of the base motion at each point is different.

The spatial variation of motion has been studied by many researchers, previously. The early studies are accomplished by Abdel-Ghaffar [65], Abdel-Ghaffar and Trifunac [66]. Some of the recent studies are carried out by Romanelli [67], Zembaty [68] and Todorovska [69] which are mentioned further in this section.

The first study [65] concerns the effects of the differential motion of the foundations on the response of a bridge. First part of the study deals with the analysis of a simple beam under harmonic excitation. Two end supports of the beam have been subjected to harmonic ground motion with different phases. The response has been obtained as displacement amplitudes at specific points of the beam in the frequency domain. In the second part of the study, a numerical method has been developed to analyze the dynamic soil-bridge interaction of a 2D bridge model. The bridge was supported by two rigid abutments with semi-circular foundation resting on elastic half-space and excited by the input motion in the form of plane SH waves. Moreover, a parametric study was carried out in order to determine the effect of the soil properties on the response of the single span bridge. The results indicate that the response depends on the stiffness, the mass and the damping characteristics of the bridge relative to that of soil. It is also stated that the symmetric modes are excited for the support motion in phase whereas the antisymetric modes are dominant when the abutments move out of phase. In addition, the peak response displacement amplitudes are magnified at the natural frequencies in the case of non-vertical excitation.

The second study accomplished by Abdel-Ghaffar and Trifunac [66] is based on the same theory with the first study. Similarly, the response of the 2D model of the multispan bridge in frequency domain is investigated (Fig. 6.1). In this case, the following issues are discussed:

- the effect of span length to the response,
- the ratio of successive span length,
- the ratio of rigidity of girders to that of the soil,
- the effect of angle of the traveling SH wave.

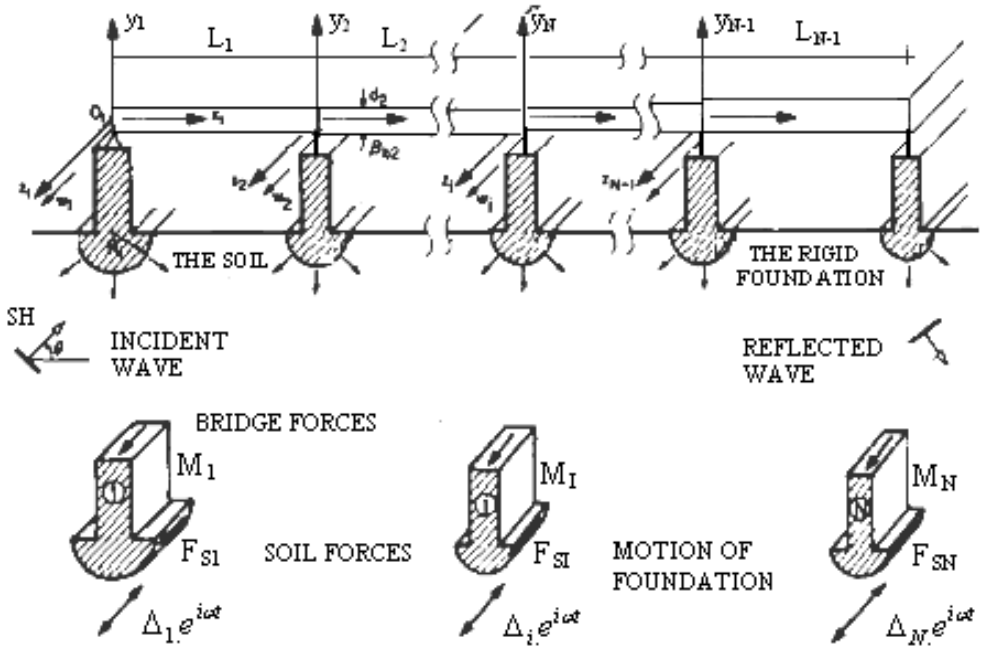

Figure 6.1 : 2D Multispan bridge under the effect of SH waves [66].

The effect of traveling seismic waves has also been studied by Werner et al. [70]. A numerical procedure has been developed to analyze the dynamic response of the soil-structure system. The bridge system has been modeled using finite element methods and the soil has been modeled employing boundary elements as a homogeneous elastic half space.

Another study carried out by the same researchers [29] involves the three dimensional seismic response of a bridge under the effect of the seismic waves using the same numerical procedure described above. The dynamic response of a single span bridge resting on a soft soil medium has been obtained using the developed methodology (Fig. 6.4). The traveling seismic effect has been discussed considering

the incident wave angle and the displacement amplitude on different sections of the bridge. For SH wave angle $\theta_V = \theta_H = 0$, the wave propagation is parallel to the longitudinal direction of the bridge and the particle motion is in the transverse direction. The plots of the response indicate that the structure displacements are essentially antisymetric about the midspan when odd multiples of the half wavelength are equal to the bridge span. For incident wave angle $\theta_V = 90$ and $\theta_H = 0$, the waves propagate vertically and the particle motion is identical at every point of the foundation. Hence, there is no traveling wave effect and bridge response amplitudes are symmetrical about the midspan for this case.

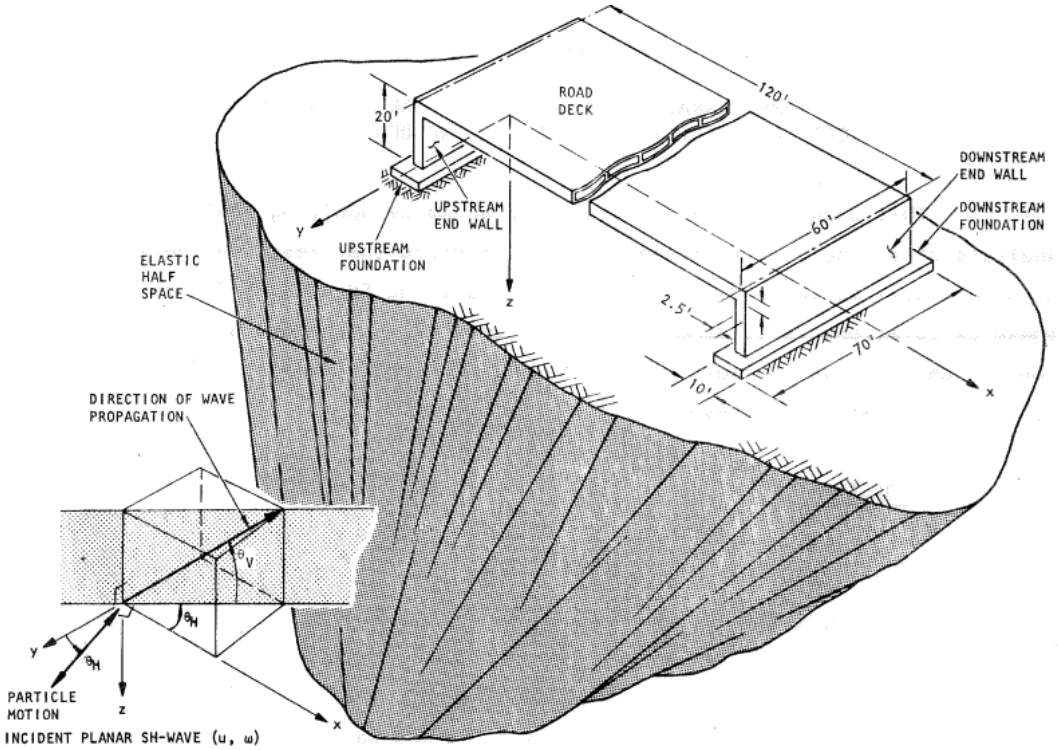

Figure 6.2 : The 3D bridge model under the effect of SH waves [70].

The recent studies on this subject generally focus on the spatial variations of the ground motion due to the size of the structure or heterogeneities of the underlying soil. The effect of this differential motion is also named as the “wave passage effect” which is the phase shift of the seismic arrivals at different parts of the structure. The study of Romanelli et al. [67] deals with the wave passage effect to assess the importance of the non-synchronous seismic excitation of long structures. Another study conducted by Zembaty [68] concerns the random vibrations of a bridge under the propagating seismic excitations and the joint effects of the pseudostatic and the dynamic vibrations. In addition, Todorovska [69] has studied the wave passage effect

and the dynamic soil-structure interaction on the response of the base-isolated buildings with embedded foundations.

6.3 The Sample Problem

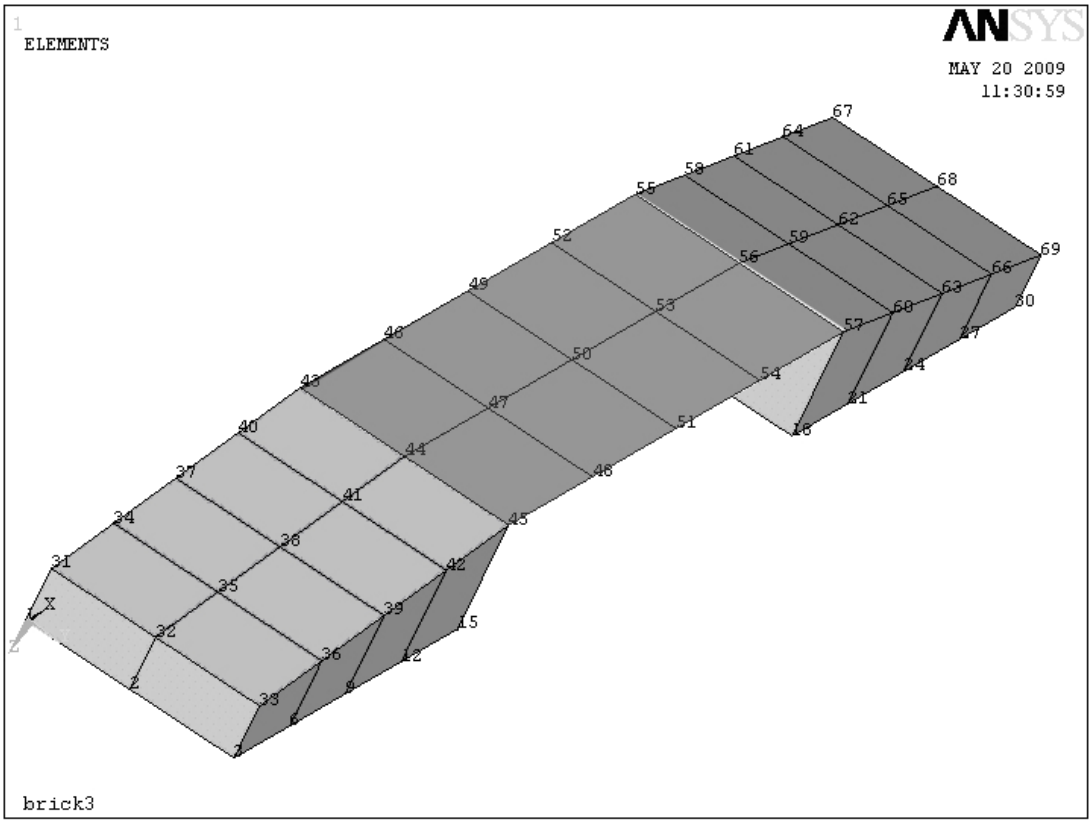

Figure 6.3 : 3D Finite element model of the bridge.

The numerical procedure developed in this study has been used to analyze the wave propagation effect for a bridge-backfill system of 84 meters length and 12 meters width (Fig. 6.3). The finite element modeling of the superstructure has been accomplished by ANSYS [60] using the eight node brick element (SOLID45) for the backfill; elastic thin shell element (SHELL63) for the road deck and the membrane shell element (SHELL41) for the retaining walls surrounding the backfill soil. The brick element has translational degrees of freedom, u_x, u_y and u_z at each node. The thin shell element that is used for modeling the roadway slab has 4 degrees of freedom at each node; translations in the *x*, *y*, and *z* directions and rotation about *y*-axis. The elastic membrane element representing the surrounding walls has only translational degrees of freedom in *x*, *y*, and *z* directions (Figure 6.4). The material and the geometrical properties of the finite element model are summarized in Table 6.1.

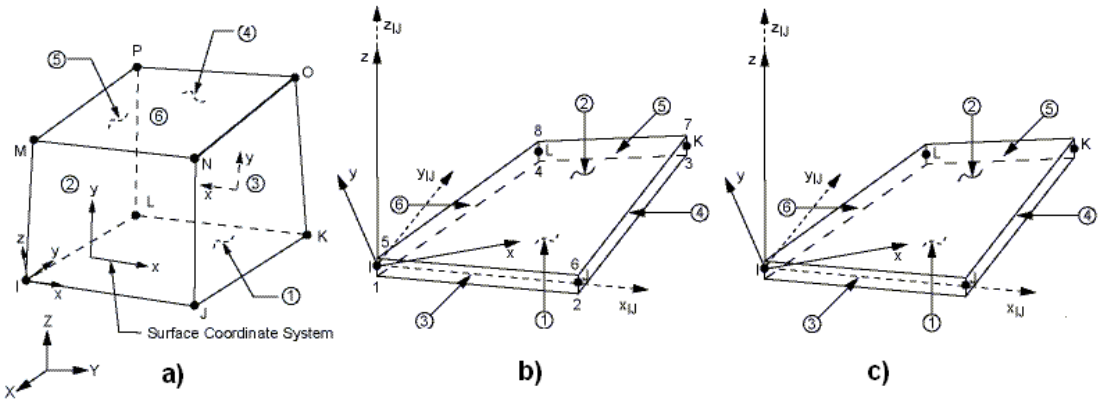

Figure 6.4 : Solid, thin shell and membrane elements [60].

Table 6.1: Physical and material properties of the bridge

MATERIAL PROPERTIES	BACKFILL	RETAINING WALLS	BRIDGE DECK	SOIL
Modulus of Elasticity (N/m^2)	1.82x10^8	1.99x10^{10}	1.99x10^{10}	1.82x10^8
Poisson's Ratio	0.33	0.15	0.15	0.33
Type of Finite Element	Brick	Plane Stress-Membrane Shell	Elastic Thin Shell	Elastic Half-Space
Thickness	--	0.3 m	1.0 m	---
DOF at each node of the element	u_x, u_y, u_z	u_x, u_y, u_z	u_x, u_y, u_z, r_y	u_x, u_y, u_z
Number of Elements	20	16	8	16

Prior to the dynamic analysis of soil-structure system, a modal analysis has been performed in order to determine the free vibration characteristics of the bridge: natural frequencies, mode shapes and modal participation factors. The eigenvector of each mode is normalized to the mass matrix. In addition, the mass matrix and the stiffness matrix are obtained and partitioned as upper nodes and interface in order to use in the substructuring. Some of the natural modes of bridge backfill system are presented in Figs. A.1 to A.4. Since the natural frequencies vary within the wide range of 1.37 Hz and 150 Hz., it has been difficult to distinguish between the natural modes concerning the roadway slab and the backfill. Thus, a modal analysis of the

road deck has been carried out apart from the bridge-backfill system. The natural frequencies and the mode shapes involving the bridge deck are shown in Fig. A.5. The dominant frequencies in the dynamic response of bridge backfill system are identified by examining the modal participation factors and the effective masses of each natural mode of the system in the next section.

6.4 The Modal Participation Factors

The modal participation factor Γ_n is a measure of the contribution of each mode to the dynamic response of the structure. For any arbitrary mode *n*, the equation of motion can be expressed as:

$$\ddot{y}_n(t) + 2\xi_n \omega_n \dot{y}_n(t) + \omega^2 y_n(t) = \frac{\{\phi_n\}^T \{p(t)\}}{M_n} \qquad \textbf{(6.1)}$$

where ω_n : the nth natural frequency of the structure, ξ_n : the damping ratio of the nth mode, ω: the excitation frequency, $\{\phi_n\}^T$: the transpose of the nth eigenvector, $\{p(t)\}$: the load vector and M_n: the modal mass (generalized mass) determined as $M_n = \{\phi_n\}^T [M] \{\phi_n\}$.

For the dynamic analysis developed, the mode shape vectors are normalized to the lumped mass matrix. Therefore, the modal mass for each mode is unity. For the case of base excitation under earthquake loading, the effective earthquake loading vector, $\{p_{eff}(t)\}$ is expressed as:

$$\{p_{eff}(t)\} = [M]\{r\}.\ddot{v}_g(t) \qquad \textbf{(6.2)}$$

where $\{r\}$ is the displacement transformation vector which is composed of displacements at each degrees of freedom resulting from unit support displacement and $\ddot{v}_g(t)$ is the earthquake time history. For a multistory building under the horizontal ground motion, the vector $\{r\}$ is simply a unit column vector. Introducing the upper equation into the equation of motion, the formulation becomes:

$$\ddot{y}_n(t) + 2\xi_n \omega_n \dot{y}_n(t) + \omega^2 y_n(t) = \frac{\{\phi_n\}^T [M]\{r\}}{\{\phi_n\}^T [M]\{\phi_n\}} \ddot{v}_g(t) \quad \textbf{(6.3)}$$

Considering the total dynamic response of the structure, the importance of each mode depends on the spatial distribution of the earthquake loading. The contribution of the individual modes is expressed in terms of the modal participation factor, Γ_n which is defined as [62];

$$\Gamma_n = \frac{\{\phi_n\}^T [M]\{r\}}{\{\phi_n\}^T [M]\{\phi_n\}} \quad \textbf{(6.4)}$$

Since eigenvectors are normalized to the mass matrix in this study, the modal participation factors are simply the upper part of the fraction. In addition to the modal participation factors, the effective mass of each natural mode is calculated revealing the contribution of each mode. Effective mass is defined as:

$$M_n^* = \frac{(\Gamma_n)^2}{\{\phi_n\}^T [M]\{\phi_n\}} \quad \textbf{(6.5)}$$

Examining the effective masses of the modal analysis of bridge deck, it is clearly observed that the bending mode in *x-z* plane (first mode), the bending mode in *x-y* plane (7th mode), 11th mode are the dominant modes in *z*, *y* and *x* directions, respectively (Fig. 6.11). The modal analysis of the bridge deck has 27 degrees of freedom. However, except for the first bending mode in Z direction (1.04 Hz) and mode number 7 (bending in *x-y* plane), none of the bridge deck modes has significant effect on the dynamic response of the bridge backfill system.

Observing the natural mode shapes and the effective mass of each mode of the total system reveal different results (Tables 6.2 to 6.4).

In the *z* direction;

- The first mode shape coincides with the first bending mode of the bridge deck and is a dominant mode similar to the modal analysis of the bridge deck comparing the effective mass values.
- The following dominant modes are modes 45, 57, 75, 87 and 92 corresponding to backfill deformation.

- The modes 57 and 75 are the coupled modes. Both bridge slab and the backfill part deform extensively.
- The effective masses are distributed uniformly among these modes indicating that each of these modes has almost the same effect on the dynamic response.

The results in the *y* direction are summarized below:

- The most dominant modes in the *y* direction are the 5th and the 12th modes with 9.42 Hz and 10.51 Hz frequencies, respectively. In both modes, the backfill part is deformed.
- The other dominant modes in the *y* direction (20, 31) have the same effect on the dynamic response. These modes are related to the deformation of the backfill parts.
- Mode 48 coincides with 7th mode of the bridge deck which is the bending mode in *x*-*y* plane.

The results in the *x* direction are summarized below:

- Mode numbers 13, 17, 58 and 71 have significant effective masses in the *x* direction. Especially, the lower mode 13 having a natural frequency of 10.71 Hz has the highest effective mass among the other modes indicating that it is one of the dominant modes in X direction. The corresponding mode shapes reveal that these modes refer to the backfill deformation.

Table 6.2: Natural modes of the bridge-backfill system.

mode	frequency	*x* direction effective mass	*x* direction mass fraction	*y* direction effective mass	*y* direction mass fraction	*z* direction effective mass	*z* direction mass fraction
1	1.04	0.00	0.00	0.00	0.00	**75079.40**	**0.23**
2	4.16	3.15	0.00	0.00	0.00	0.00	0.23
3	9.06	0.00	0.00	0.00	0.00	2445.40	0.24
4	9.42	0.00	0.00	0.00	0.00	0.00	0.24
5	9.42	0.00	0.00	**102155.00**	**0.32**	0.00	0.24
6	9.86	20230.20	0.06	0.00	0.32	0.00	0.24
7	9.87	0.00	0.06	0.00	0.32	17.34	0.24
8	10.25	903.44	0.07	0.00	0.32	0.00	0.24
9	10.26	0.00	0.07	0.00	0.32	24.42	0.24
10	10.34	0.00	0.07	919.86	0.32	0.00	0.24
11	10.35	0.00	0.07	0.00	0.32	0.00	0.24
12	10.51	0.00	0.07	**117836.00**	**0.69**	0.00	0.24
13	10.71	**110023.00**	**0.41**	0.00	0.69	0.00	0.24
14	10.83	0.00	0.41	0.00	0.69	0.00	0.24
15	10.83	0.00	0.41	14225.40	0.73	0.00	0.24

Table 6.2 (Continued): Natural modes of the bridge-backfill system.

mode	frequency	*x* direction effective mass	*x* direction mass fraction	*y* direction effective mass	*y* direction mass fraction	*z* direction effective mass	*z* direction mass fraction
16	11.12	0.00	0.41	0.00	0.73	85.82	0.24
17	11.17	**72429.10**	**0.63**	0.00	0.73	0.00	0.24
18	11.72	0.00	0.63	0.00	0.73	3916.85	0.25
19	11.73	0.00	0.63	0.00	0.73	0.00	0.25
20	11.73	0.00	0.63	**24531.10**	**0.81**	0.00	0.25
21	12.13	11616.50	0.67	0.00	0.81	0.00	0.25
22	12.43	0.00	0.67	0.00	0.81	18.39	0.25
23	12.64	162.02	0.67	0.00	0.81	0.00	0.25
24	12.76	0.00	0.67	0.00	0.81	1574.46	0.26
25	12.81	0.00	0.67	0.00	0.81	0.00	0.26
26	12.81	0.00	0.67	3148.61	0.82	0.00	0.26
27	12.96	13325.40	0.71	0.00	0.82	0.00	0.26
28	13.65	0.00	0.71	0.00	0.82	9503.42	0.29
29	13.78	3379.33	0.72	0.00	0.82	0.00	0.29
30	13.83	0.00	0.72	0.00	0.82	0.00	0.29
31	13.83	0.00	0.72	**35067.50**	**0.93**	0.00	0.29
32	14.65	0.00	0.72	0.00	0.93	838.95	0.29
33	14.65	2159.95	0.73	0.00	0.93	0.00	0.29
34	14.89	0.00	0.73	0.00	0.93	655.00	0.29
35	14.89	4426.35	0.74	0.00	0.93	0.00	0.29
36	15.14	0.00	0.74	0.00	0.93	5582.74	0.31
37	15.15	7.61	0.74	0.00	0.93	0.00	0.31
38	15.36	0.00	0.74	0.00	0.93	0.00	0.31
39	15.36	0.00	0.74	126.18	0.93	0.00	0.31
40	16.10	0.00	0.74	0.04	0.93	0.00	0.31
41	16.85	0.00	0.74	0.00	0.93	0.00	0.31
42	16.93	0.00	0.74	0.00	0.93	0.00	0.31
43	16.93	0.00	0.74	1866.03	0.93	0.00	0.31
44	17.12	0.00	0.74	0.00	0.93	0.00	0.31
45	17.34	0.00	0.74	0.00	0.93	**30135.90**	**0.40**
46	17.34	80.31	0.74	0.00	0.93	0.00	0.40
47	18.59	0.00	0.74	7.63	0.93	0.00	0.40
48	21.95	0.00	0.74	18305.50	0.99	0.00	0.40
49	22.74	0.00	0.74	0.00	0.99	0.84	0.40
50	22.90	0.00	0.74	0.00	0.99	21633.00	0.47
51	22.90	871.82	0.74	0.00	0.99	0.00	0.47
52	23.40	0.25	0.74	0.00	0.99	0.00	0.47
53	24.46	0.00	0.74	0.00	0.99	7.79	0.47
54	31.43	0.00	0.74	0.00	0.99	1633.78	0.48
55	32.53	0.00	0.74	0.00	0.99	0.00	0.48
56	32.57	490.69	0.75	0.00	0.99	0.00	0.48
57	32.58	0.00	0.75	0.00	0.99	**24958.80**	**0.55**
58	36.67	**31985.90**	**0.85**	0.00	0.99	0.00	0.55
59	37.38	0.00	0.85	319.34	0.99	0.00	0.55
60	37.68	0.00	0.85	0.00	0.99	2407.47	0.56
61	38.45	0.00	0.85	0.00	0.99	0.00	0.56
62	39.25	0.00	0.85	0.00	0.99	3571.84	0.57
63	39.26	18775.10	0.90	0.00	0.99	0.00	0.57
64	40.66	0.00	0.90	1478.61	0.99	0.00	0.57
65	42.08	0.00	0.90	0.00	0.99	0.00	0.57

Table 6.2 (Continued): Natural modes of the bridge-backfill system.

mode	frequency	*x* direction effective mass	*x* direction mass fraction	*y* direction effective mass	*y* direction mass fraction	*z* direction effective mass	*z* direction mass fraction
66	42.63	0.00	0.90	0.00	0.99	2778.70	0.58
67	42.65	660.49	0.91	0.00	0.99	0.00	0.58
68	42.82	0.00	0.91	208.28	1.00	0.00	0.58
69	43.48	0.00	0.91	0.00	1.00	0.00	0.58
70	43.89	0.00	0.91	0.00	1.00	88.84	0.58
71	43.89	23131.70	0.98	0.00	1.00	0.00	0.58
72	43.89	0.00	0.98	4.32	1.00	0.00	0.58
73	44.07	0.00	0.98	0.00	1.00	0.00	0.58
74	44.84	1013.73	0.98	0.00	1.00	0.00	0.58
75	44.89	0.00	0.98	0.00	1.00	**40038.60**	**0.71**
76	45.19	0.00	0.98	1253.56	1.00	0.00	0.71
77	45.22	0.00	0.98	0.00	1.00	0.00	0.71
78	47.88	1268.46	0.99	0.00	1.00	0.00	0.71
79	48.02	0.00	0.99	0.00	1.00	1830.42	0.71
80	48.37	0.00	0.99	15.37	1.00	0.00	0.71
81	48.46	0.00	0.99	0.00	1.00	0.00	0.71
82	48.77	134.24	0.99	0.00	1.00	0.00	0.71
83	49.31	0.00	0.99	0.00	1.00	2561.21	0.72
84	51.07	0.00	0.99	34.69	1.00	0.00	0.72
85	51.09	0.00	0.99	0.00	1.00	0.00	0.72
86	51.10	481.64	0.99	0.00	1.00	0.00	0.72
87	51.12	0.00	0.99	0.00	1.00	**30301.70**	**0.81**
88	53.42	0.00	0.99	24.63	1.00	0.00	0.81
89	56.99	8.75	0.99	0.00	1.00	0.00	0.81
90	59.22	0.00	0.99	0.00	1.00	0.00	0.81
91	59.22	0.00	0.99	15.38	1.00	0.00	0.81
92	59.25	0.00	0.99	0.00	1.00	**30404.30**	**0.91**
93	59.25	1632.13	0.99	0.00	1.00	0.00	0.91
94	59.66	72.43	0.99	0.00	1.00	0.00	0.91
95	62.37	0.00	0.99	0.00	1.00	411.19	0.91
96	64.85	0.00	0.99	0.00	1.00	0.00	0.91
97	69.32	0.00	0.99	90.84	1.00	0.00	0.91
98	74.61	0.00	0.99	8.55	1.00	0.00	0.91
99	74.61	0.00	0.99	0.00	1.00	0.00	0.91
100	74.68	2364.11	1.00	0.00	1.00	0.00	0.91
total mass				**321648**			

6.5 The Response of the Bridge-Backfill System under Harmonic Excitation

Harmonic response analysis is a technique used to determine the steady-state response of a structure to loads or displacements that vary harmonically with time. The purpose is to determine the response at varying frequencies. Using the results of the analysis, the graph of the displacement response versus the frequency is obtained at different nodal points. The "Peak" values of the response are then identified indicating important features about the dynamic behavior of the structure.

Considering the matrix of equations of motion;

$$[M]\{\ddot{u}\}+[C]\{\dot{u}\}+[K]\{u\}=\{F_a\} \qquad \textbf{(6.6)}$$

$\{F_a\}$: the applied load vector; [M]: the mass matrix; [C]: the damping matrix; [K]: the stiffness matrix and $\{\dot{u}\},\{\ddot{u}\}$ and $\{u\}$: the acceleration, the velocity and the displacement vectors of the nodes, respectively. Since there is the structural damping, points of the structure move with the same frequency but not always in the same phase. Therefore, the displacement vector (and the force vector) can be defined as:

$$\{u\}=\{u_{max}\}e^{i(\omega t+\phi)} \qquad \textbf{(6.7)}$$

where $\{u_{max}\}$: the maximum displacement vector; ϕ: displacement phase shift and ω: the angular frequency of harmonic motion.

In order to determine the dynamic behavior of the bridge-backfill system, the harmonic response of the structure has been initially analyzed using ANSYS [60]. Even though the numerical study focuses on the traveling wave effect, it is of great importance to compare the peak frequencies under uniform harmonic motion with those obtained by the numerical procedure to identify the effect of the traveling seismic waves.

In the numerical procedure developed for this study, the input excitation is in the form of a plane SH wave motion. The SH wave has a displacement amplitude of 2 units with the shear wave velocity of 213 m/s and originates from an infinite distance of the elastic half-space soil medium. Since the length of the bridge-backfill system

is close to the wavelength of the seismic wave, the plane SH wave arriving to the base causes different values of the displacement at every interface node. Therefore, the excitation at the interface is not uniform.

Unlike the response under the traveling waves, the harmonic response of the structure is obtained employing uniform base excitation with harmonic displacements. Therefore, it is essential to compare the response under traveling waves with the uniform harmonic base excitation.

The harmonic analysis has been carried out for three directions; the *x* and the *y* directions separately. The displacements at the interface nodes have been constrained except for the direction of the harmonic motion for each analysis.

The displacement response has been obtained at three different nodes on the bridge deck. The graphs of the response versus frequency in each direction have been plotted for the nodes 47, 50 and 53 as shown in Figs. 6.5 to 6.6. Node 50 is the midpoint of the road deck and 47 and 53 are the closest nodes to the midpoint. Each graph indicates that the symmetric nodes 47 and 53 always move with the same amplitude and direction regardless of the direction of the harmonic motion. In addition, the response values of these nodes are always equal to or smaller than the response of the midpoint.

The peak response for the harmonic excitation in *x* direction occurs at 12 Hz and 64 Hz. Considering the mode shapes and the effective modal mass values; the first frequency coincides with a dominant natural mode (Mode No.21) in the *x* direction, which corresponds to the backfill deformation.

The peak response for the harmonic excitation in the *y* direction occurs at 11 Hz, 17 Hz and 30 Hz. The deformed shape of the response at f = 11 Hz corresponds to the 12th natural mode obtained from the modal analysis. The effective modal mass of this natural mode also implies that the peak frequency corresponds to a dominant natural frequency. Similarly, the deformed shape of the peak response at f = 30 Hz is related to a coupled mode shape (Mode Number 54), but the effective mass of the mode is not high compared to the other modes.

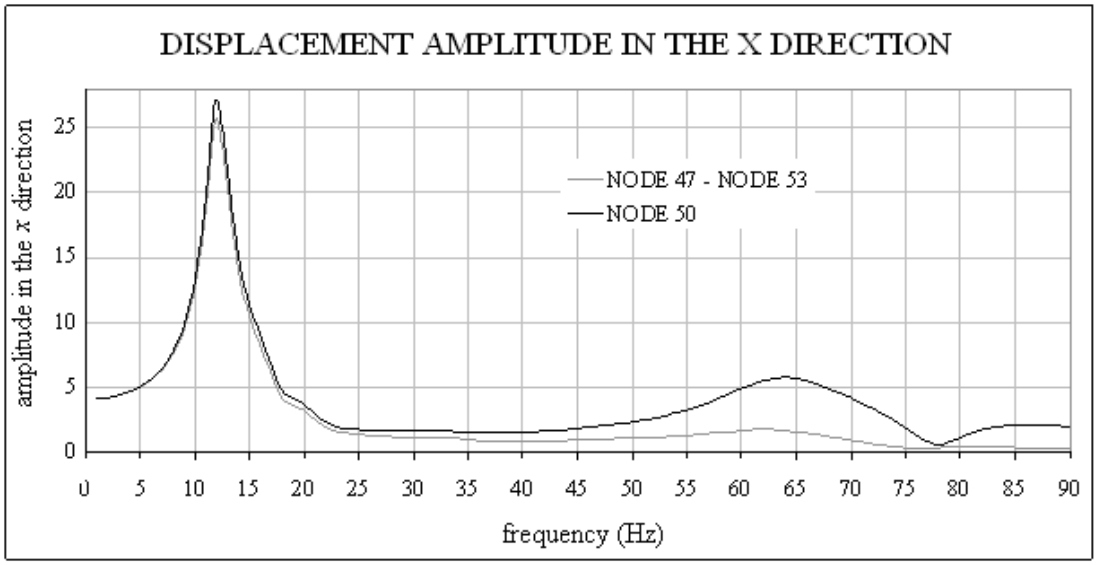

Figure 6.5 : Harmonic motion in the *x* direction.

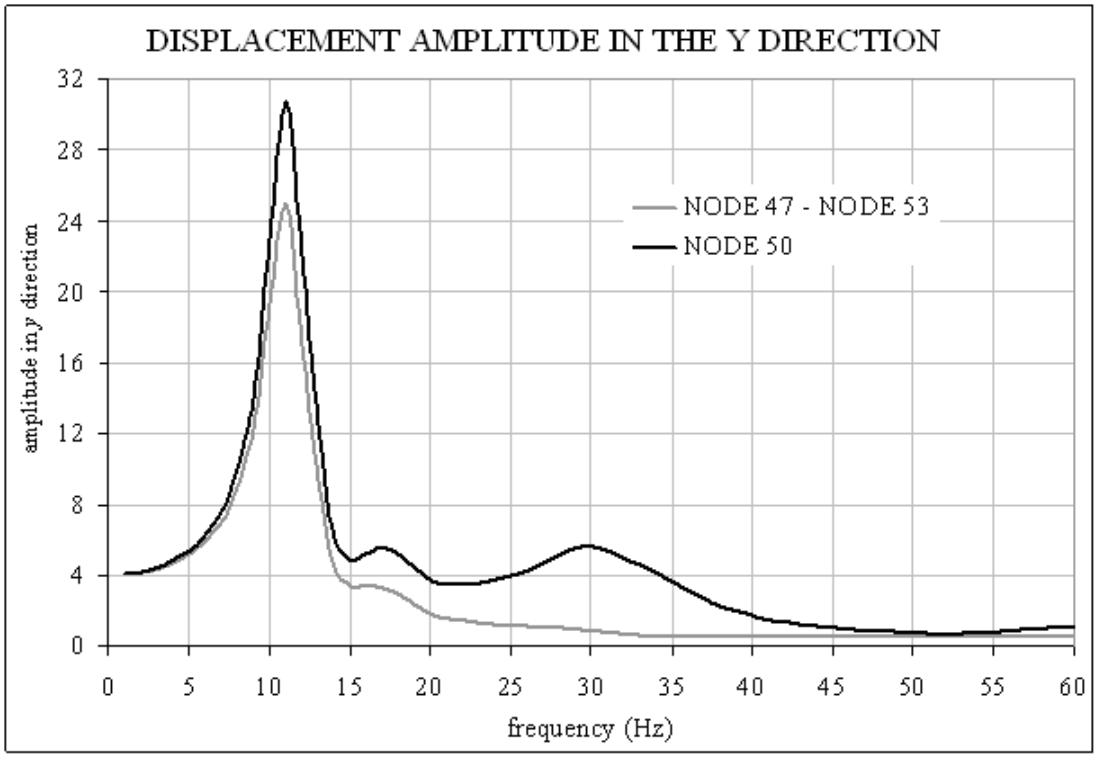

Figure 6.6 : Harmonic motion in the y direction.

6.6 The Response of Bridge-Backfill System under Plane SH Wave Excitation

The numerical analysis which has been developed for the dynamic response of the bridge under the traveling wave effect has been applied to the sample problem under three different conditions:

Case A1: The plane SH wave propagates in the three dimensional half-space which is almost a rigid soil medium.

Case B1: The backfill soil has the same dynamic properties with the underlying soil (medium clay).

Case C1: The backfill soil has a very low mass density value compared to the bridge and the underlying soil (medium clay).

The material properties of the underlying soil and the backfill soil surrounded by the retaining walls are given in Table 6.3. The displacement amplitudes in the *y* direction are plotted against the excitation frequency of the incident SH wave for Cases A1, B1 and C1 in Figs. 6.12 to 6.14. The results are discussed in the following section.

Table 6.3: Material properties of the soil for Cases A1, B1 and C1.

case	UNDERLYING SOIL				BACKFILL SOIL			
	soil type	G	ρ	v_s	soil type	G	ρ	v_s
A1	granite	2.52×10^{10}	2800	3000	med. clay	6.86×10^{7}	1500	213.85
B1	med. clay	6.86×10^{7}	1500	213.85	med. clay	6.86×10^{7}	1500	213.85
C1	med. clay	6.86×10^{7}	1500	213.85	fict. mater.	6.86×10^{7}	38.12	1341.4

υ = 0.33 (Poisson's ratio)
G = Shear modulus (N/m^2)
ρ = Mass density (kg/m^3)
v_s = Shear wave velocity (m/s)

6.7 The Discussion of the Results

Firstly, the results of the uniform harmonic motion in the *y* direction are compared with the values obtained from the numerical analysis under SH wave traveling along the *x* direction (horizontal and vertical angles of the wave, θ_H and θ_V are zero) for a very rigid soil condition. The solution under rigid soil conditions corresponds to Case A1 that is defined in Table 6.5. The peak response of the midpoint node 50 occurs at 11 Hz, 17 Hz and 30 Hz for uniform harmonic excitation as observed in Fig. 6.7. The other symmetrical nodes also reach their peak values of the amplitude at the same frequencies but with smaller amplitudes.

However, the peak response under the effect of the traveling SH wave does not occur at the same frequency values (Fig. 6.7). Displacement amplitude at the midpoint reaches its peak value at 8.5 Hz and 18 Hz. In addition, the uniform harmonic response curves of symmetrical nodes coinciding for the entire frequency range are no longer identical for the analysis of the Case A1. The curves of the response for these nodes are still smaller than the midpoint, but the displacement amplitude of node 47 is less than that of node 53 for the initial peak frequency of 8.5 Hz. Furthermore, the second peak response of node 47 is captured at 15 Hz, whereas the peak response of node 47 occurs at 14 Hz with a larger displacement amplitude.

Therefore, it can be deduced that the response for the uniform harmonic excitation and the response under SH wave propagation resemble but are not identical even for the same rigid base conditions. This is an expected consequence since the input motion at the base is different for each point with respect to the coordinates of the nodes for the Case A1. On the contrary, the uniform harmonic analysis of the bridge embankment system is conducted by applying the same uniform displacement amplitude at the base, which is the general representation of the ground motion.

Secondly, the response curves of Case A1, B1 and C1 are compared in order to determine the effect of the underlying and backfill soil conditions. Figs. 6.7 and 6.9 indicate that both the displacement amplitude and the peak response frequency increase as the underlying soil conditions get stiffer. The peak response values for Case B1 (where the underlying soil is medium clay) are captured at 1.04 Hz, 2.20 Hz, 2.60 Hz, 2.90 Hz, 4.40 Hz and 6.70 Hz. The response of the system caused by the incident SH wave is almost completely damped after the last peak value at 6.7

Hz. On the contrary, the first peak response for the rigid soil conditions (Case A1) is reached at 8.5 Hz and the motion is damped at frequency values higher than 15 Hz. In this case, it can be concluded that increasing the stiffness of soil increases both the displacement amplitude and the frequency at which the peak responses are obtained. In addition, there is a greater extent of fluctuation in the amplitude values for the case of the soft soil conditions (Case B1).

Finally, the dynamic analysis is carried out for Case C1, which has the same type of underlying soil (medium clay) as Case B1 but with a stiffer backfill material. Comparing the results of the two cases indicate that softer backfill material magnifies the ground motion. Because, the amplitude values for Case C1 slightly exceeds the initial displacement amplitude at 3.5 Hz. The rest of the peak response amplitudes are smaller than the initial value. In addition, it is clear that the response of each node on the road deck is much closer to each other than for Case B1.

Cases A1, B1 and C1 are analyzed under the effect of the traveling SH waves with amplitude of 2 units and the propagation direction coinciding with *x* axis of the bridge model. The solution of each case has been conducted by the computer program developed in this study using the methodology developed by Dendrou et al. [29]. The response curves of Case C1 indicate that the solutions obtained in this study are in good agreement with the results obtained by the authors. Verifying the developed numerical procedure in this study, the bridge-backfill models are reanalyzed implementing the revised numerical technique, which includes the effect of damping on the dynamic transformation matrix of the system. The response curves of Cases A2, B2 and C2 that are obtained by the new methodology are given in Figures 6.7 to 6.9.

Comparing the results of Case A1 and Case A2 corresponding to the rigid soil condition, it is clearly seen that the peak response amplitude occurs at the same excitation frequency (8.5 Hz) for both of the analyses. However, the response amplitude at the midpoint for Case A1 is reduced from a value of 20 units to 15 units for Case A2. Similarly, the response values of the other two nodes on the bridge deck are also smaller for Case A2. This reduction of displacement amplitude values is due to the implementation of the damping matrix into the dynamic transformation matrix. Since the response of the bridge deck is obtained by the multiplication of the dynamic transformation matrix and the response vector of the base nodes, the

reduction in the dynamic transformation matrix causes a reduction in the response curves of the superstructure.

The peak response values of Case B2 are also smaller than those of Case B1. Moreover, the displacement amplitude of Case B2 never exceeds the initial value within the frequency range of the analysis. Finally, observing the response curve of Case C2 shows that the motion is almost totally damped for the excitation frequencies higher than 1 Hz using the revised methodology.

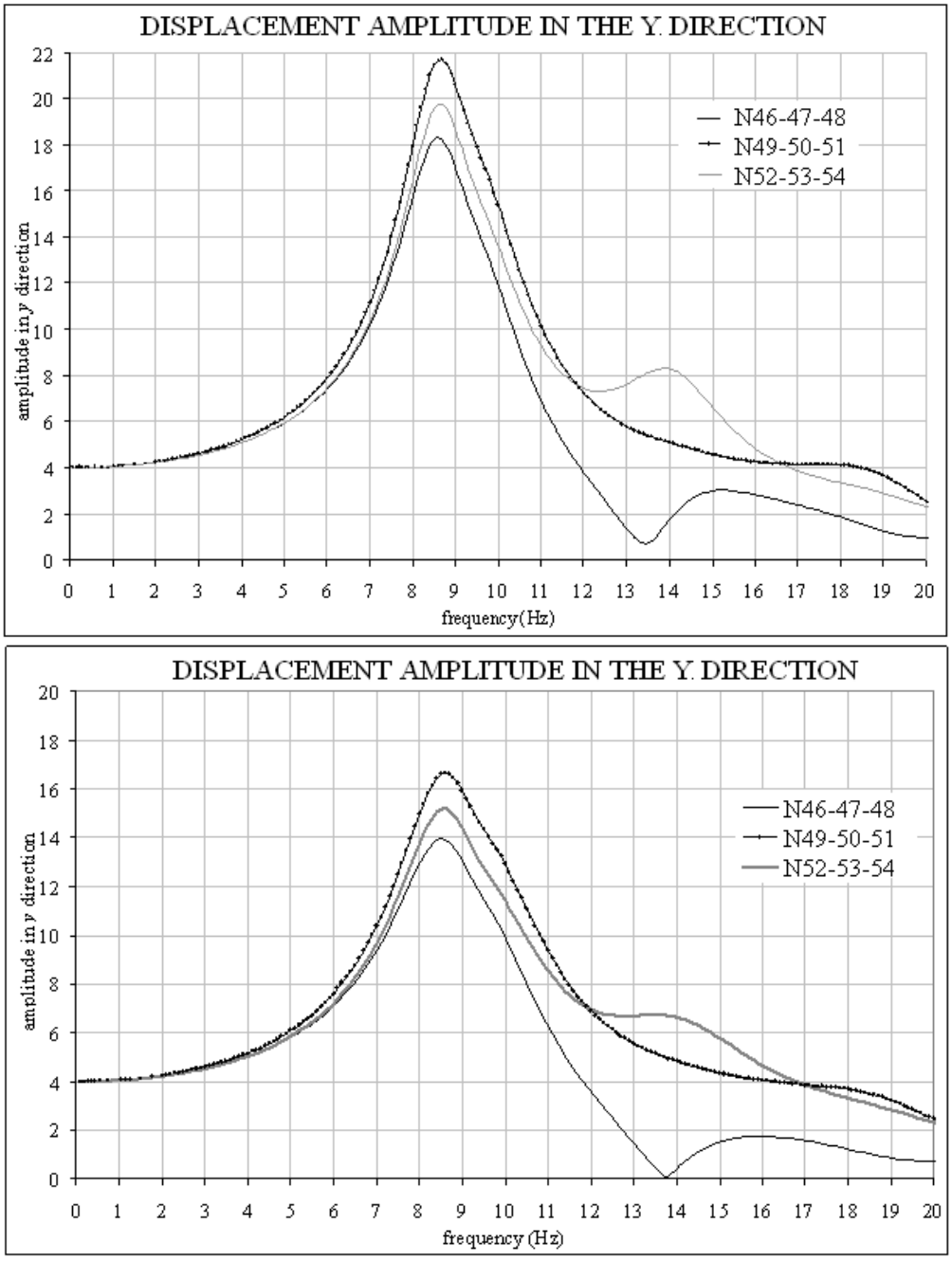

Figure 6.7 : The response in the y direction for the rigid base conditions given as Case A1 (top) and Case A2 (bottom).

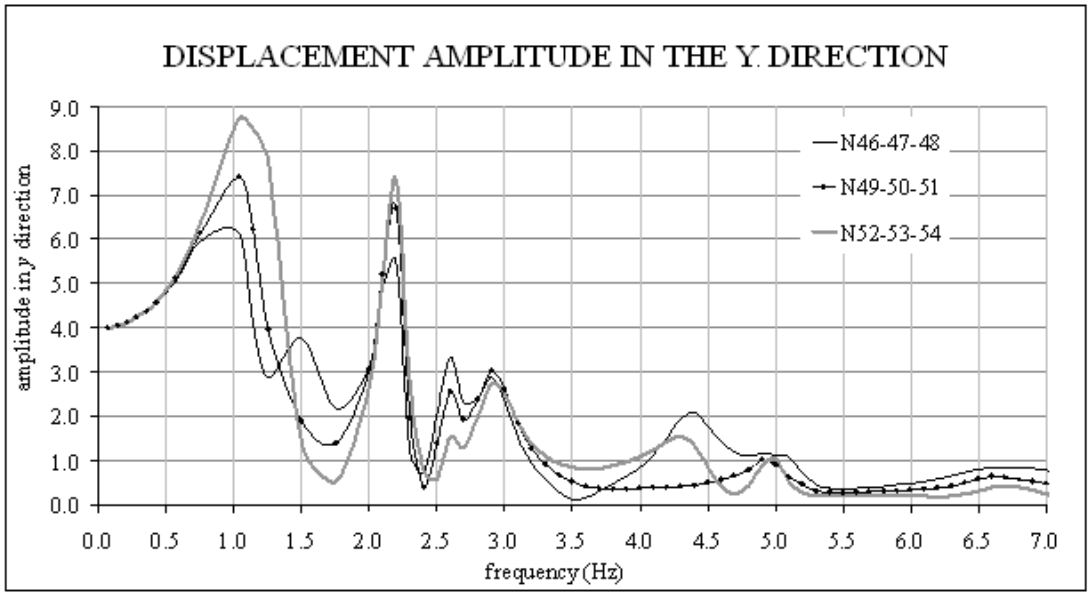

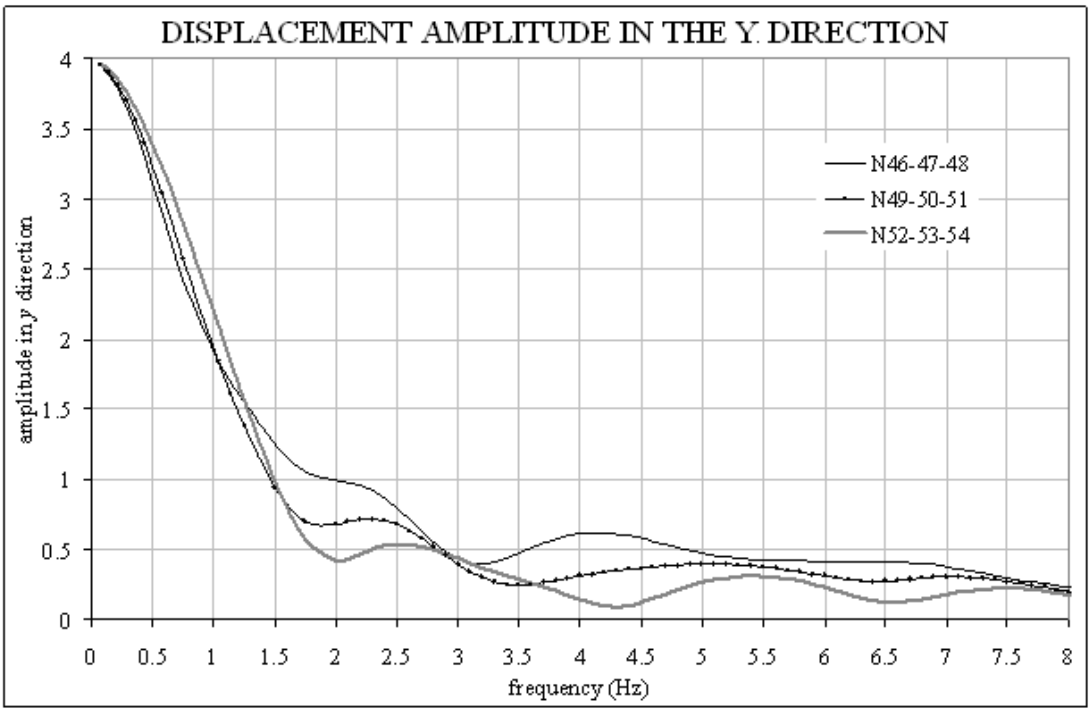

Figure 6.8 : The response in the y direction for Case B1 (top) and Case B2 (bottom).

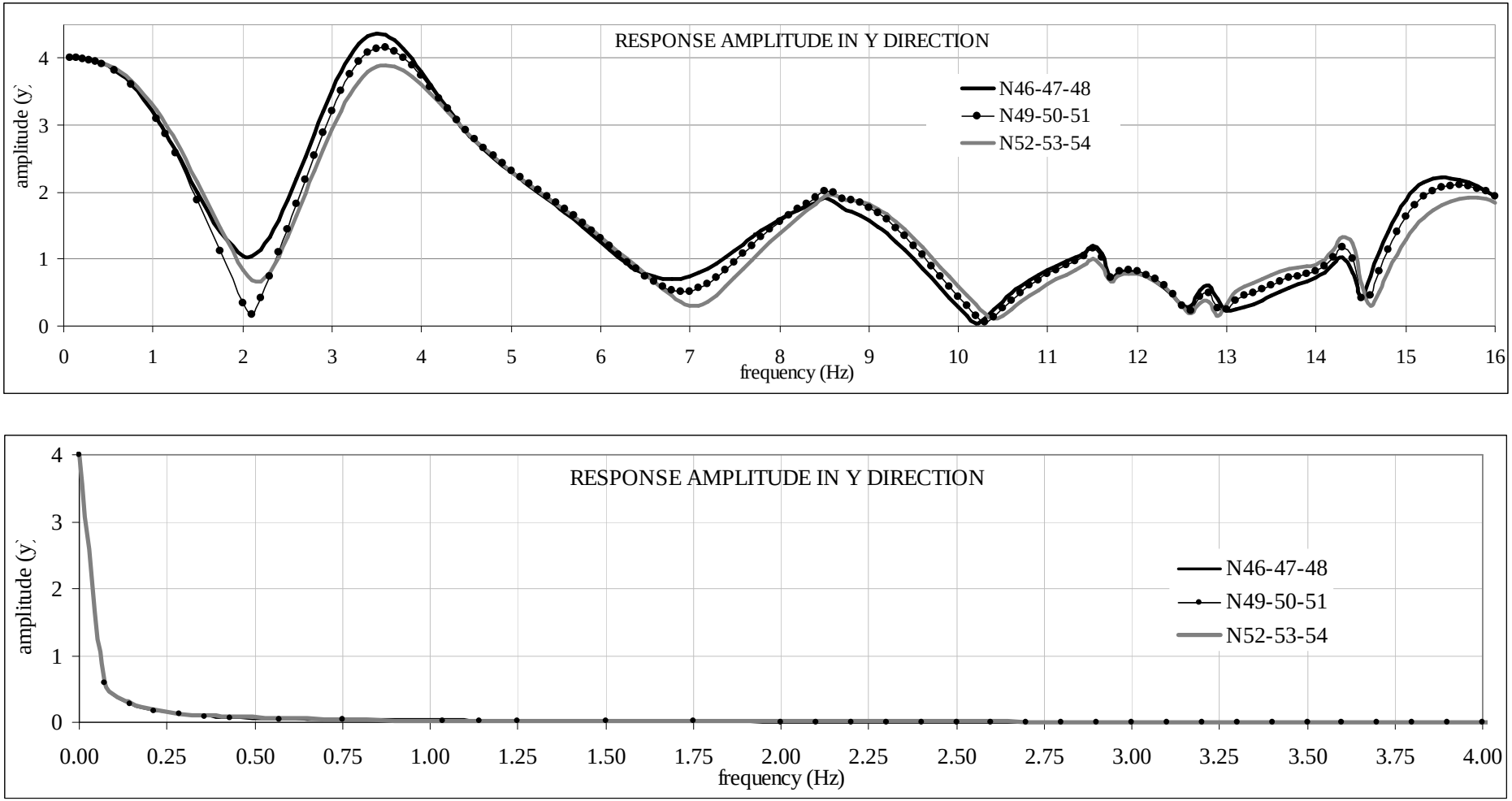

Figure 6.9 : The response in the *y* direction for Case C1 (top) and Case C2 (bottom).

7. SAMPLE PROBLEM 2: 3D MULTISTORY BUILDING

7.1 Introduction

This chapter includes the application of the proposed numerical procedure on a real multistory building in Düzce. The dynamic response curves of each story level and the foundation are obtained for stiff and soft soil conditions. The analysis of the soil-structure system is conducted for both vertically and horizontally propagating SH waves. The response for each case has been used to calculate the maximum drift ratio of the existing building. Eventually, the damage state or level of the structure has been identified using the provisions prepared by FEMA [16,17]. The results are discussed in the last section of this chapter.

7.2 Simplified Equivalent Single-Degree-Of-Freedom (SDOF) System for the Coupled Soil-Structure System

The frequency of the soil-structure system to be analyzed by the numerical procedure developed is compared with the results obtained by the equivalent single degree of freedom (SDOF) representation of the 3D structure. The derivation of the formula to determine the frequency of the coupled system will be summarized by the following equations.

Equations of motion of a an equivalent single degree of freedom (SDOF) soil-structure system are given as:

$$-m\omega^2(u+u_0+h\phi+k(1+2\zeta i)u=m\omega^2u_g \qquad \textbf{(7.1)}$$

$$-m\omega^2(u+u_0+h\phi+k_h(1+2\zeta_x i+2\zeta_g i)u_o=m\omega^2u_g \qquad \textbf{(7.2)}$$

$$-m\omega^2(u+u_0+h\phi+k_r(1+2\zeta_\phi i+2\zeta_g i)\phi=mh\omega^2u_g \qquad \textbf{(7.3)}$$

where m: the effective mass of the structure in its fundamental mode; ω : the excitation frequency of the input motion; h: the effective height of the structure

determined for its fundamental mode; k: the lateral stiffness of mass; ζ : the hysteretic damping ratio of the structure; k_h : spring coefficient of foundation; ζ_x : the hysteretic damping ratio of the foundation; ζ_g : the hysteretic damping ratio of the soil; u_0 : the displacement amplitude of foundation; u_g : the displacement amplitude of the ground motion; u: the displacement amplitude of mass due to elastic deformation of the SDOF system; ϕ : the rocking amplitude of the mass (Fig. 7.1).

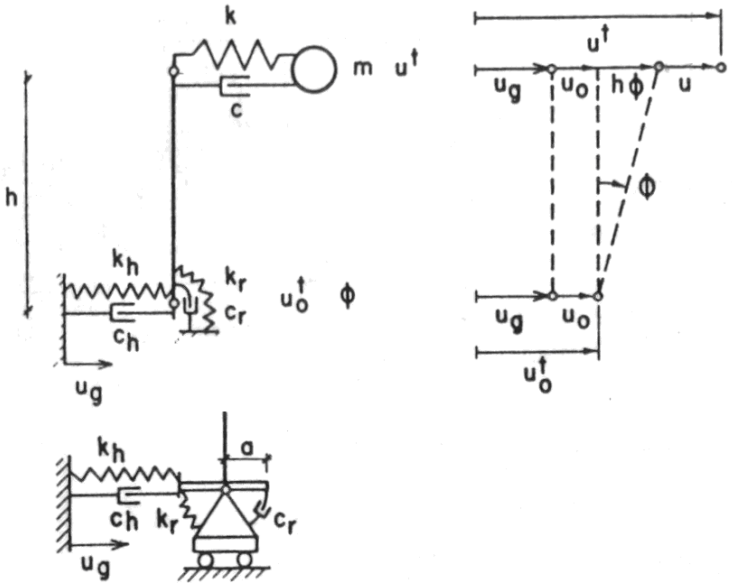

Figure 7.1 : The single degree of freedom model for soil-structure interaction [18].

The set of equations of motion are represented as a single matrix;

$$\begin{bmatrix} \frac{\omega_s^2}{\omega^2}(1+2\zeta i)-1 & -1 & -1 \\ -1 & \frac{\omega_h^2}{\omega^2}(1+2\zeta_x i+2\zeta_g i)-1 & -1 \\ -1 & -1 & \frac{\omega_r^2}{\omega^2}(1+2\zeta_\phi i+2\zeta_g i)-1 \end{bmatrix} \begin{Bmatrix} u \\ u_o \\ h\phi \end{Bmatrix} = \begin{Bmatrix} 1 \\ 1 \\ 1 \end{Bmatrix} u_g \qquad \textbf{(7.4)}$$

where ω_s : the fixed based natural frequency of the structure; ω_h : the natural frequency of the structure without rocking vibration; ω_r : the natural frequency of the structure without horizontal vibration;.

Eliminating u_0 and $h\phi$ form the above equation yields;

$$u_0 = \frac{\omega_s^2}{\omega_h^2}\frac{(1+2\zeta i)}{(1+2\zeta_x i+2\zeta_g i)}u \qquad \textbf{(7.5)}$$

$$h\phi = \frac{\omega_s^2}{\omega_r^2}\frac{(1+2\zeta i)}{(1+2\zeta_\phi i+2\zeta_g i)}u \tag{7.6}$$

u is derived as:

$$\left(1+2\zeta i-\frac{\omega^2}{\omega_s^2}-\frac{\omega^2}{\omega_h^2}\frac{(1+2\zeta i)}{(1+2\zeta_x i+2\zeta_g i)}-\frac{\omega^2}{\omega_r^2}\frac{(1+2\zeta i)}{(1+2\zeta_\phi i+2\zeta_g i)}\right).u = \frac{\omega^2}{\omega_s^2}u_g \tag{7.7}$$

The properties of the SDOF system are given by the natural frequency $\tilde{\omega}$, the ratio of the hysteretic damping $\tilde{\zeta}$ and the equivalent effective seismic input $\tilde{u}_g$. The parameters given by the tilde (~) denote the properties of an equivalent oscillator replacing the real system. The equation of motion is given as:

$$(-m\omega^2 + i\omega\tilde{c} + \tilde{k})u = m\omega^2\tilde{u}_g \tag{7.8}$$

where

$$\tilde{\omega}^2 = \frac{\tilde{k}}{m} \tag{7.9}$$

$$\tilde{c} = \frac{2\tilde{k}\tilde{\zeta}}{m} \tag{7.10}$$

Eq. (7.8) can also be expressed as:

$$\left(1+2\tilde{\zeta}i-\frac{\omega^2}{\tilde{\omega}^2}\right)u = \frac{\omega^2}{\tilde{\omega}^2}u_g \tag{7.11}$$

For an undamped system where $\zeta_x = \zeta_r = \zeta_g = \zeta = 0$ and $\omega = \tilde{\omega}$, the coupled frequency of the system given in Eq. 6.6 can be represented as [22]:

$$\frac{1}{\varpi^2} = \frac{1}{\omega_s^2}+\frac{1}{\omega_h^2}+\frac{1}{\omega_r^2} \tag{7.12}$$

where the fixed based frequency of the structural mass ω_s, the natural frequency of the mass with horizontal vibration ω_h and the natural frequency of the mass with rocking vibration ω_r are defined as:

$$\omega_s^2 = \frac{k}{m} \tag{7.13}$$

$$\omega_h^2 = \frac{k_h}{m} \tag{7.14}$$

$$\omega_r^2 = \frac{k_r}{mh^2} \tag{7.15}$$

7.3 Two-Degree-Of-Freedom System for the Coupled Soil-Structure System

In addition to the simplified SDOF system that is described in the previous section, the dynamic characteristics of the soil-structure system are also compared by an alternative simplified method which is composed of two masses representing the building and the foundation (Figure 7.2) [18].

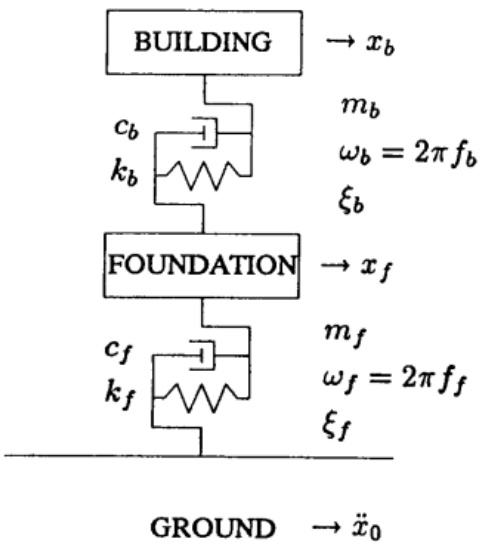

Figure 7.2 : Two degree of freedom system for the soil-structure system [18].

The spring-dashpot between the two masses concerns the stiffness and the damping characteristics of the building and the latter represents the stiffness and the damping of the foundation, which is determined using the soil properties. The motion of the coupled system is assumed to be in the horizontal direction and the rocking motion is neglected for the linear system. The dynamic characteristics of the soil-structure system is determined for its fundamental mode [10]. Two equations of motion can be written for the system as given below;

$$m_f \ddot{y}_f + c_f \dot{y}_f + k_f y_f - c_b \dot{y}_b - k_b y_b = -m_f \ddot{x}_0 \tag{7.16}$$

$$m_b(\ddot{y}_f + \ddot{y}_b) + c_b\,\dot{y}_b + k_b\,y_b = -m_b\,\ddot{x}_0 \qquad \textbf{(7.17)}$$

where m_b: the mass of the building; k_b: the stiffness of the building (for the fixed based condition); c_b: the damping of the building (for fixed based condition); m_f: the mass of the foundation; k_f: the stiffness of the foundation; c_f: the damping of the foundation. The stiffness and the damping parameters of the foundation is determined assuming that there exists no building on the foundation. The final natural frequencies of the soil-structure system are derived from Eqs. (7.13) and (7.14) as [71];

$$\omega_{1,2}^2 = \frac{1}{2}\left[\omega_f^2 + (1+\mu)\omega_b^2 \pm \sqrt{\left[\omega_f^2 + (1+\mu)\omega_b^2\right]^2 - 4\omega_f^2\omega_b^2}\right] \qquad \textbf{(7.18)}$$

where $\mu = m_b / m_f$: the mass ratio; $\omega_f = \sqrt{k_f / m_f}$: the natural frequency of the foundation without the building; $\omega_b = \sqrt{k_b / m_b}$: the fixed based natural frequency of the building. Natural frequency of the foundation is determined using Hall's Analog [72] that is based on a SDOF system representing the horizontal and the rocking vibrations of a rigid circular footing. The equation of the harmonic motion for a rigid circular disk considering merely the horizontal excitation is;

$$m\ddot{u} + c_x\,\dot{u} + k_x u = Q_0 e^{i\omega t} \qquad \textbf{(7.19)}$$

where u: the horizontal displacement at the surface of half-space; Q_0: the amplitude of the harmonic force applied horizontally at the center of rigid foundation; m: the mass of the foundation; k_x: the spring constant and c_x: the damping constant determined as:

$$k_x = \frac{32(1-\mu)Gr_0}{7-8\mu} \qquad \textbf{(7.20)}$$

$$c_x = \frac{18.4(1-\mu)}{7-8\mu} r_0^2 \sqrt{\rho G} \qquad \textbf{(7.21)}$$

where G : the shear modulus of the soil; μ: the Poisson's ratio of the soil; ρ: the mass density of the soil and r_0: the equivalent radius of a rectangular foundation.

Considering the harmonic rocking motion without horizontal vibrations, the equation of motion can be written as:

$$I_\phi \ddot{\phi} + c_\phi \dot{\phi} + k_\phi \phi = M_{y0} e^{i\omega t} \qquad \textbf{(7.22)}$$

where ϕ : the angle of rotation of the foundation; I_ϕ: the mass moment of inertia; M_{y0}: the amplitude of the harmonic rocking moment; k_ϕ : the spring constant and c_ϕ : the damping constant determined as:

$$k_\phi = \frac{8Gr_0^3}{3(1-\mu)} \qquad \textbf{(7.23)}$$

$$c_\phi = \frac{0.8r_0^4\sqrt{\rho G}}{(1-\mu)(1+B_\phi)} \qquad \textbf{(7.24)}$$

where B_ϕ is calculated as:

$$B_\phi = \frac{3(1-\mu)I_\phi}{8\rho r_0^5} \qquad \textbf{(7.25)}$$

Natural frequency of the foundation is determined using the two equations of motion for free vibration. Finally, the value of ω_f is implemented in Eq. (7.15) in order to calculate the frequencies of the coupled motion.

7.4 Response of Two-Degree-Of-Freedom Model to Earthquake Ground Motion

In Sections 7.2 and 7.3, the given formulations are employed in order to determine the natural frequencies of the soil-structure system using simplified models instead of the detailed finite elements model. Response of the 3D soil-structure system is also analyzed by an alternative formulation based on the dynamic equations of a representative Two-Degree-of-Freedom model. The displacement amplitude values due to the horizontal harmonic ground motion are compared with the results of the numerical model.

The representative model has two degrees of freedom; horizontal displacement of the concentrated mass concerning the structure and the horizontal displacement of the foundation. The time dependent variables of the system are the horizontal ground motion $u_g(t)$, the horizontal displacement of foundation $u_b(t)$, the deformation of the

structure $u(t)$, the total horizontal displacement of the structural mass $u_t(t)$, which are shown in Figure 7.3.

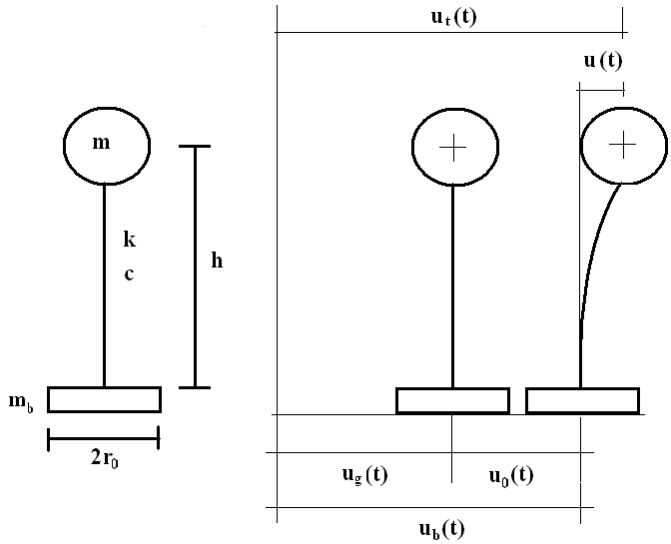

Figure 7.3 : Two-degree of freedom model.

The displacement of the foundation $u_b(t)$ and the deformation of the mass $u(t)$ are expressed in terms of the harmonic ground motion $u_g(t) = Ae^{i\omega t}$ through the use of transfer functions defined as:

$$u_b(t) = \Omega u_g(t) \tag{7.26}$$

$$u(t) = \Pi u_g(t) \tag{7.27}$$

The equation of motion for the mass can be written as:

$$m\ddot{u}_t(t) + c\dot{u}(t) + ku(t) = 0 \tag{7.28}$$

Since the total displacement of the mass is expressed as $u_t(t) = (\Omega + \Pi)\, u_g(t)$, Eq. (7.26) can also be written as:

$$-m\omega^2(\Omega + \Pi)\, u_g(t) + ci\Pi\omega u_g(t) + k\Pi\, u_g(t) = 0 \tag{7.29}$$

The dynamic equilibrium equation of motion at the foundation level is defined as:

$$m_b\, \ddot{u}_b(t) + m\ddot{u}_t(t) + P(t) = 0 \tag{7.30}$$

where $P(t) = \overline{K}_x \cdot u_0(t)$: the force applied to the foundation by the underlying soil, $\overline{K}_x$ is the frequency-dependent foundation impedance which is determined as:

$$\overline{K}_x = k_x K_x \tag{7.31}$$

where K_x is calculated as:

$$K_x = \frac{8Gr_0}{2-\mu} \tag{7.32}$$

and the dimensionless coefficient k_x is determined using Fig. 7.4 [73] for dimensionless frequency $a_0 = \omega r_0/v_s$ where v_s is shear wave velocity of the soil. Using the above equations, Eq. (7.28) can be rewritten in terms of transfer functions as:

$$-m_b\omega^2\Omega\, u_g(t) - m\omega^2(\Omega + \Pi)\, u_g(t) + \overline{K}_x(\Omega - 1)\, u_g(t) = 0 \tag{7.33}$$

Eventually, Eqs. (7.27) and (7.31) are rearranged in matrix form in order to determine the transfer functions, Ω and Π. The set of equations can be written as:

$$\begin{bmatrix} 1 & \left(1 - \dfrac{k}{m\omega^2} - \dfrac{ci}{m\omega}\right) \\ \left(1 + \dfrac{m_b}{m} - \dfrac{\overline{K}_x}{m\omega^2}\right) & 1 \end{bmatrix} \begin{Bmatrix} \Omega \\ \Pi \end{Bmatrix} = \begin{Bmatrix} 0 \\ -\dfrac{\overline{K}_x}{m\omega^2} \end{Bmatrix} \tag{7.34}$$

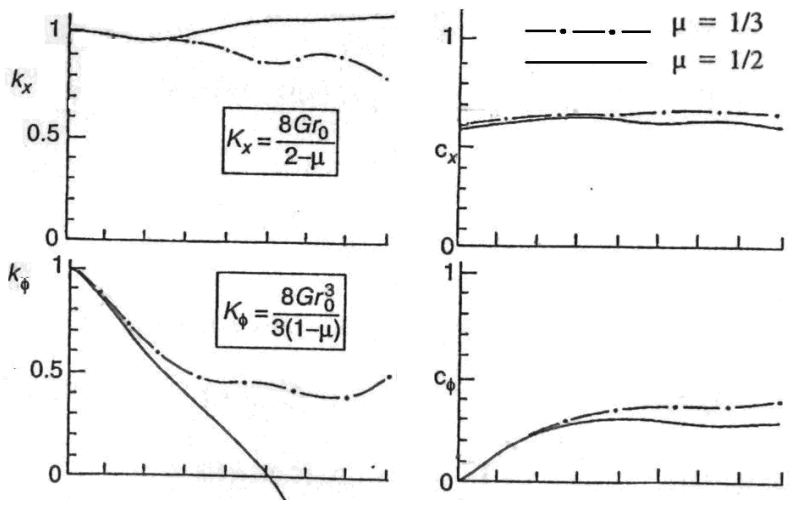

Figure 7.4 : Coefficients in impedance functions of a rigid massless circular footing resting on the elastic half-space [73].

7.5 Verification of the Numerical Procedure: A Simplified Three Dimensional Frame

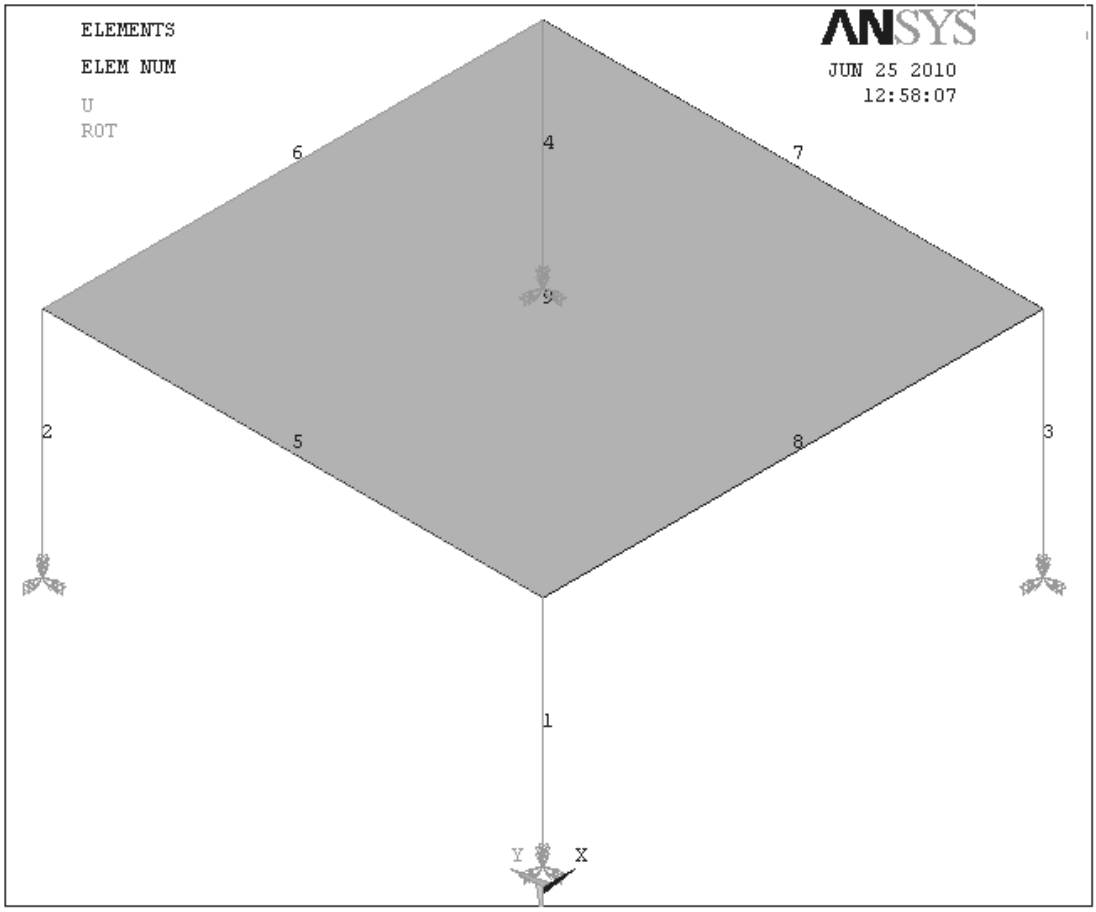

Figure 7.5 : Three dimensional modeling of the single story structure.

Before analyzing a multistory building composed of many degrees of freedom, the numerical model that is developed is simplified as a single story structure (Fig. 7.5). The system is composed of a raft foundation, a single shell element for the floor slab; four beams and four columns. The soil structure system is excited by a vertical SH wave propagating in the *x* direction. The amplitude of the seismic wave $2A_0$ is equal to 2 cm. The material properties that are used for the detailed numerical model is given in Table 7.1. However, the solution of the simplified model is accomplished for the soil conditions given as Soil A.

The results of the simplified numerical analysis show that the peak displacement response amplitude of the structure (in the *y* direction) relative to its foundation is 0.072 cm at 8.55 Hz (Figs. 7.6, 7.7 and 7.8). Therefore, the fundamental frequency of the fixed based structure in the *y* direction has been reduced from 10.46 Hz to 8.55 Hz due to the soil-structure interaction effect under the harmonic seismic motion. For

verification of this result, the frequency of the soil structure system is compared with the results obtained using Eqs. 7.13, 7.16 and 7.32 which have been derived from the lumped mass-spring-dashpot SDOF and Two-Degree-of freedom models as given in Sections 7.2, 7.3 and 7.4. The results clearly show that the frequency obtained using the numerical analysis developed in this study is in good agreement with the results obtained by the formulations previously defined in the literature (Table 7.2).

Table 7.1: Mechanical and material properties of soil-structure system.

Mechanical/ Material Property	Structure	Foundation	Soil A	Soil B
Modulus of Elasticity (N/m^2)	3×10^{10}	3×10^{10}	-	-
Shear Modulus of Elasticity (N/m^2)	-	-	6×10^7	2.52×10^{10}
Mass Density (kg/m^3)	2550	2550	1500	2800
Poisson's Ratio	0.20	0.20	0.33	0.33
Shear Wave Velocity, v_s (m/sec^2)	-	-	200	3000.00
Type of Finite Element	Columns - Beams: 3D Elastic Beam Slab: Elastic Shell	Membrane Shell		
Geometric Properties of Finite Elements	Slab Thickness: 24 cm Column Dimension: 60x40 cm^2 Beam Dimension: 47x20 cm^2 Foundation Thickness: 20 cm		Elastic Half-Space	

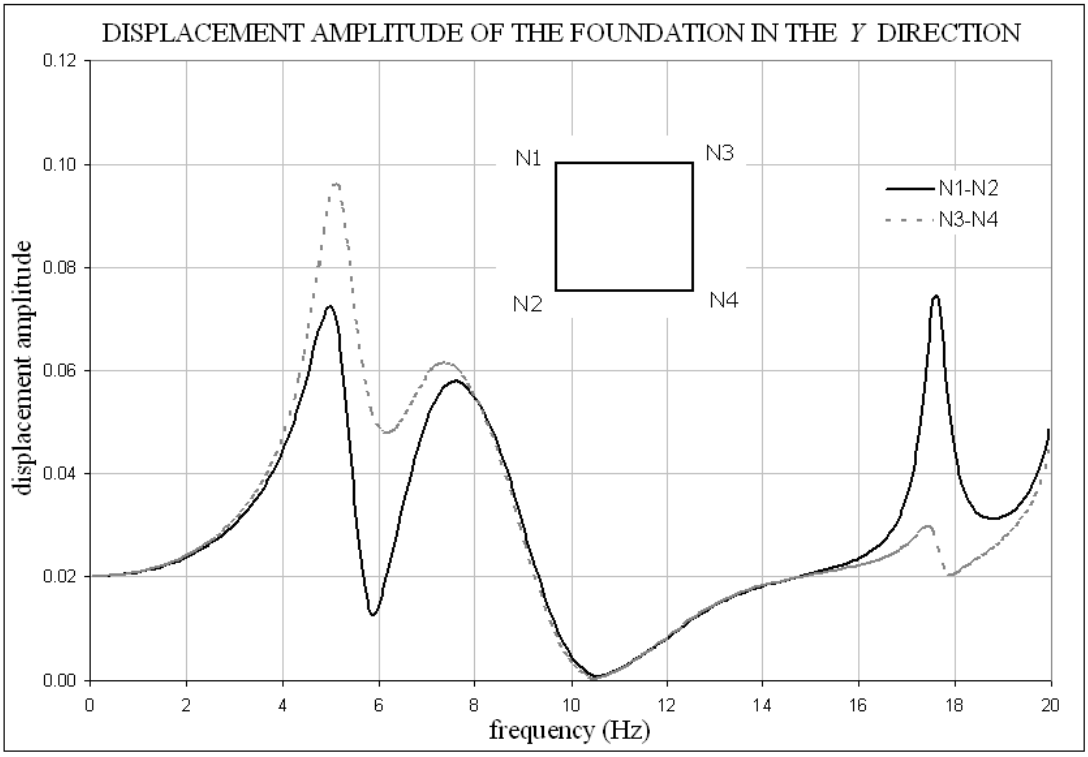

Figure 7.6 : Response of one story building at the foundation.

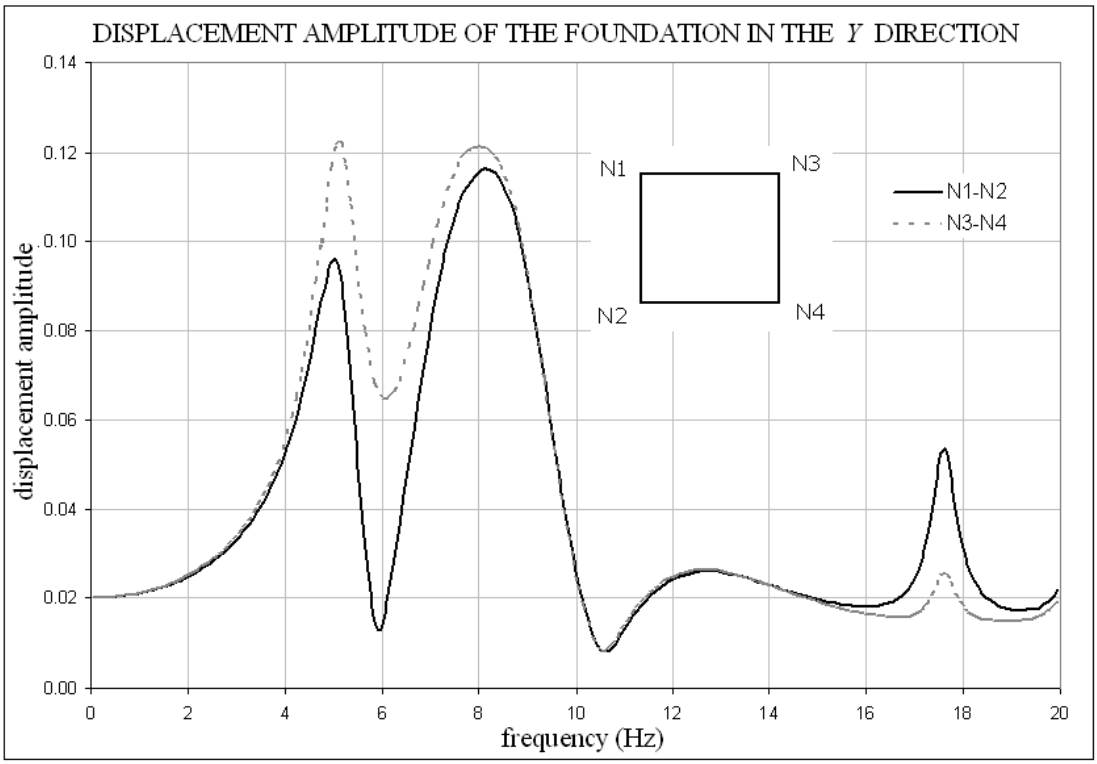

Figure 7.7 : Response of one story building at the first story level.

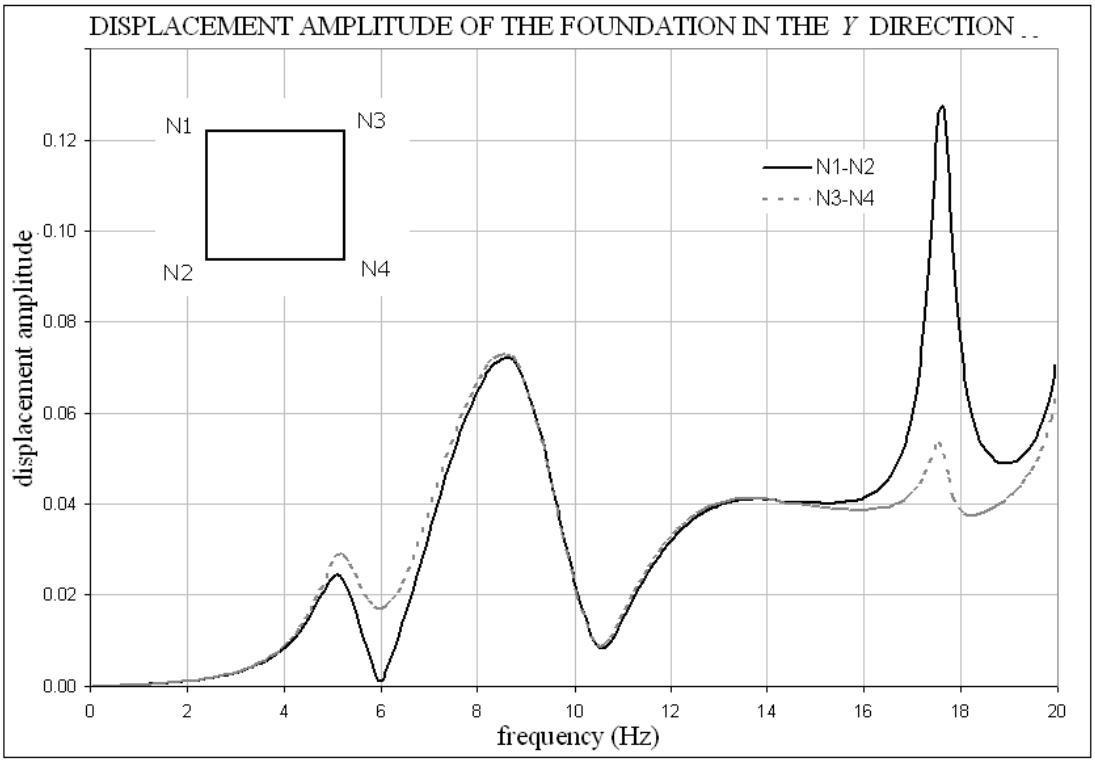

Figure 7.8 : Relative displacement of the first story level with respect to foundation.

The displacement response of the soil-structure system has been obtained for increasing excitation frequencies at the foundation and first story levels as shown in Figs. 7.6 and 7.7. Eventually, the relative displacement response of the first story level has been plotted in Fig. 7.7, which is the horizontal motion of the roof relative to the base.

Table 7.2: Comparison of the natural frequency of the soil-structure system..

Frequency of soil-structure system	Equation No.	Natural frequency of the structure f_y (Hz)	Frequency of the coupled system f_1 (Hz)
Simplified Equivalent SDOF System	Equation (7.13)	10.46	8.92
Two-Degree-of-Freedom System	Equation (7.16)	10.46	9.03
Two-Degree-of-Freedom System	Equation (7.32)	10.46	9.71
3D Modeling of Soil-Structure System (This Study)	-	10.46	8.65

Table 7.3: Comparison of the displacement amplitude values in y direction.

Peak response of soil-structure system	3D modeling of the soil-structure system	Idealized 2DOF mass-spring-dashpot model
Total response of the structure $\|u_t(t)\|$	11.04	12.69
Response of the structure relative to the base $\|u(t)\|$	8.45	10.86
Response of the foundation $\|u_b(t)\|$	4.06	2.12

The peak displacement amplitudes that are obtained by the numerical analysis of the system are compared with the results obtained by the analytical solution that is determined using the equations of motion for the idealized 2DOF system in Section 7.4. The peak values of the response are obtained by using the transfer functions that are defined to express the total response of the structure $u_t(t)$, the deformation of the structure $u(t)$ and the response of the foundation $u_b(t)$ in terms of the ground motion $u_g(t)$. These results are compared with the values obtained by this study in Table 7.3.

The results for the total response of the structure show that the analytical solution of the 2DOF system is compatible with the numerical solution. However, there is a discrepancy between the peak values of the relative response. Since the response of the structure relative to the base $u(t)$ are directly related to the deformation of the

structure, the relative motion of the lumped mass representing the structure is overestimated for the idealized 2DOF model.

In addition, there is a difference between the response of the foundation $u_b(t)$ obtained by the 2DOF system and the results of the numerical analysis. This difference depends on the fact that the response of the foundation is a function of the coupled stiffness matrix as well as the stiffness matrices of the structure and the foundation for the 3D numerical analysis. On the contrary, the solution of the idealized model does not include a spring constant representing the coupled stiffness of the system.

The results show that the displacement values and the shifted fundamental frequencies obtained from the developed numerical analysis as well as the existing formulations are in good agreement with each other. Therefore, the verification of the numerical procedure developed in this study is accomplished.

7.6 Three Dimensional Modeling of A Reinforced Concrete Multistory Building

After verification of the numerical procedure that is developed in this study for a simple model, three-dimensional modelling of an existing 6-story building in Bolu has been accomplished using the developed numerical procedure (Figs. 7.9 and 7.10). Finite element modelling of the building has been developed using the building drawings that had been reproduced by the surveying team of researchers from Purdue University after the 1999 Düzce Earthquake [74].

The surveying data show that the building has a surface foundation resting on clay soil conditions. The floor slab has a thickness of 12 cm and the dimensions of the raft foundation are 19.4 m (in *x* direction), 20.4 m (in the *y* direction) and the thickness is 30 cm. Material properties and the soil conditions of the soil-structure system are listed in Table 7.1. The Soil Type A, B refer to the stiff clay and hard rock soil conditions, respectively. The foundation surface, which is the interface of the soil-structure interaction, is discretized by 30 rectangular elements as shown in Fig. 7.9.

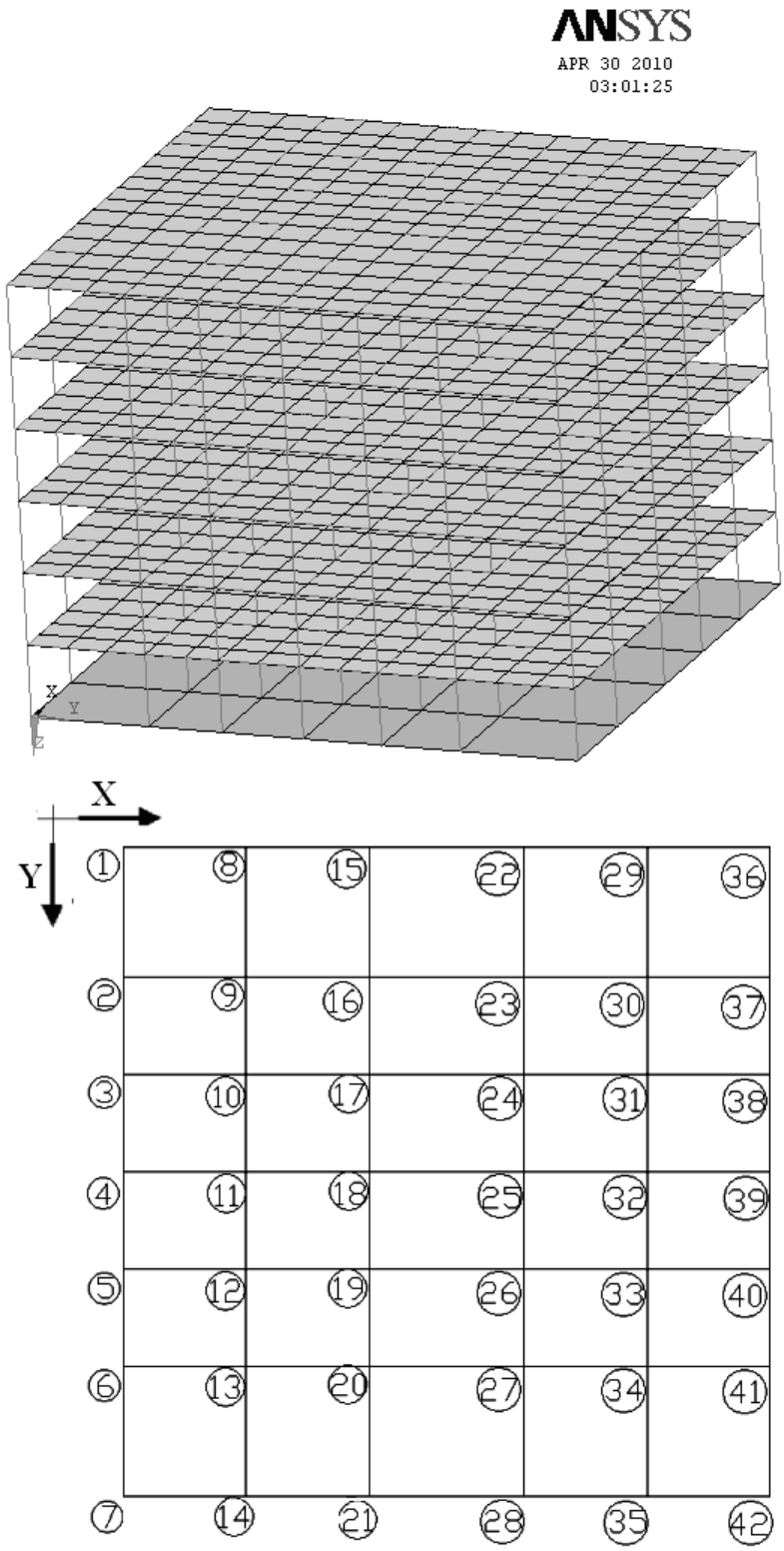

Figure 7.9 : FEM of the building and discretization of the soil-structure interface.

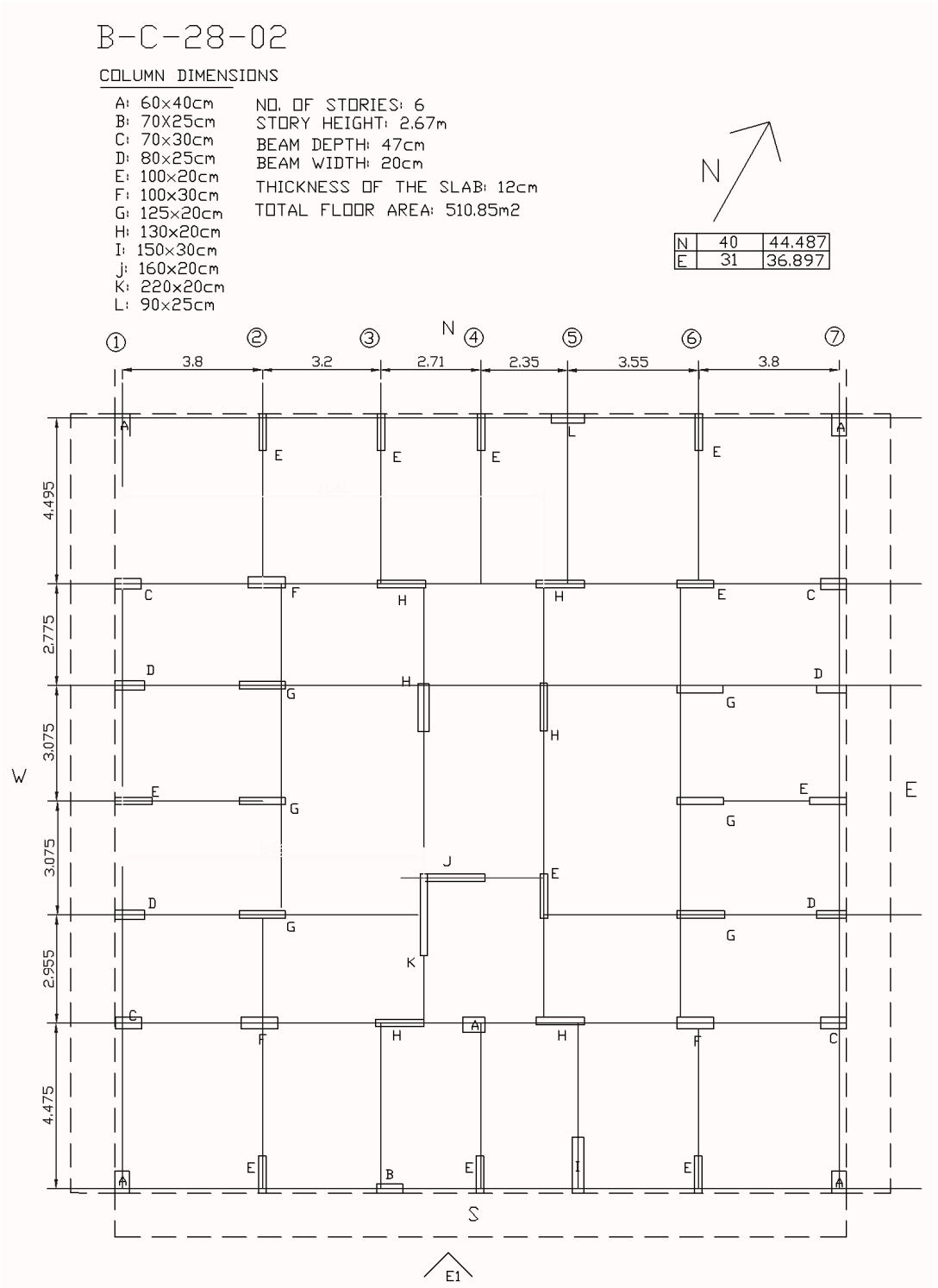

Figure 7.10 : Plan section of the multistory building [74].

Table 7.4: The natural frequencies, the proportional damping and the effective masses for the first 20 modes.

Mode	Frequency (Hz)	Proportional damping	Effective mass (X)	Effective mass (Y)	Effective mass (Z)
1	1.70	0.05	**133027.0**	0.0	0.0
2	2.13	0.05	0.0	**130635.0**	0.0
3	2.24	0.05	5.3	1435.1	0.0
4	5.92	0.09	11224.4	0.0	0.1
5	7.51	0.11	0.0	10967.7	0.0
6	7.87	0.11	0.1	732.2	0.0
7	11.97	0.16	3447.4	0.0	0.2
8	15.49	0.21	0.3	2735.2	0.2
9	16.12	0.22	0.6	945.0	0.1
10	19.06	0.25	1.0	6.1	**27383.5**
11	19.14	0.25	0.4	10.3	8416.5
12	20.01	0.27	1504.8	0.0	16.3
13	20.74	0.28	0.5	6.7	20015.4
14	21.16	0.28	0.0	6.3	15393.5
15	21.84	0.29	0.1	1.1	1493.3
16	22.04	0.29	1.0	0.3	1579.7
17	22.13	0.29	0.0	0.2	189.0
18	22.33	0.30	1.3	0.3	8299.6
19	22.36	0.30	0.1	0.0	4123.3
20	22.39	0.30	3.5	1.3	1196.5
Sum of effective masses:			**149217.9**	**147482.9**	**88107.2**

7.7 Discussion of the Results

The results of the numerical analysis of the soil structure system have been discussed considering the topics listed below;

- the peak displacement and the frequency values that are obtained for increasing excitation frequency;
- the dynamic response of the building under seismic wave motion;
- the interstory drift and the drift ratios at each story level at the peak response frequency;
- the torsional irregularity factor at each story level at the peak response frequency;

- the damage level related to the drift ratios obtained at the peak excitation frequency.

Table 7.5: The summary of the results.

Response of the soil-structure system	SOIL A (soft soil)		SOIL B (rigid soil)	
	Vertical SH wave	Horizontal SH wave	Vertical SH wave	Horizontal SH wave
Peak displacement response amplitude and the frequency at the base	3.37 cm 1.25 Hz	3.39 cm 1.25 Hz	2.01 cm 1.95 Hz	2.02 cm 2.05 Hz
Peak response displacement amplitude and the frequency at the 6th story	8.49 cm 1.35 Hz	9.02 cm 1.35 Hz	25.60 cm 2.15 Hz	25.21 cm 2.15 Hz
Ratio of transfer functions for the acceleration	Peak value at 1.85 Hz	Peak value at 1.95 Hz	Peak value at 2.15 Hz	Peak value at 2.15 Hz
Displacement response amplitude at the 6th story relative to the base	6.59 cm	7.06 cm	26.3 cm	26.0 cm
Torsional irregularity factor at the peak response frequency	1.068 at 1st story	1.198 at 1st story	1.071 at 1st story	1.060 at 1st story
Drift ratio for each story	0.0058 at 1st story	0.0062 at 1st story	0.0269 at 1st story	0.0266 at 1st story

7.7.1 Effect of the soil-structure interaction on the fundamental frequency of the structure

The reinforced concrete building that is chosen as a sample problem is analyzed under the effect of the traveling SH wave with an amplitude of 1 cm and a varying vertical angle between 0^0 (horizontally propagating) and 90^0 (vertically propagating). Considering the local coordinate system of the soil-structure interface (Fig. 7.9), the vertically incident SH wave propagates along the *z* direction and causes a free-field harmonic motion in the *y* direction at each node of the surface foundation. Similarly, the particle motion of the horizontally incident SH wave is in the *y* direction but the direction of propagation is along the *x* direction. Since the out-of-plane motion of the SH wave is independent of the angle of incidence, the amplitudes of the incident and the reflected waves are equal and in phase. Therefore, the amplitude of free-field displacement caused by the SH wave at the surface of the soil is always twice the amplitude of the wave which can also be noticed from the wave equation given in Eq. (3.52) .

The most important aspect of soil-structure phenomenon is that it causes a reduction in the natural vibration frequency of the structure under seismic excitation. This

reduction is larger for very soft soil conditions and the shift of the natural frequency is negligible for rigid soil conditions. Observing the displacement response curves obtained from the numerical analysis (Figs. B.1 through B.8), the shift of the fundamental frequency in the *y* direction is larger for the soft soil conditions (Soil A) and it is smaller for the rigid soil conditions (Soil B). Therefore, the results agree with the previous studies confirming the validity the developed numerical model.

Since the soil-structure system is under the effect of a vertical or a horizontal incident SH wave, the dynamic base excitation invokes the fundamental fixed base mode of the structure in the *y* direction with a natural frequency of 2.13 Hz. The peak values of the response curves indicate that the natural frequency of the structure is reduced to 1.25 Hz and 1.95 Hz for Soil A and Soil B, respectively.

The previous study conducted by Şafak E. [10] suggests a powerful tool to indicate the effect of the soil-structure interaction on the natural frequency of the coupled system. Fourier amplitude spectra (FAS) of acceleration records at the top and foundation levels are obtained for a seismic motion. The ratio of FAS for the top and foundation levels $|R|$ is identical to the ratio of the transfer functions for the acceleration as $|R| = |H_b/H_f|$. This ratio always has a peak at the fixed base fundamental frequency of the structure regardless of the underlying soil conditions unless there exists a rocking motion. As a contribution of this study, this useful technique has been employed as an indicator of the soil-structure interaction.

In the study of Şafak [10], the ratio of the FAS has been used to identify the soil-structure interaction for the buildings from vibration recordings. Referring to this study, the identification method has been applied in this research in a different way. Instead of the ratio of the FAS obtained from real vibration recordings, the acceleration response ratio of the 6th story and the foundation are determined under the effect of the SH waves using the developed numerical procedure. The results confirm the validity of this technique for the developed numerical model for the dynamic soil-structure analysis (Figs. B.9-B.12).

The response curves that are obtained for four different conditions show that the effect of the wave propagation can be observed for weak soil condition (Soil A) and horizontal SH wave. This is an expected result, because wave propagation effect is significant for long structures having comparable dimensions with the wavelength of the incident wave. Since the size of the building (about 20 m) is not long in

comparison with the wavelength (about 100 m for 2 Hz), the effect of the wave propagation causes a small shift in the frequencies corresponding to the peak response of the propagation even for the soft soil conditions.

7.7.2 Effect of soil-structure interaction on the peak displacement response of the soil-structure system

Apart from the effect of the soil-structure interaction on the fundamental frequency of the fixed base building, the second issue that is discussed is the peak response amplitudes, which are important concerning the design process of the structure. The peak response that is attained at the fundamental frequency of the system at the base does not vary to a great extent due to soil conditions and direction of the incident wave. However, the response at the top story for the rigid soil conditions (which is about 25 cm) is substantially higher than that of the system with the soft soil conditions (9 cm). This indicates that the stiffness and the shear wave velocity of the underlying soil have a major influence on the response of the structure at the fundamental frequency. As the stiffness of the underling soil increases under constant initial SH wave amplitude, the force exerted on the structure due to the base excitation increases as well. Therefore, the horizontal displacement of the roof increases, depending on the increase of the excitation force due to the seismic motion.

Torsional irregularity factor which is the ratio of the maximum relative interstory drift to the average relative interstory drift is determined at the peak response frequency of each case (Table 7.5). The results reveal that the torsional irregularity factor is below the limiting value which is stated as 1.20 in the Turkish Earthquake Code for both types of the soil under the vertical wave propagation [75]. The torsional irregularity factor determined by the dynamic analysis for the rigid soil condition (Soil B) under horizontal wave propagation is also very close to the results obtained for the vertical wave propagation. However, this factor is comparably higher than the rest of the cases for the soft soil conditions (Soil A) under horizontal wave propagation, still lower than the limiting value.

7.7.3 Damage identification using the drift ratio

Finally, the most important issue that is discussed using the results of the numerical analysis is the story drift and the drift ratio of each story. As the main objective of this study, a numerical procedure has been developed to analyze the soil-structure system under the effect of the seismic wave motion; and to determine the displacement response at each node of the system for varying excitation frequencies. Using the peak displacement response at the fundamental frequency, the drift ratio of each story is obtained. Subsequently, a damage identification procedure is introduced employing the damage states described in the technical manual of HAZUS [16] in terms of the drift ratios considering the effect of the soil-structure interaction. The proposed procedure is described in Fig. 7.11.

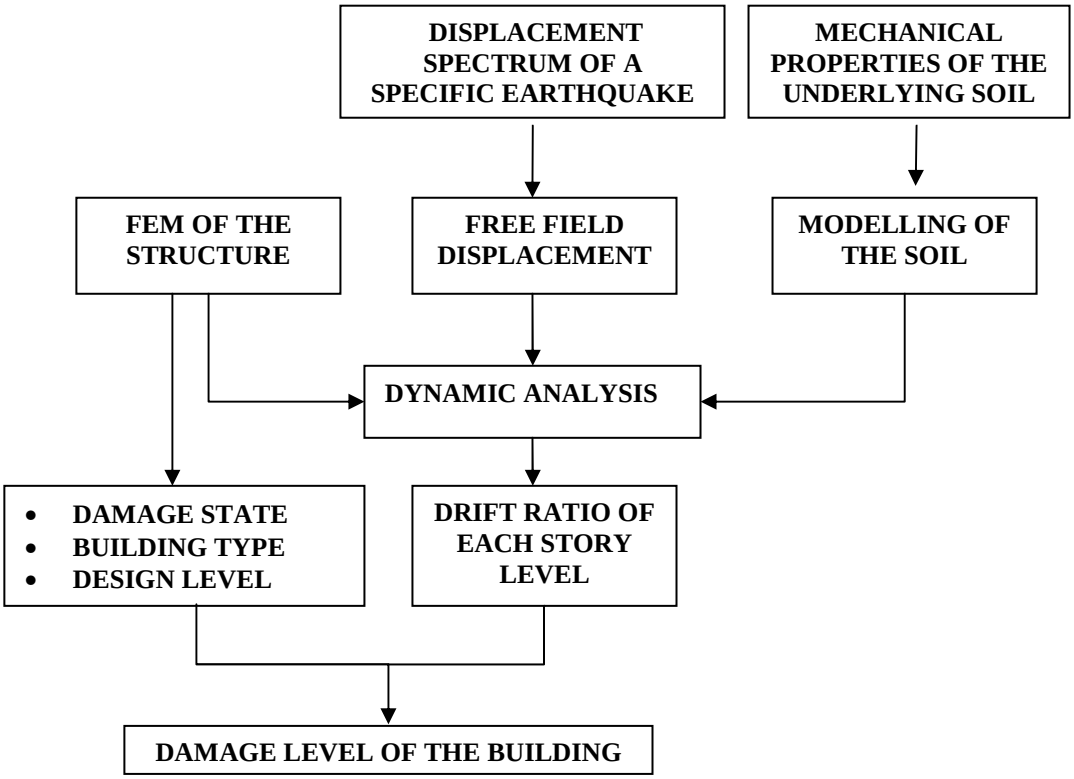

Figure 7.11 : The procedure proposed for the damage identification.

HAZUS99 Technical Manual [16] defines the structural damage states as “Slight”, “Moderate”, “Extensive” and “Complete” for 16 basic building types. For the numerical example that is analyzed, the 6-story building falls into the model building type of “Reinforced Concrete Moment Resisting Frame (C1M)” which is in the mid-rise range. Seismic design levels of buildings are classified as “High-Code”, “Moderate-Code”, “Low Code” and “Pre-Code” according to the seismic zones. The

drift limits that are described with respect to the damage states in HAZUS99 [16] are listed in Table 7.6.

Table 7.6: Drift ratio at the threshold of the damage state for C1M building type according to HAZUS99 [16].

Seismic design level	Slight	Moderate	Extensive	Complete
High-code	0.0033	0.0067	0.0200	0.0533
Moderate-code	0.0033	0.0058	0.0156	0.0400
Low-code	0.0033	0.0053	0.0133	0.0333
Pre-code	0.0027	0.0043	0.0107	0.0267

Similarly, FEMA 356 [17] restricts the drift ratios with respect to the structural performance levels and ranges defined as Immediate Occupancy (S-1), Damage Control Range (S-2), Life Safety (S-3), Limited Safety Range (S-4), Collapse Prevention (S-5) and Not Considered (S-6). The drift limits for concrete frames stated in FEMA 356 Prestandard [17] are summarized in Table 7.7. Finally, The Turkish Earthquake Resistant Design Code [75] states the drift limit as the smaller value of 0.0035 and 0.02/R where R is the structural behavior factor.

Table 7.7: Structural performance levels and damage given by FEMA 356 [17].

Drift ratio	Structural performance levels		
	Collapse prevention (S-5)	Life safety (S-3)	Immediate occupancy (S-1)
Transient	0.04	0.02	0.01
Permanent	0.04	0.01	negligible

Examining the interstory drift results obtained by the analysis of soil-structure system (Figs. C.1-C.4), the maximum drift ratio of the building, which is built on stiff clay (Soil A), is estimated as 0.0058 and 0.0062 for the vertical and the horizontal incident SH wave, respectively. These two values are just below the limits corresponding to the moderate damage state for high-code seismic design level given in HAZUS99 [16]. Considering the Turkish Earthquake Resistant Design Code [75], the drift limit is given as 0.0035 or 0.02/R = 0.005 where R is four for the reinforced concrete framed structures. The calculated values of the drift ratio do not satisfy the requirements given by the Turkish Code [75].

The maximum inter-story drift ratios estimated for the soil-structure system with rigid soil condition (Soil B) are about 0.0266 for both the vertical and the horizontal

wave propagation. These values exceed the drift limit for extensive damage state according to the high-code design level defined by HAZUS99 [16]. They are also slightly higher than the limit for the Life Safety structural performance level suggested by FEMA 356 [17].

Examining the story levels versus interstory drift ratio plots in (Figs. C.1 –C.8), it is obvious that the maximum drift ratios are attained at the first story levels and decrease linearly with increasing story levels. Therefore, the most critical part is the first story when the structure is under the effect of the seismic waves causing horizontal motion of the structure.

The initial amplitude of the SH wave which is taken as $2A_0 = 2$ cm, corresponds to a mild earthquake ground motion using the response spectra obtained for 1999 the Düzce Earthquake [76]. The results of the dynamic analysis of the soil-structure system for the existing soil conditions (Soil A) also indicate that the damage level of the building under the given SH wave excitation is close to the damage of the building that is stated as slightly damaged by the research team [74].

8. CONCLUSIONS AND RECOMMENDATIONS

The interaction of the soil with the foundation under seismic loading plays an important role on the performance of the structure. Especially, the dynamic behavior of structures resting on soft soil is strongly affected by the interaction of the soil and the foundation. The extent and the type of the effect mainly depend on the stiffness of the underlying soil; the stiffness, the mass and the geometric properties of the structure and the shape and the type of the foundation system. Thus, the influence of the soil-structure interaction has always been an important issue that has drawn the attention of the researchers throughout many years.

Many methods have been developed to deal with the dynamic analysis of the structures that are built on soft soil. The basic approach to the solution of the problem is to model the total soil-structure system and to analyze the total system under the effect of the seismic excitation whether in the time domain or in the frequency domain. The techniques to analyze the problem are mainly categorized in two groups as the direct method and the substructure method. The numerical modeling of the structure is generally conducted by the Finite Elements technique for both of the methods. Nevertheless, the Finite Element or the Boundary Element methods can be implemented for the modeling of the soil medium.

In this study, a coupled Finite Element-Boundary Element (FE-BE) methodology is introduced for the modeling of the soil-structure system. The dynamic analysis of the soil-structure model is accomplished by the “Substructure Method” under the effect of the traveling seismic waves. The total system is substructured as the structure and the unbounded soil. Then, the structure is modelled using the Finite Elements Method and the modeling of the soil medium is carried out by the Boundary Element Method. Eventually, the two models are coupled at the soil-structure interface using the displacement compatibility and the dynamic equilibrium equations at the soil-structure interface. The dynamic response of the structure is obtained by the numerical solution of the set of the dynamic equilibrium equations under the effect of

the traveling seismic wave motion at the interface nodes, which are determined by the elastic wave theory.

Finally, a drift-based damage identification technique is introduced for the multistory buildings using the peak response at each story level. The response is obtained by the solution of the soil-structure model that is generated using the developed numerical procedure.

8.1 Conclusions

Using the numerical procedure, a three dimensional bridge-backfill system has been analyzed under the effect of the traveling SH waves for different soil conditions. Initially, three different bridge-backfill model was generated. Among these, the solution of Case C1 was used for the verification of the implemented procedure comparing the response curves with those obtained by Dendrou et. al. [26]. The results were in good agreement with the previous study.

Using the same methodology, the solution of Case A1 and Case B1 has been carried out as a parametric study to determine the effect of the soil conditions on the dynamic response of the soil-structure system. Examining the results of analyses, it is concluded that;

- Increasing the stiffness of the soil underlying the structure, increases the peak response of the bridge under constant wave amplitude.
- The results of the dynamic analysis for each case under constant SH wave amplitude reveal that the excitation frequency that the peak response occurs increases as the soil gets stiffer.
- The response of the bridge-backfill system has also been obtained by uniform harmonic excitation. Comparing the results of the harmonic analysis with those of Case A1 (rigid soil conditions), it was observed that the motion of the bridge deck was symmetrical about the center of the bridge at the peak frequency for the harmonic motion, but the response of the symmetrical nodes were not identical for the solution of Case A1. This was an indication of the traveling seismic wave effect. Since the direction of the propagation for the incident SH wave coincided with the longitudinal axis of the bridge, the deck was subjected to a non-uniform seismic motion at each point.

After presenting and discussing the results of Case A1, B1 and C1, the same models were reanalyzed using the improved methodology. In this case, the bridge models were named as Case A2, B2 and C2. The conclusions withdrawn from the comparison of the results are discussed below.

- The revised numerical technique includes the effect of damping on the dynamic transformation matrix of the system. Using the new formulation, the peak displacement amplitudes of the bridge deck for all of the cases are reduced since the reduction in the dynamic transformation matrix causes a reduction in the response curves of the superstructure as well.
- Comparing the results of the solutions corresponding to the rigid soil condition (Case A1 and Case A2), it was observed that the peak response amplitude occurred at the same excitation frequency despite the reduction in the amplitude values.
- For the bridge-backfill system resisting on stiff clay, the response was again reduced by the revised methodology. In addition, the displacement amplitude of Case B2 never exceeded the initial value within the frequency range of the response curve.

As a second sample problem, three-dimensional modelling of an existing 6-story building in Bolu has been accomplished using the developed numerical procedure. Dynamic analysis of the building resting on raft foundation was carried out for two different soil conditions; soil types A and B corresponding to the stiff clay and the rigid soil conditions. In addition, the sample problem was analyzed under the effect of the traveling SH waves with two different incident angles as 90^0 (vertically propagating) and 0^0 (horizontally propagating). The conclusions withdrawn from the results are listed below;

- Comparing the displacement response curves obtained from the analyses for the soft and stiff soil conditions, there is a reduction in the fundamental frequency for both of the soil conditions. However, this reduction is observed to be larger for the response of the structure with the soft soil condition and the shift of the natural frequency is negligible for the rigid soil condition. This is an expected result because the effect of the soil-structure interaction causes a reduction of the fundamental frequency of the structure under

seismic excitation. Thus, the proposed methodology can also serve as an efficient tool to identify the change in the dynamic properties of the structures caused by the dynamic soil-structure interaction.

- Şafak E. [10] introduced a simple technique to identify the effect of the SSI using the vibration recordings. The FAS of the acceleration records at the roof and the foundation levels were obtained for seismic motion. The author stated that the ratio of the FAS for the top and the foundation levels always had a peak at the fixed base fundamental frequency of the structure if the rocking motion of the system had a negligible impact on the response. This was used as an indicator of the SSI by the author. This approach has been applied in this dissertation as well. However, instead of the acceleration records of a real seismic motion, the ratio of the acceleration response of the 6th story and the foundation were determined under the effect of the SH waves using the developed numerical procedure. The results were satisfactory. Regardless of the soil conditions, the ratios of the acceleration response always peaked at the fixed based natural frequency of the structure.
- Obtaining the displacement response of the multistory building by the proposed methodology, the horizontal displacement values at each story level were used to evaluate the drift ratio at the peak response. The structural damage was identified in terms of the maximum drift ratio, using the structural performance levels defined in FEMA 356 [18] or the damage states given in HAZUS99 [17]. The results showed that the structural damage of the building built on stiff clay were just below the limits corresponding to the moderate damage state for the high-code seismic design level given in HAZUS99 [17]. For rigid soil conditions, the results exceeded the drift limit for extensive damage state according to the high-code design level (corresponding to the fourth seismic zone in UBC) defined by HAZUS99 [17].

8.2 Contributions

The major contributions of this study are summarized below;

- An effective computational tool has been developed in order to obtain the dynamic response of a structure under the effect seismic waves.
- The methodology introduced in this study originates from a previous numerical approach that is conducted for the dynamic analysis of a simple bridge-backfill system [26]. Improving the formulation and the numerical procedure, the new computational tool is capable of solving various types of structures such as buildings, suspension bridges or bridge-backfill systems etc. with a great number of structural nodes.
- The new methodology provides an improved formulation of the dynamic transformation matrix of the soil-structure system, which relates the displacement response amplitude vector of the soil-structure interface with the dynamic response of the structural nodes. It has been observed that the response obtained by the previous techniques excluded the damping matrix of the structure in the dynamic transformation matrix. However, this assumption has led to the overestimated values of the structural response. Including the effect of the damping in the formulation, more realistic response values are obtained by the solution of the soil-structure system.
- The technique introduced by Şafak E. [10] for the identification of the SSI using the vibration recordings was adopted in this numerical study. Alternatively, instead of the ratio of the FAS of the top and foundation levels obtained from the acceleration records of a real seismic motion, the ratio of the acceleration response of the 6th story and the foundation were determined using the developed numerical procedure. Since the ratios of the acceleration response have peaks at the fixed based natural frequency of the structure regardless of the soil conditions, this approach has been proposed as a simple method for the identification of the SSI of the multistory buildings which is one of the contributions of this study.
- This study introduces an efficient technique for a drift-based damage identification for multistory buildings using the dynamic response at each story level. Obtaining the displacement response of a multistory building under the effect of the seismic waves, the horizontal displacement values at each story level are used to evaluate the drift ratio at the peak response. Using

the structural performance levels defined in FEMA 356 [18] or the damage states given in HAZUS99 manual [17], the structural damage is identified in terms of the maximum drift ratio values of the building.

8.3 Recommendations for The Future Work

- Developing the coupled BE-FE methodology, the soil medium is represented as an elastic half space. However, in reality the underlying soil deposits are mostly composed of layers with different mechanical properties. This heterogeneity considerably affects the vibrations of the foundations and the superstructure as well. The types of soil composing the layers can cause an amplifying effect on the seismic waves reaching soil-structure interface. This amplification can lead to an increased response of the superstructure. Thus, further work is necessary for the implementation of the layered soil medium as a soil model within the computer program.
- As a further research, a vibration-based study on a multistory building can be conducted in order to verify the results of the dynamic soil-structure model developed in this study and to improve the proposed methodology. Thus, a new technique can be introduced for the identification of soil-structure interaction based on vibration recordings of a future earthquake motion and the results obtained form the proposed numerical procedure.
- The computer program that has been developed is capable of obtaining the displacement and the acceleration response of any point of a multistory building excited by the seismic waves through the soil. Implementing a layered soil model within the computer program, the same drift-based damage identification technique can be used to assess the damage levels of the buildings that are founded on layered soil medium.

REFERENCES

[1] **Todorovska, M. I. and Trifunac, M. D.,** 1990: *Analytical model for building-foundation-soil interaction,* **CE 90-01**, Department of Civil Engineering, University of Southern California, Los Angeles, California.

[2] **Todorovska, M. I. and Trifunac, M. D.,** 1990: A note on the propagation of earthquake waves in buildings with soft first floor, *Journal of Engineering Mechanics*, ASCE, Vol. **116**, No. 4, pp. 892-900.

[3] **Todorovska, M. I. and Trifunac, M. D.,** 1991: *Radiation damping during two-dimensional, in-plane building-soil interaction,* **CE 91-01**, Department of Civil Engineering, University of Southern California, Los Angeles, California.

[4] **Todorovska, M. I. and Trifunac, M. D.,** 1992: Effects of the Input Base Rocking on the Relative Response of Long-Buildings on Embedded Foundations, *European Earthquake Eng.*, Vol. **VI**, No. 1, 36-46.

[5] **Trifunac, M. D., Ivanovic, S. S., Todorovska, M. I.,** 2001. Apparent Periods of a Building. I: Fourier Analysis, *Journal of Structural Engineering,* ASCE, **127**(5), 517-526.

[6] **Trifunac, M. D., Ivanovic S. S., Todorovska, M. I.,** 2001. Apparent Periods of a Building. II: Time-Frequency Analysis, *Journal of Structural Engineering*, ASCE, **127**(5), 527-537.

[7] **Todorovska, M. I. and Trifunac, M. D.,** 2006. *Impulse Response Analysis of the Van Nuys 7-story Hotel during 11 earthquakes (1971-1994): One-dimensional wave propagation and inferences on global and local reduction of stiffness due to Earthquake Damage,* Dept. of Civil Engineering Report **CE 06-01**, University of Southern California, Los Angeles, California.

[8] **Şafak, E.,** 1999. Wave propagation formulation of seismic response of multi-story buildings. *Journal of Structural Eng.*, ASCE, **125**(4), 426-437.

[9] **Clinton, J. F., Bradford S. C., Heaton T. H., and Favela J.,** 2006. The Observed Wander of the Natural Frequencies in a Structure, *Bulletin of the Seismological Society of America,* Vol.**96**, No.1, pp-237-257.

[10] **Şafak, E.** 1995. Detection and identification of soil-structure interaction in buildings from vibration recordings, *Journal of Structural Engineering*, ASCE, Vol.**121**, No.5, May 1995, pp.899-906.

[11] **Şafak, E. and Çelebi, M.,** 1992. Recorded seismic response of Pacific Park Plaza: Part II – System identification, *Journal of Structural Engineering*, ASCE, Vol.**118**, No.6, June 1992, pp.1566-1589.

[12] **Çelebi, M., and Şafak, E.,** 1992. Seismic response of Pacific Park Plaza: Part I - Data and preliminary analysis, *Journal of Structural Engineering*, ASCE, Vol.**118**, No.6, June 1992, pp.1547-1565.

[13] **Trifunac, M. D., and Biot, MA.,** 2006. Response Spectrum, *Soil Dynamics and Earthquake Engineering*, **26**(6-7), 491-500.

[14] **Ewing, W.M., Jardetsky, W.S. and Press F.,** 1957. *Elastic Waves in Layered Media*, McGraw-Hill, New York.

[15**] Lamb, H.,** 1904. On the Propagation of Tremors over the Surface of an Elastic Solid, *Philosophical Transactions of the Royal Society of London*., A, **203**:1-42.

[16] **HAZUS99,** 1999. Earthquake Loss Estimation Methodology, Technical Manual, *FEMA***,** National Institute of Building Science, Washington, D.C.

[17] **FEMA 356**, 2000. Prestandard and commentary for the seismic rehabilitation of buildings., *FEMA*, ASCE, Washington, D.C.

[18] **Wolf, J.P. and Song C.,** 2000. The scaled boundary finite-element method a primer: derivation. *Computers and Structures*, **78**. 191-210.

[19] **Hunter P. and Pullan A.,** 2001. *FEM/BEM Notes*. Department of Engineering Science, The University of Auckland.

[20] **Sandler, I.S.,** 1981. A method of successive approximations for structure interaction problems, *Computational Methods for Infinite Domain Media Structure Interaction*, Applied Mechanics Division, Vol.**46**, ASME, 67-82.

[21] **Wolf, J.P.,** 1991. Consistent lumped-parameter models for unbounded soil: physical representation. *Earthquake Engineering and Structural Dynamics*; **20**:11–32.

[22] **Wolf, J.P.,** 1985. *Dynamic Soil–Structure Interaction*. Prentice-Hall, Englewood Cliffs, NJ.

[23] **Lehmann L. and Borsutzky, R.,** 2006. Seismic Analysis of Structures: Influence of the Soil, *First European Conference on Earthquake Engineering and Seismology*, Geneva, Switzerland, Paper Number: **933**.

[24] **Lysmer, J. and Kuhlmeyer, R.**, 1969. Finite dynamic model for infinite media**,** *J. of Eng. Mech. Division*, ASCE, **95**, 859-875.

[25] **Engquist, B. and Majda, A.,** 1977. Absorbing boundary conditions for the numerical simulation of waves, *Math. of Computation*, **31**, 629-651.

[26] **Liao, Z. and Wong, H.**, 1984. A transmitting boundary for the numerical simulation of elastic wave propagation. *Soil Dyn. and Earthquake Eng.*, **3**, 174-183.

[27] **Weber, B.,** 1994. Rational transmitting boundaries for time-domain analysis of dam-reservoir interaction. *Ph.D. Dissertation*, Inst. of structural engineering, Swiss Federal Institute of Technology (ETH).

[28] **Lymser, J., Tabatabaie, M., Tajirian, F., Vahdani, S., and Ostadan, F.** 1981. *SASSI A System for Analysis of Soil-Structure Interaction*, **UCB/GT 81-02**, University of California, Berkeley, CA..

[29] **Dendrou, B.,** 1983. *A methodology for the dynamic analysis of bridge/abutment/backfill systems subjected to traveling seismic waves,* Agbabian Associates, National Science Foundation, **CEE-8007518.**

[30] **Villaverde, R.,** 2009. *Fundamental Concepts of Earthquake Engineering*, University of California, Irvine, California, USA.

[31] **Perelman D.S. and Parmelee R.A. et al.,** 1968**.** Seismic response of single-story interaction systems. *Journal of Structural Division*, ASCE; **94**:2597–2608.

[32] **Parmelee, R.A., Perelman, D.S. , Lee S.L.,** 1969. Seismic response of multiple-story structures on flexible foundations. *Bulletin of the Seismological Society of America*; **59**:1061–1070.

[33] **Jennings P.C. and Bielak J.** 1973. Dynamics of building soil interaction. *Bulletin of the Seismological Society of America*; **63**:9– 48.

[34] **Ghaffer-Zadeh M. and Chapel, F**., 1983. Frequency-independent impedances of soil–structure interaction systems in horizontal and rocking modes. *Earthquake Engineering and Structural Dynamics*; **11**:523–540.

[35] **Ehlers, G.,** 1942. The effects of soil flexibility on vibrating systems. *Beton und Eisen*; **41**:197–203 [in German].

[36] **Meek J.W. and Veletsos, A.S.,** 1974. Simple models for foundations in lateral and rocking motions. *Proceedings of the 5th World Conference on Earthquake Engineering*, Vol. **2**, Rome, 2610–2613.

[37] **Veletsos, A.S. and Nair, D.V.V.,** 1974. Torsional vibration of viscoelastic foundations, *Journal of Geotechnical Engineering Division*, ASCE, **100**:225–246.

[38] **Meek, J.W. and Wolf, J.P.** 1992. Cone models for homogeneous soil, *Journal of Geotechnical Engineering*, ASCE, **118**:667–685.

[39] **Meek, J.W. and Wolf, J.P.,** 1993. Cone models for nearly incompressible soil, *Earthquake Engineering and Structural Dynamics*, **22**:649–663.

[40] **Meek, J.W. and Wolf, J.P.,** 1993. Why cone models can represent the elastic half-space, *Earthquake Engineering and Structural Dynamics*, **22**:759–771.

[41] **Veletsos, A.S. and Nair, D.V.V.,** 1974. Response of torsionally excited foundations, *Journal of Geotechnical Engineering Division*, ASCE, **100**:476–482.

[42] **Wolf, J.P.,** 1994. *Foundation Vibration Analysis Using Simple Physical Models*, Prentice-Hall: Englewood Cliffs, NJ.

[43] **Wolf, J.P.,** 1991. Consistent lumped-parameter models for unbounded soil: physical representation, *Earthquake Engineering and Structural Dynamics*, **20**:11–32.

[44] **Wolf, J.P. and Somaini, D.R.,** 1986. Approximate dynamic model of embedded foundation in time domain, *Earthquake Engineering and Structural Dynamics*, **14**:683–703.

[45] **Nogami, T. and Konagai, K.,** 1986. Time domain axial response of dynamically loaded single piles, *Journal of Engineering Mechanics*, ASCE, **112**:1241–1249.

[46] **De Barros, F.C.P. and Luco, J.E.,** 1990. Discrete models for vertical vibrations of surface and embedded foundations, *Earthquake Engineering and Structural Dynamics*, **19**:289–303.

[47] **Jean, W.Y., Lin, T.W., and Penzien, J.,** 1990. System parameters of soil foundations for time domain dynamic analysis, *Earthquake Engineering and Structural Dynamics*, **19**:541–553.

[48] **Paronesso, A. and Wolf, J.P.,** 1995. Global lumped-parameter model with physical representation for unbounded medium, *Earthquake Engineering and Structural Dynamics*, **24**:637–654.

[49] **Wolf, J.P.,** 1997. Spring-dashpot-mass models for foundation vibrations. *Earthquake Engineering and Structural Dynamics*, **26**:931–949.

[50] **Kramer, S.L.,** 1996. *Geotechnical Earthquake Engineering*, Prentice Hall, Upper Saddle River, New Jersey.

[51] **Sykes L.R. and Evernden J.F.,** 1989. The verification of a comprehensive nuclear test ban. *Scientific American*, **743**. W.H. Freeman and Company.

[52] **García, J.,** 2003. Reduction of seismically induced structural vibrations considering soil-structure interaction. *Ph.D. (Dr.-Ing.) Dissertation*, Ruhr-Universität Bochum, Germany.

[53] **Graff, K. F.,** 1973. *Waves in Semi-Infinite Media*, Wave Motion in Elastic Solids, Dover.

[54] **Achenbach, J. D.,** l973. *Wave Propagation in Elastic Solids*, North-Holland Publishing Company/American Elsevier, Amsterdam/New York.

[55] **Apsel, R. J. and Luco, J. E.,** 1983. On the Green's functions for a layered half-space. Part I, *Bulletin of the Seismological Society of America*. **4**: 909-929.

[56] **Apsel, R. J. and Luco, J. E.,** 1983. On the Green's functions for a layered half-space. Part II, *Bulletin of the Seismological Society of America*. **73**: 931-951.

[57] **Love, A.E.H.,** 1927. *A Treatise on Mathematical Theory of Elasticity*. 4th edition, Cambridge University Press.

[58] **Wong, H.L.,** 1975. *Dynamic soil-structure interaction*. Technical Report: Caltech **EERL-75-01**. California Institute of Technology.

[59] **Elorduy, J., Nieto, J. A., and Szekely, E. M.,** 1967. 'Dynamic response of bases of arbitrary shape subjected to periodic vertical loading', Proceedings, *International Symposium on Wave Propagation & Dynamic Properties of Earth Materials*, Univ. of New Mexico, Albuquerque, Aug., pp 105-121.

[60] **ANSYS** Multiphysics Solutions. *http://www.ansys.com/*, Release 11.0. ANSYS Incorporated; 2007. accessed at 02.09.2010.

[61] **MATLAB R2010b**. 1994-2011 The MathWorks, Inc. accessed at 04.04.2011 *http://www.mathworks.com/index.html?s_cid=pl_homepage*

[62] **Clough, R. W and Penzien, J.,** 1993. *Dynamics of Structures*, McGraw-Hill, New York,. ISBN 0-07-011394-7.

[63] **Dendrou, B, Werner, S.D., and Toridis, T.,** 1985. Three dimensional response of a concrete bridge system to traveling seismic waves, *Computers and Structures*, **20**:593–603.

[64] **Hall, W.S. and Oliveto, G.,** 2003. *Boundary Element Methods for Soil-Structure Interaction*, Kluwer Academic Publishers.

[65] **Abdel-Ghaffar, A.M.**, 1977. *Studies on the effect of differential motions of two foundations upon the response of the superstructure of a bridge*, **EERL 77-02**, Pasadena, Ca.,, California. Inst. of Tech. Earthquake Engineering Research Lab. Report, 87p.

[66] **Abdel-Ghaffar, A.M. and Trifunac, M.D.,** 1977. Antiplane dynamic soil-bridge interaction for incident plane SH-waves, *Earthquake Engineering and Structural Dynamics*, Vol.**5**, Issue 2, pp. 107-129.

[67] **Romanelli, F., Vaccari, F., and Panza, G.F.,** 2003. Realistic Modelling of the Seismic Input: Site Effects and Parametric Studies, *Journal of Seismology and Earthquake Engineering*, Vol. **5**, No. 3.

[68] **Zembaty Z.,** 1997. Vibrations of bridge structure under kinematic wave excitations', *Journal of Structural Engineering*, ASCE, **123**, 479-488.

[69] **Todorovska, M.I.,** 1994. The effects of the wave passage and the dynamic soil-structure interaction on the response of base-isolated buildings on rigid embedded foundations, in G. Duma (Ed.), *Proc. 10th European Conf. Earthquake Engrg*, Aug. 28 - Sept. 2, 1994, Vienna, Austria. Sess. 5.3: Base isolation, Balkema, Rotterdam, 1995, Vol**. 1**, pp. 733-738.

[70] **Werner, S.D., Lee, L.C., Wong, H.L., and Trifunac, M.D.,** 1977. *An Evaluation of the Effects of Traveling Seismic Waves on the Three-Dimensional Response of Structures*, Report No. **R-7720-4514**, Agbabian Associates, El Segundo, California.

[71] **Timoshenko, S., Young, D.H., and Weaver, Jr. W.,** 1974. *Vibration Problems in Engineering*. John Wiley and Sons, New York.

[72] **Richart, F.E., Hall, J.R., and Woods, R.D.,** 1970. *Vibrations of Soils and Foundations*, Prentice-Hall Inc., New Jersey, 27.

[73] **Gazetas, G.,** 1983. Analysis of machine foundation vibrations: State of the art., *International Journal of Soil Dynamics and Earthquake Engineering* **2**(1) 2–42.

[74] **Url 1** <*http://cobweb.ecn.purdue.edu/~anatolia/*>, accessed at 02.07.2010.

[75] **T.C. Bayındırlık ve İskan Bakanlığı, Afet İşleri Genel Müdürlüğü,** *Deprem Bölgelerinde Yapılacak Binalar Hakkında Yönetmelik,* 2007, Resmi Gazete, Sayı : 26551, 03.05.2007.

[76] **Bakır P.G., Roeck G.D., Degrande G., Wong K.K.F**., 2007. Site dependent response spectra and analysis of the characteristics of the strong ground motion due to the 1999 Düzce Earthquake in Turkey, *Engineering Structures*, Vol.**29**, 1939-1956.

APPENDICES

APPENDIX A : Mode Shapes of The Bridge-Backfill System.

APPENDIX B : Response of The Six-Story Building.

APPENDIX C : Displacement Response and Interstory Drift Ratio at The Story Levels.

APPENDIX A.

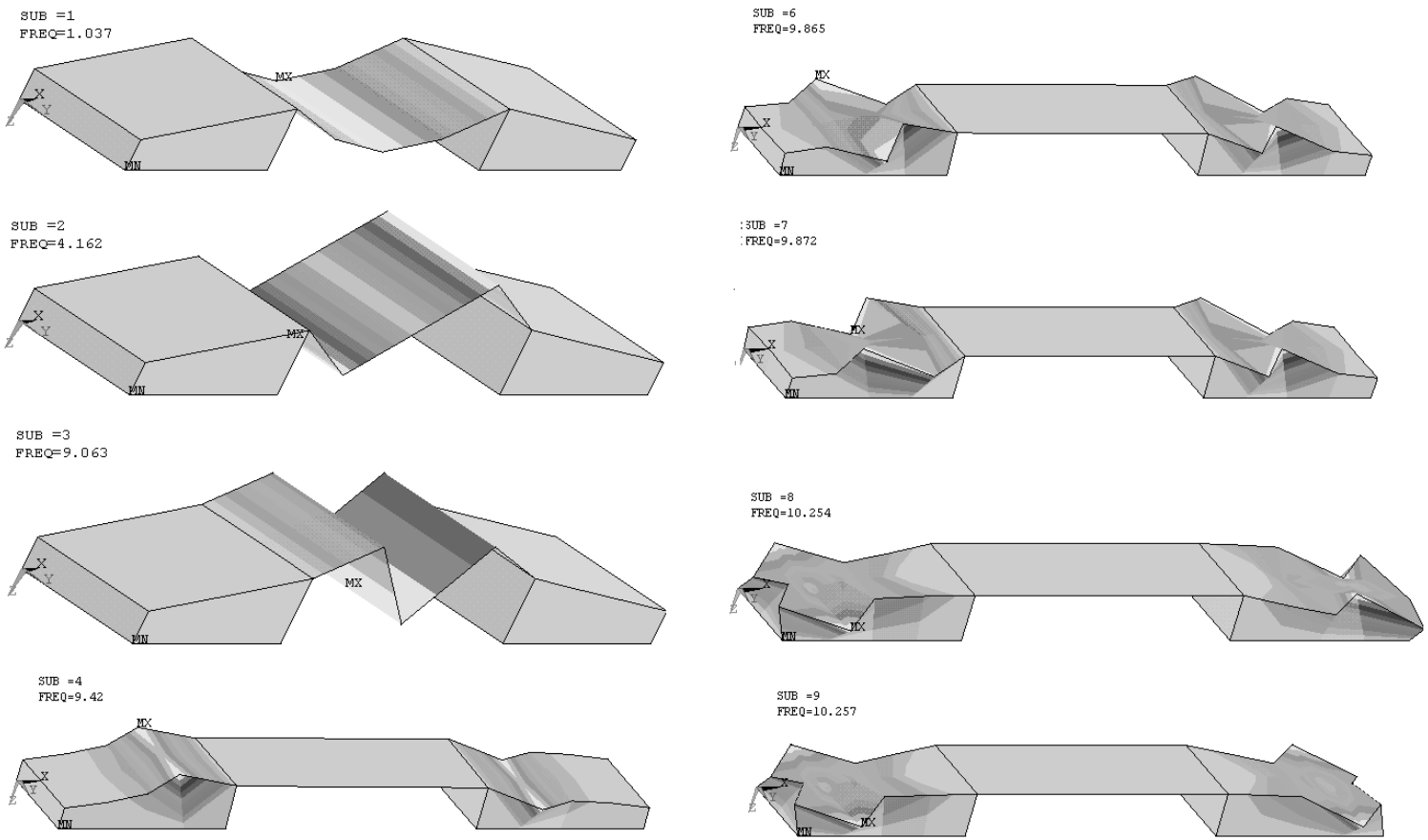

Figure A.1 : Mode shapes of the bridge (1-9).

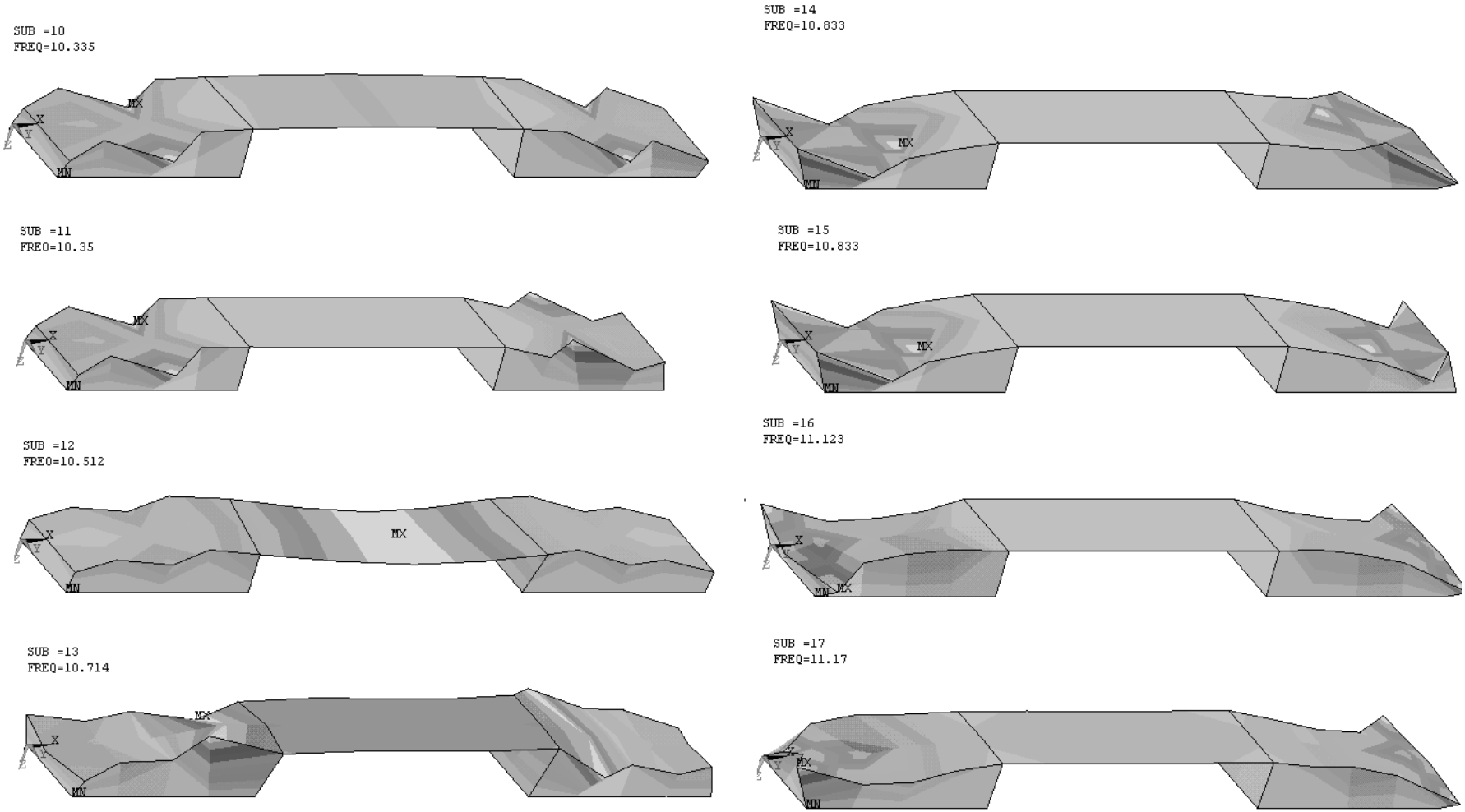

Figure A.2 : Mode shapes of the bridge (10-17).

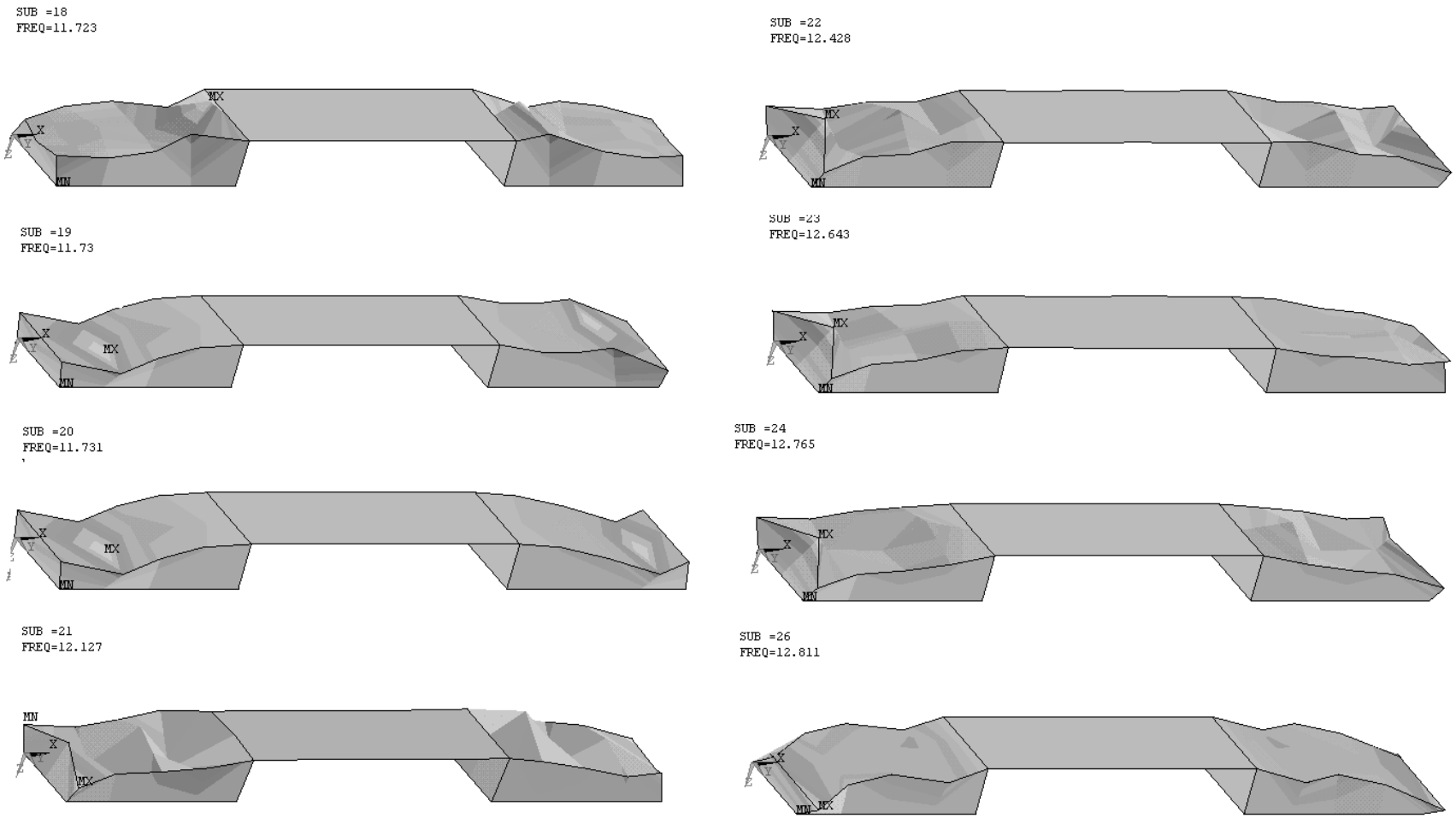

Figure A.3 : Mode shapes of the bridge (18-26).

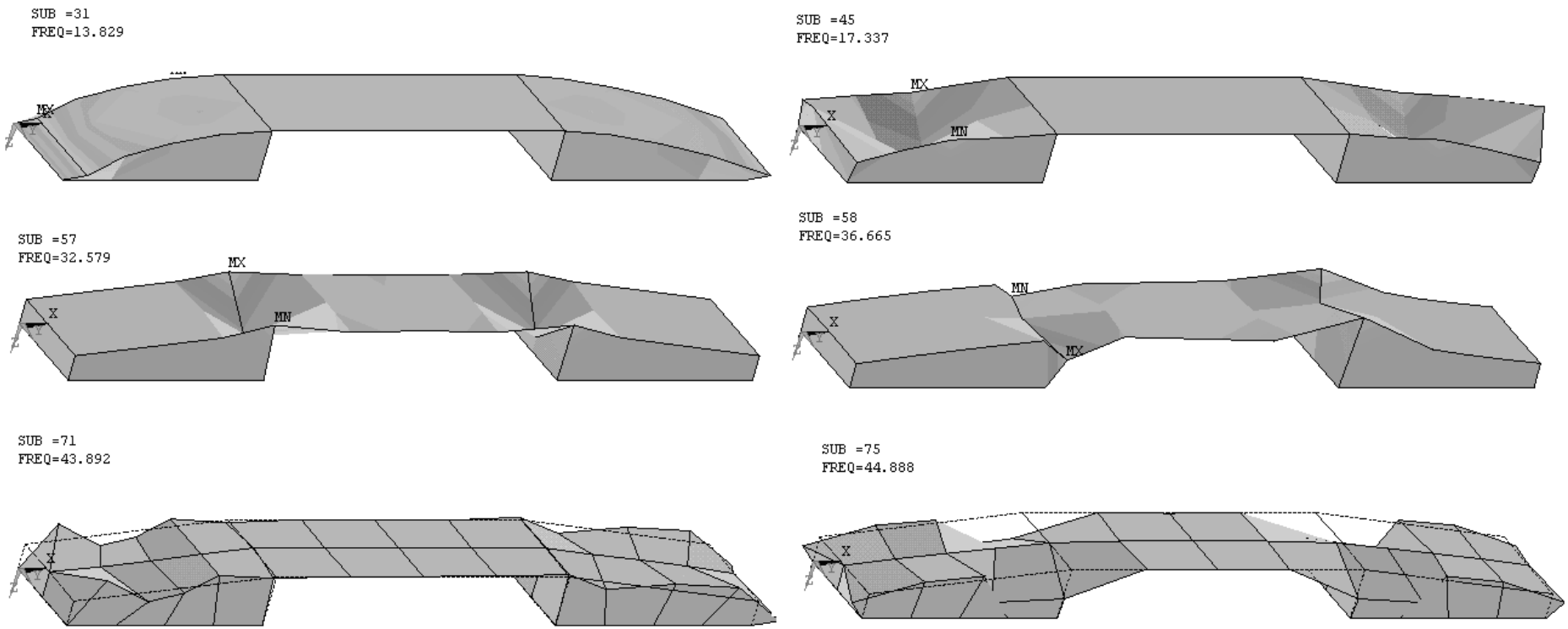

Figure A.4 : Mode shapes of the bridge (31, 45, 57, 58, 71, 75).

SET	FREQ. (Hz)	EFF. MASS	MODE SHAPE	SET	FREQ. (Hz)	EFF. MASS	MODE SHAPE	SET	FREQ. (Hz)	EFF. MASS	MODE SHAPE
1	1.04	74969.9 Z	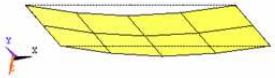	10	24.46	Y	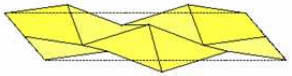	19	85.37	X	
2	4.17	Z	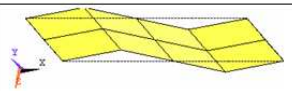	11	39.67	74539.3 X	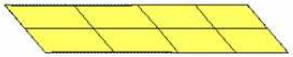	20	90.40	X	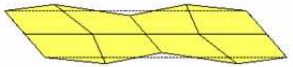
3	9.07	2206.91 Z	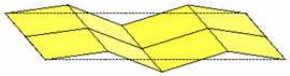	12	40.63	X	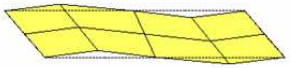	21	91.02	588.689 X	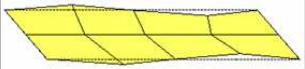
4	16.10	Z	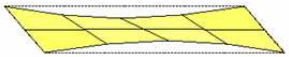	13	59.22	7257.03 Y	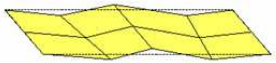	22	96.66	1902.85 X	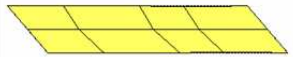
5	16.88	Y	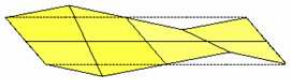	14	65.26	145.622 X	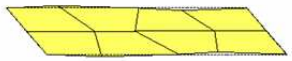	23	102.41	8.02811 Y	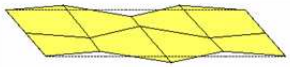
6	18.59	Y	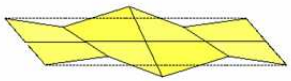	15	72.06	Y	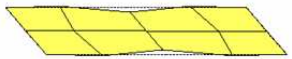	24	104.00	0.32 X	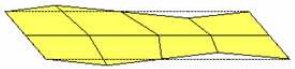
7	20.05	68952.6 Y	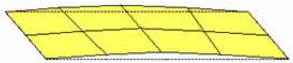	16	76.37	X	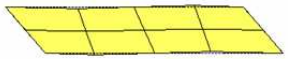	25	108.60	X	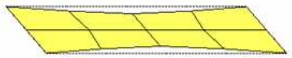
8	22.74	Y		17	77.13	X	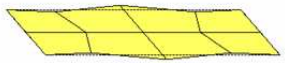	26	127.82	X	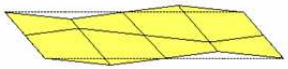
9	23.41	Y	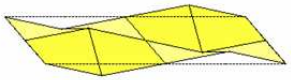	18	83.23	958.98 Y	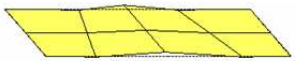	27	148.90	0.12 Y	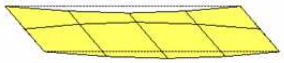

Figure A.5 : Mode shapes of the bridge deck.

APPENDIX B.

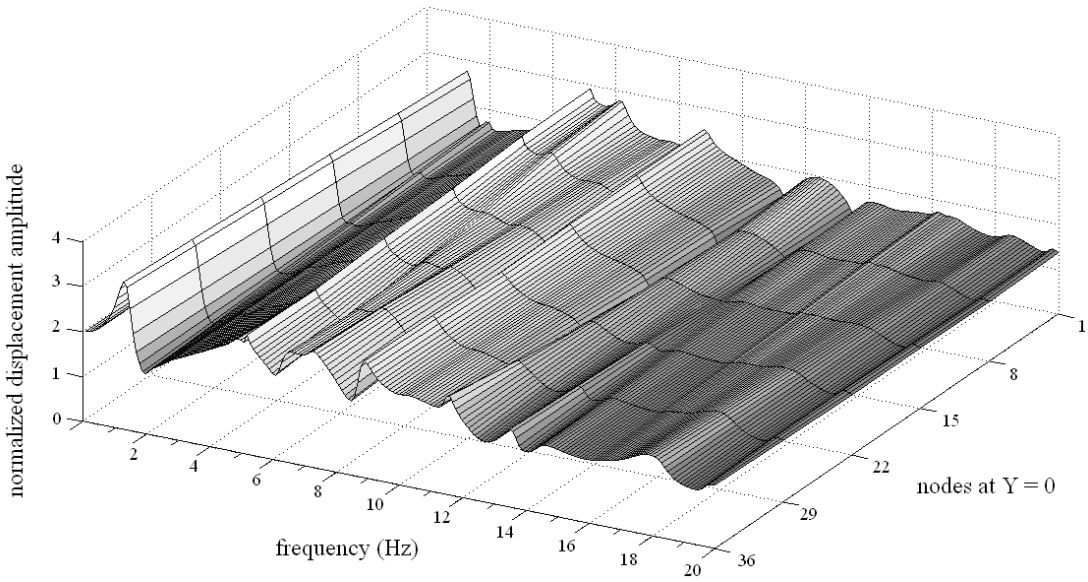

Figure B.1 : Displacement response at the foundation normalized with respect to the base excitation for the Soil A and the vertical SH wave.

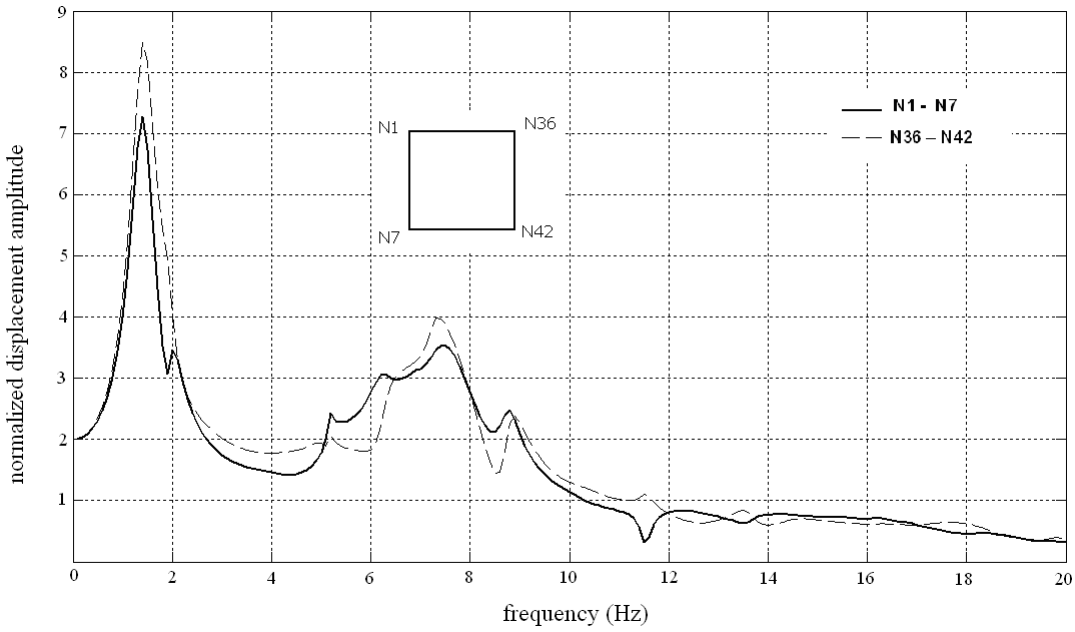

Figure B.2 : Displacement response at the sixth story normalized with respect to the base excitation for the Soil A and the vertical SH wave.

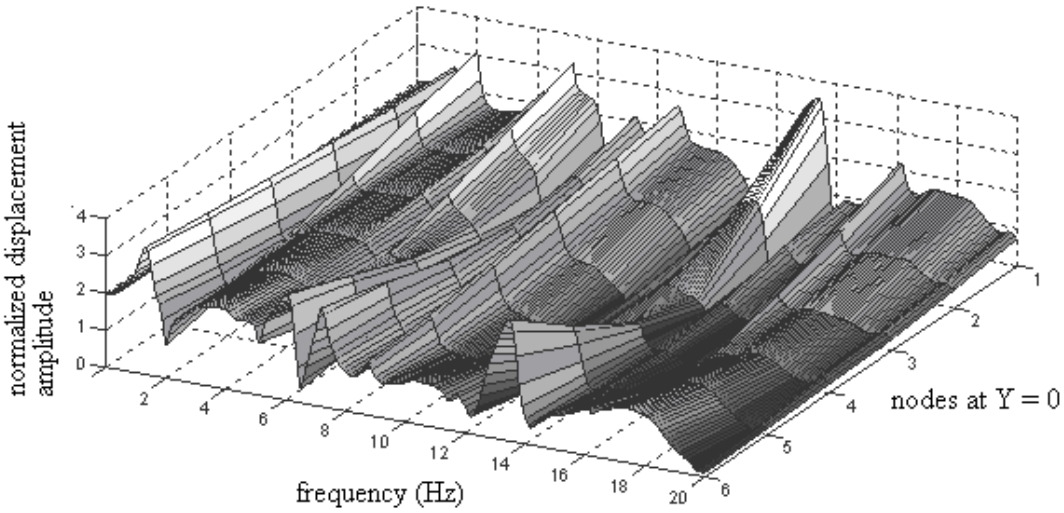

Figure B.3 : Displacement response at the foundation normalized with respect to the base excitation for the Soil A and the horizontal SH wave.

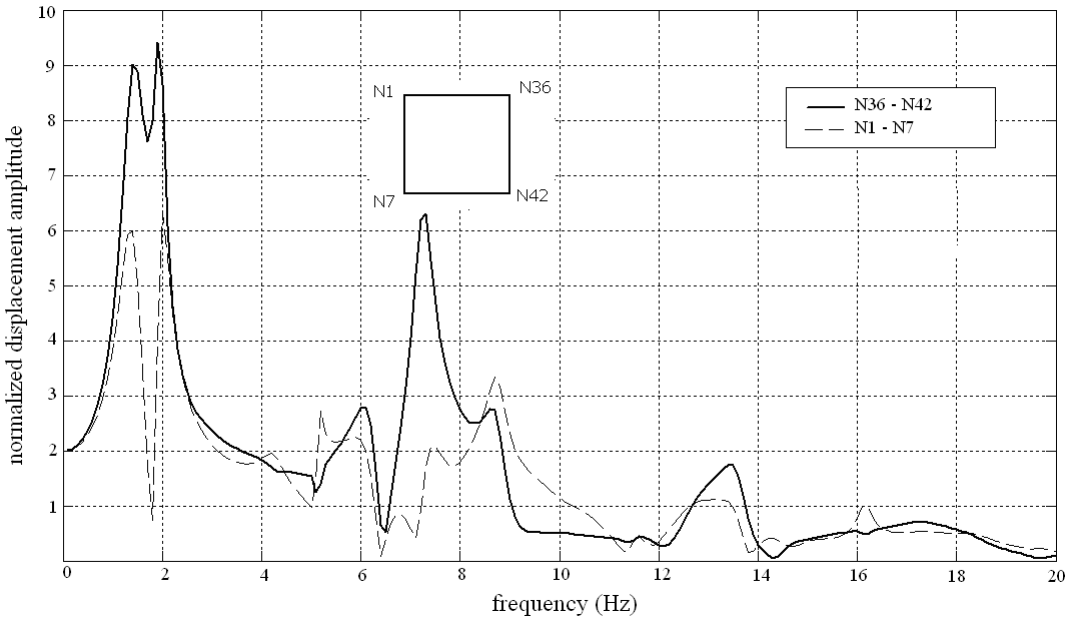

Figure B.4 : Displacement response at the 6th story normalized with respect to the base excitation for the Soil A and the horizontal SH wave.

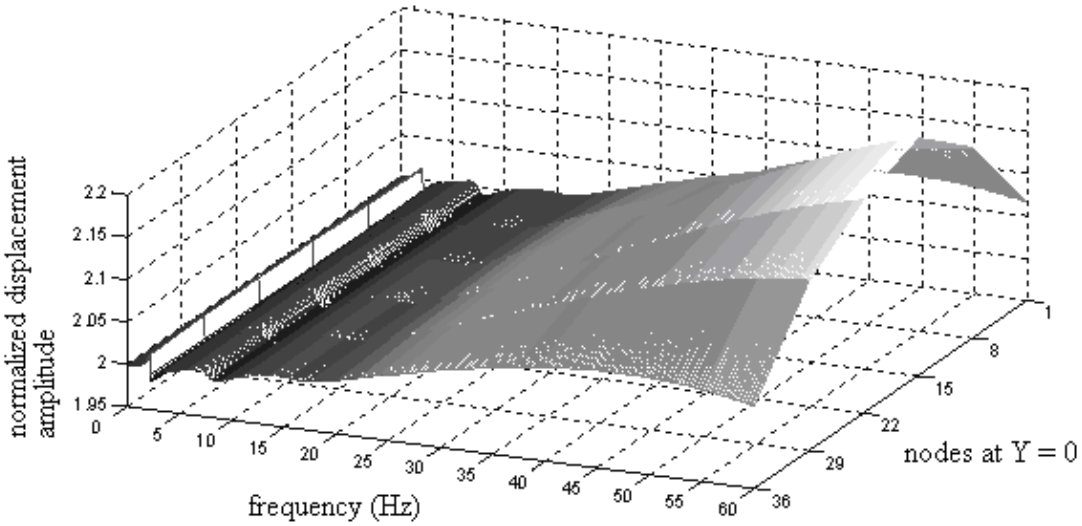

Figure B.5 : Displacement response at the foundation normalized with respect to the base excitation for the Soil B and the vertical SH wave.

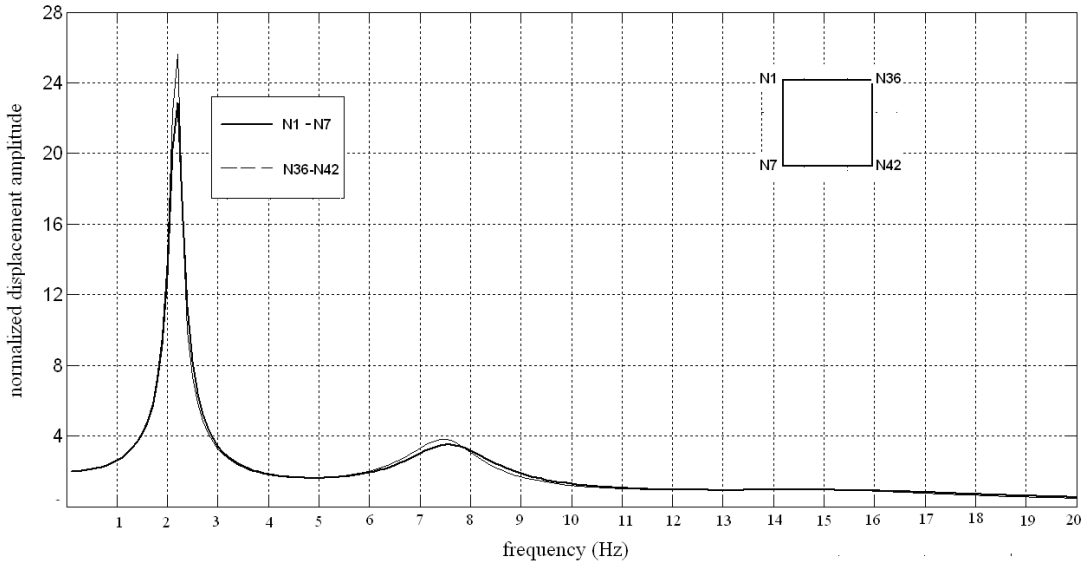

Figure B.6 : Displacement response at the 6th story normalized with respect to the base excitation for the Soil B and the vertical SH wave.

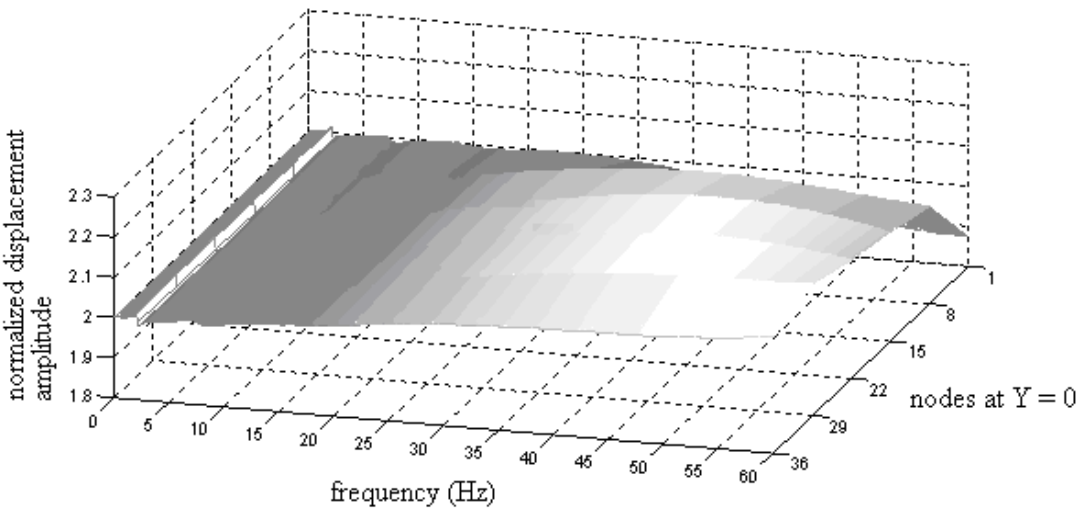

Figure B.7 : Displacement response at the foundation normalized with respect to the base excitation for the Soil B and the horizontal SH wave.

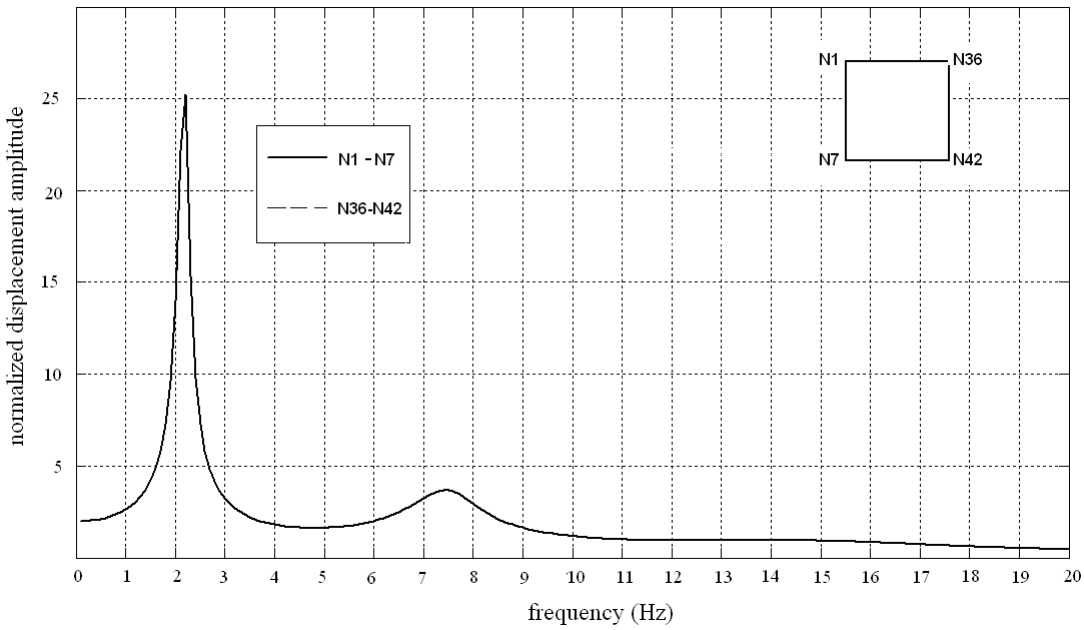

Figure B.8 : Displacement response at the 6th story normalized with respect to the base excitation for the Soil B and the horizontal SH wave.

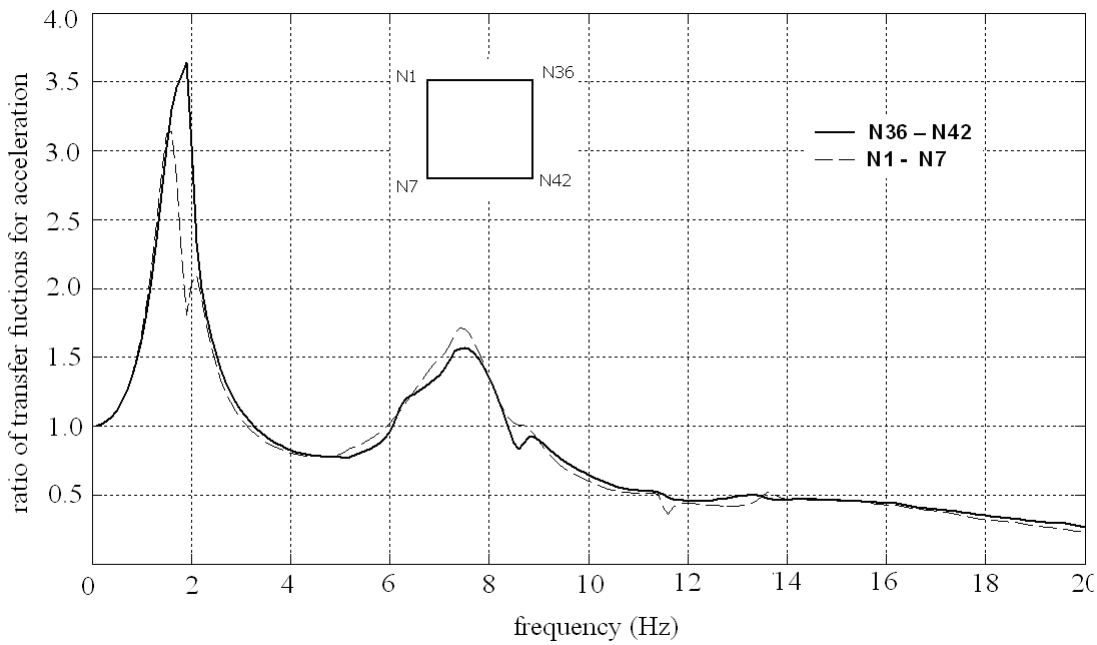

Figure B.9 : Ratio of the acceleration response (top/base) for the Soil A and the vertical SH wave.

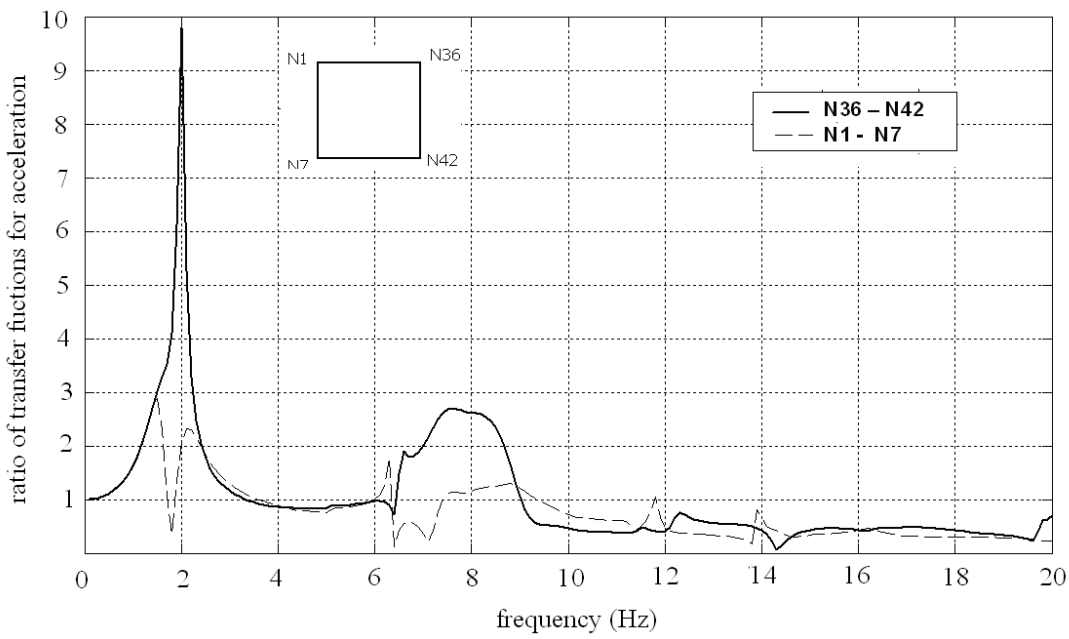

Figure B.10 : Ratio of the acceleration response (top/base) for the Soil A and the horizontal SH wave.

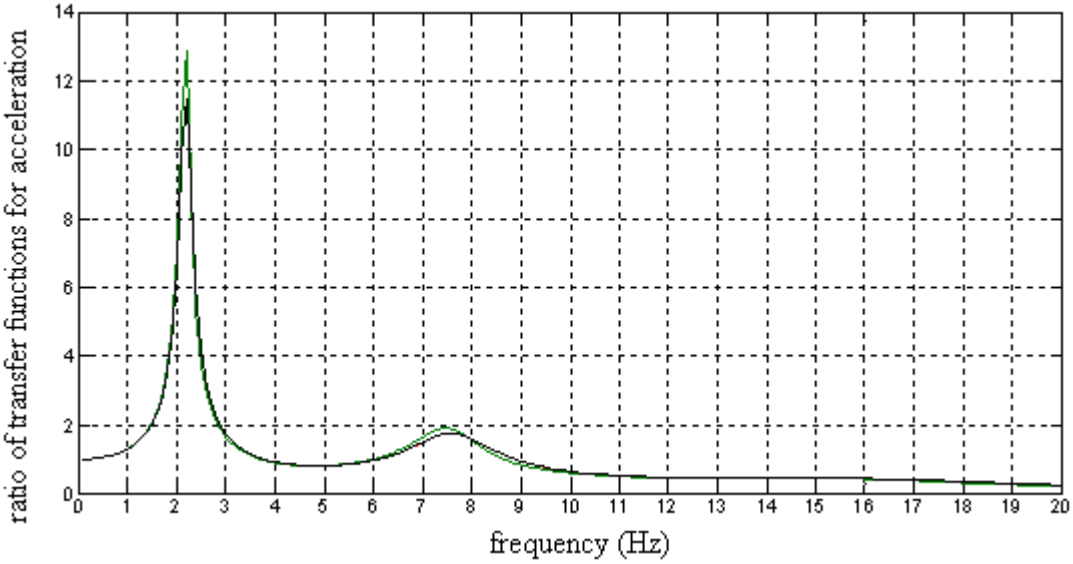

Figure B.11 : Ratio of the acceleration response (top/base) for the Soil B and the vertical SH wave.

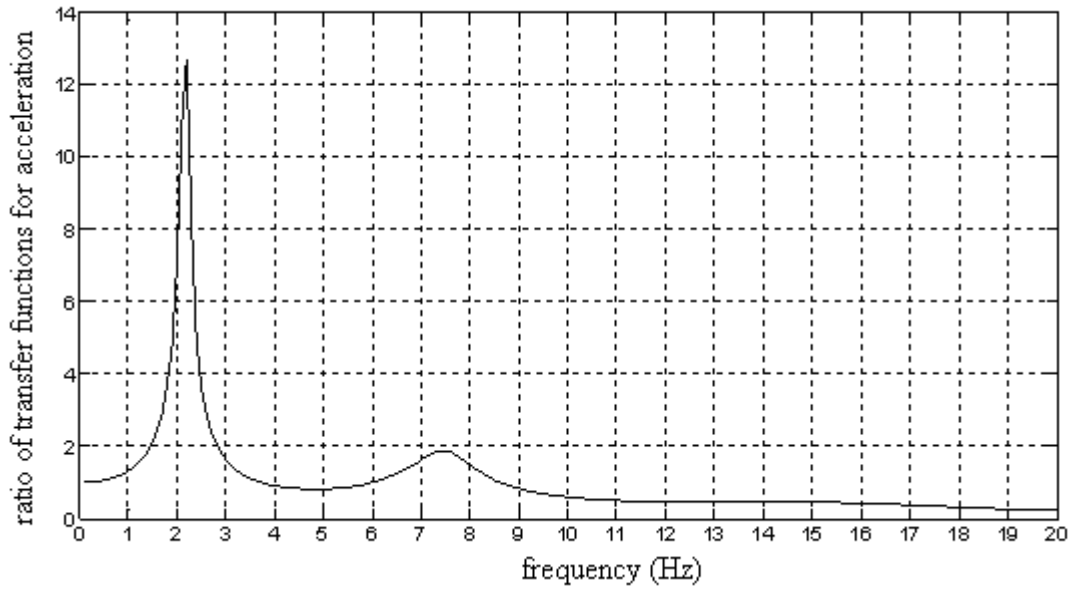

Figure B.12 : Ratio of the acceleration response (top/base) for the Soil B and the horizontal SH wave.

APPENDIX C.

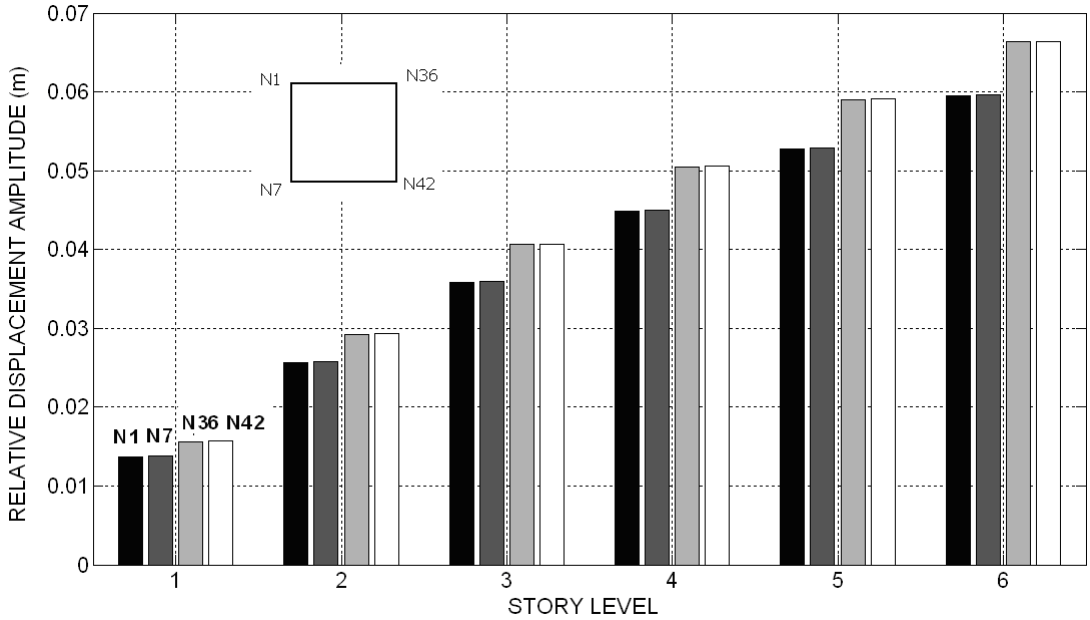

Figure C.1 : Displacement response of the story levels relative to foundation at f = 1.45 Hz for the Soil A and the vertical SH wave motion.

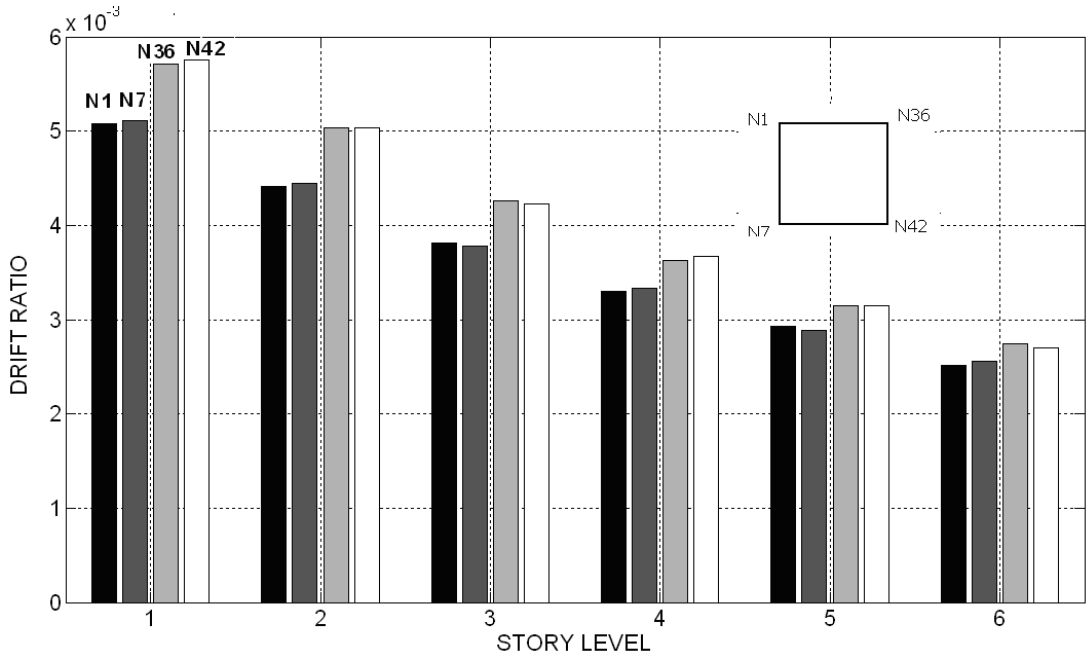

Figure C.2 : Interstory drift ratio at f = 1.45 Hz for the Soil A and the vertical SH wave motion.

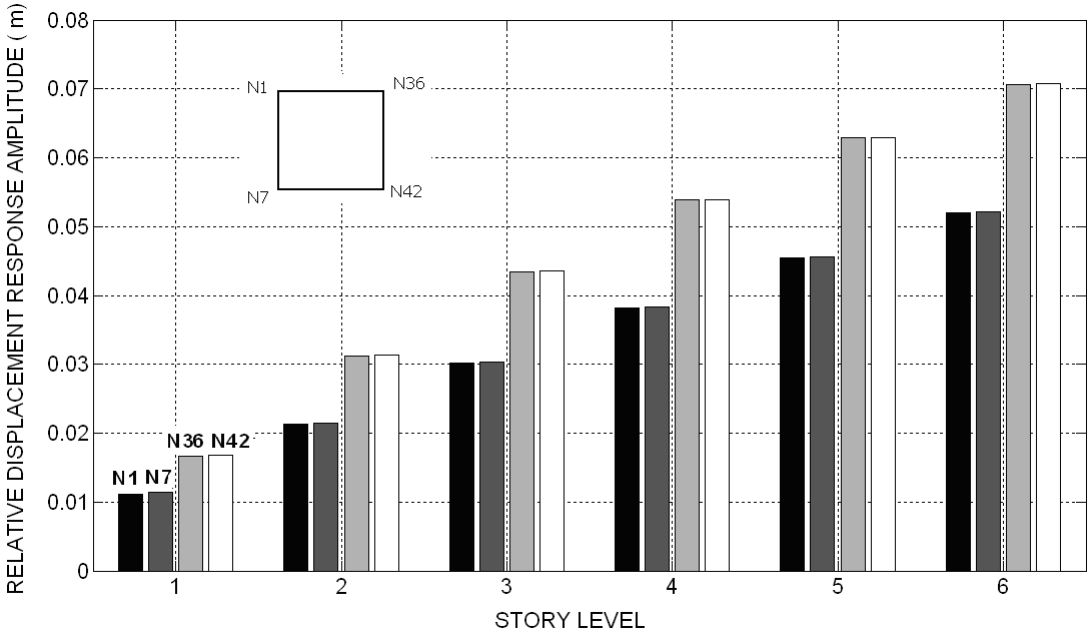

Figure C.3 : Displacement response of the story levels relative to foundation at f = 1.45 Hz for the Soil A and the horizontal SH wave motion.

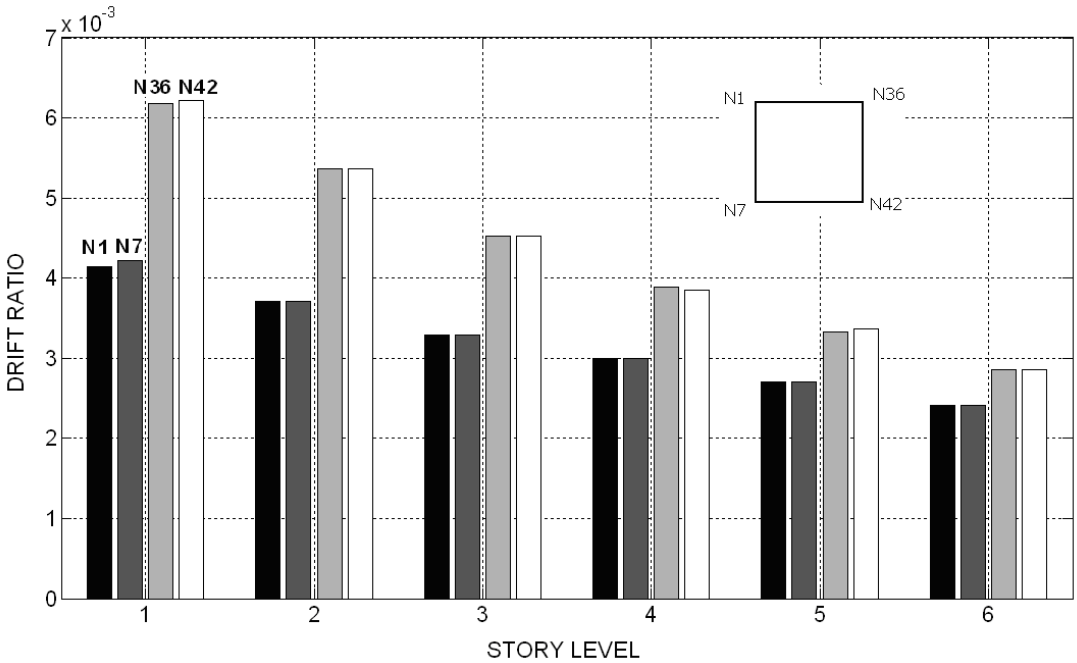

Figure C.4 : Interstory drift ratio at f = 1.45 Hz for the Soil A and the horizontal SH wave motion.

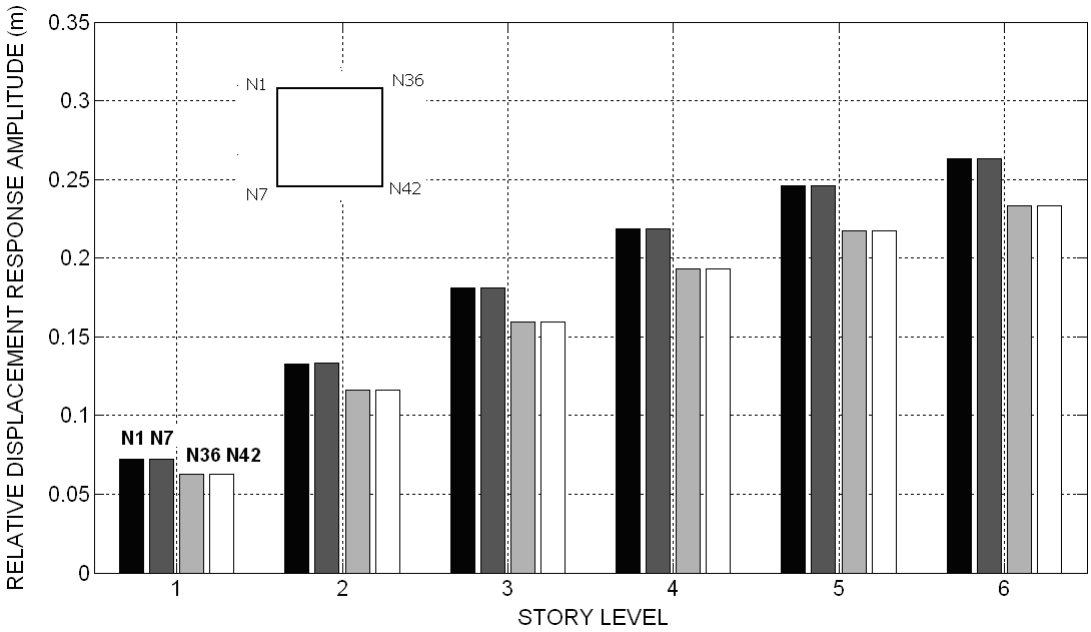

Figure C.5 : Displacement response of the story levels relative to foundation at f = 2.15 Hz for the Soil B and the vertical SH wave motion.

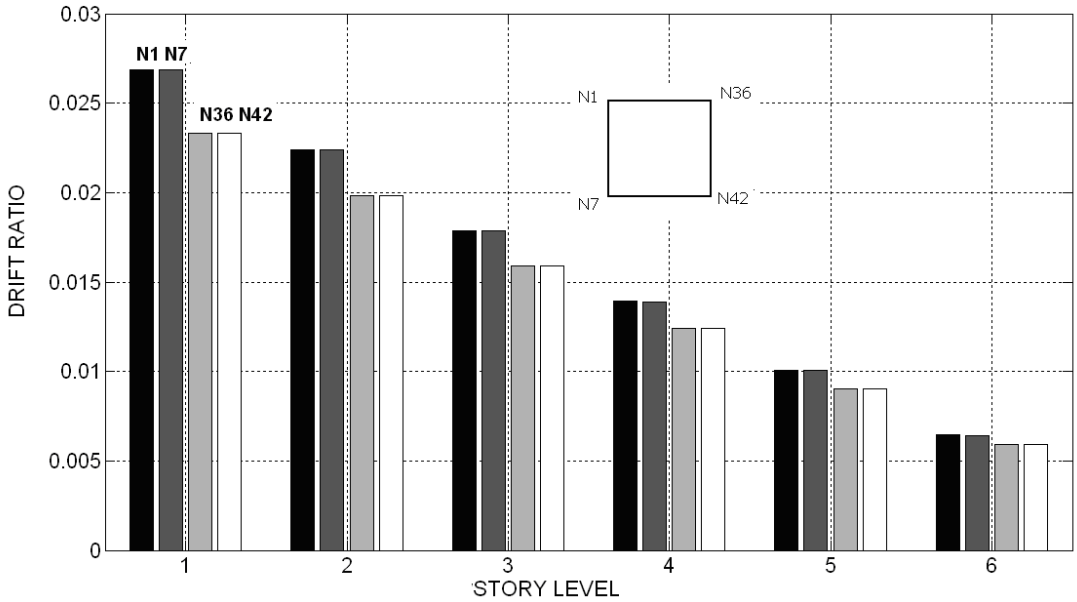

Figure C.6 : Interstory drift ratio at f = 2.15 Hz for the Soil B and the vertical SH wave motion.

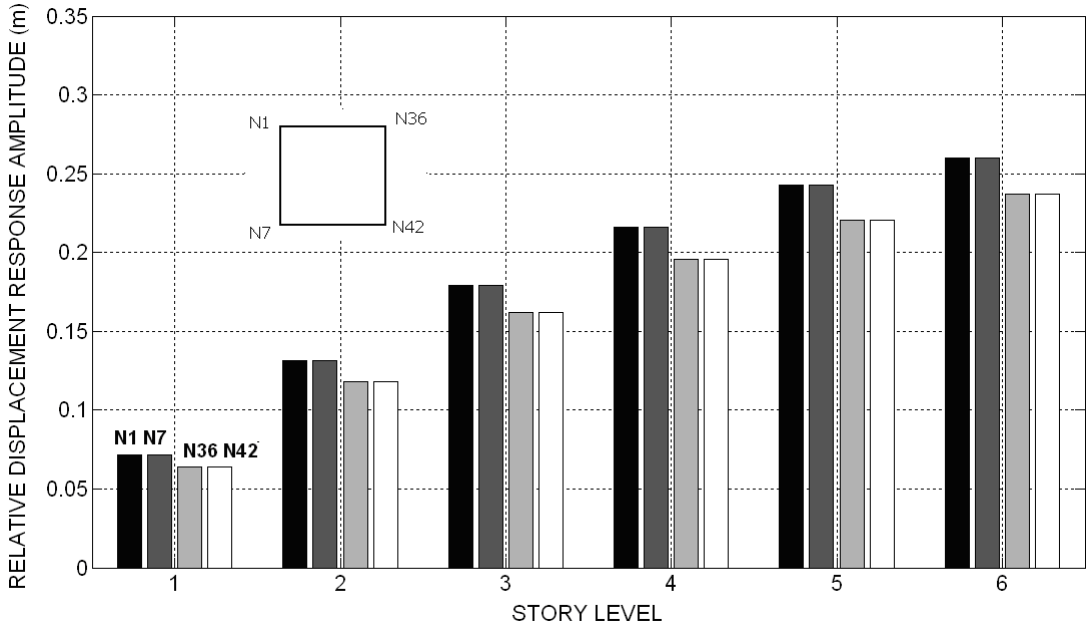

Figure C.7 : Displacement response of the story levels relative to foundation at f = 2.15 Hz for the Soil B and the horizontal SH wave motion.

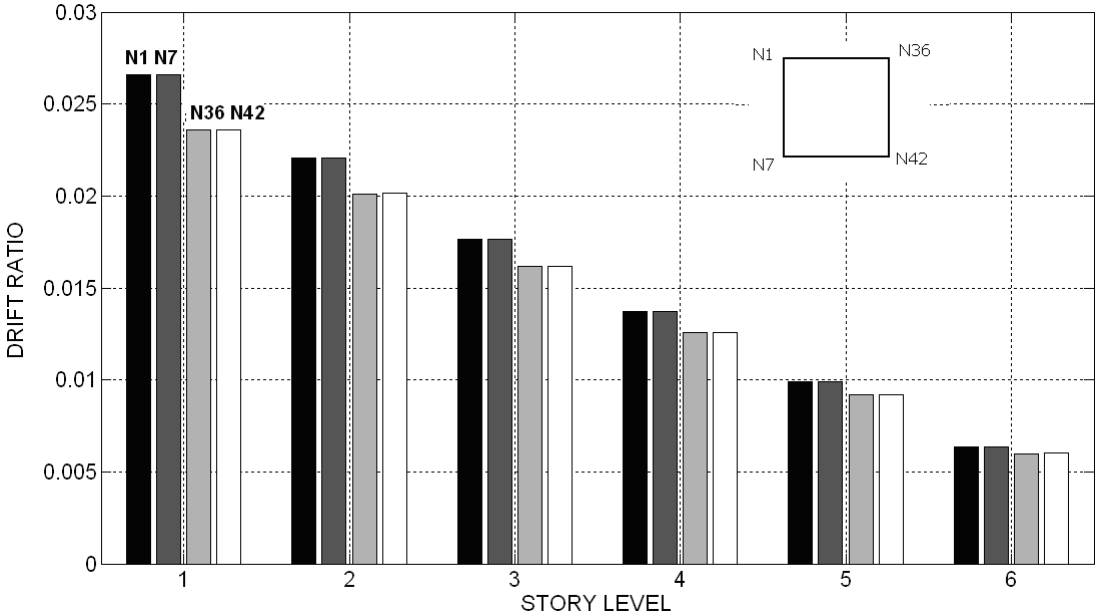

Figure C.8 : Interstory drift ratio at f = 2.15 Hz for the Soil B / horizontal SH wave motion.

CURRICULUM VITAE

Candidate's full name: Ayşe Elif ÖZSOY ÖZBAY

Place and date of birth: İstanbul – 14.09.1975

Permanent Address: Ataköy 9. Kısım B.12 D.38 Bakırköy/İSTANBUL

Universities and Colleges attended:

B.S. in Civil Engineering 1994-1999
Boğaziçi University, Faculty of Engineering

M.S. in Civil Engineering (GPA: 3.46) 1999-2003
Boğaziçi University, Faculty of Engineering

Ph.D. in Civil Engineering (GPA: 3.69) 2003-
Structural Engineering
İstanbul Technical University

Publications:

- **Özsoy E.Ö.,** Bakır P.G., (2010), "*Sonlu eleman-sınır eleman yöntemi ile yapı-zemin etkileşiminin deprem dalgalarının yayılımı etkisi altında analizi*", IZAS2010.
- **Özsoy A.E.** and Özgen K., 2005. "*Perdelerdeki Boşlukların Yatay Ötelenmeye Etkisi*", Deprem Sempozyumu Kocaeli 2005, pp: 444 – 450.
- Köksal H. O., Doran B., **Özsoy A. E.** and Alacalı S. N., 2004. "*Nonlinear Modeling of Concentrically Loaded Reinforced Blockwork Masonry Columns*", Canadian Journal of Civil Engineering, Vol.**31**: 1012 – 1023. **(SCI-Expanded)**
- Karakoç C., Köksal H. O. & **Özsoy A. E.,** 2003. "*The Behavior of Reinforced Blockwork Masonry Columns under Axial Compression*", Fourth International Conference on Earthquake Resistant Engineering Structures, ERES IV, Ancona, Italy, WIT Press, Southampton, U.K., pp: 371 – 379.